SAND2017-5122PE

Exceptional service in the national interest

Sandia National Laboratories

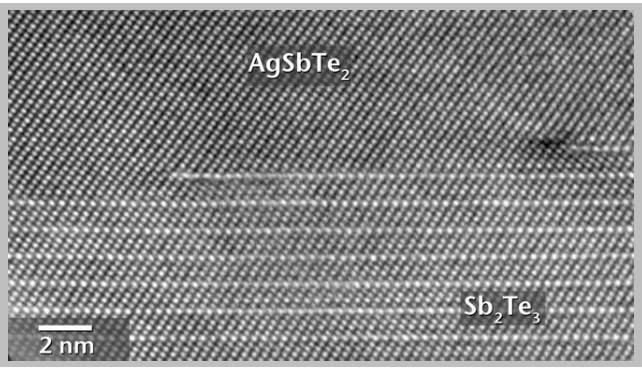

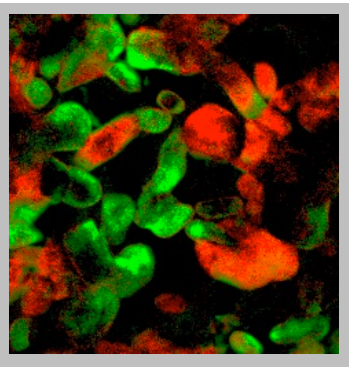

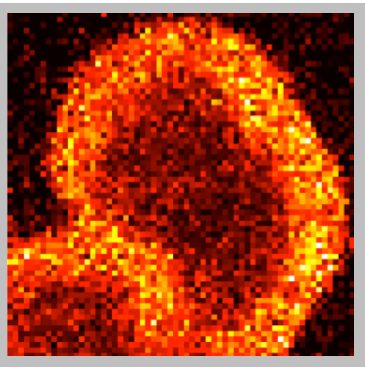

More Than Just a Picture: Answering Scientific Questions with Advanced Electron Microscopy

Carnegie Science | Geophysical Laboratory

Joshua D. Sugar

May 8, 2017

U.S. Department of Energy | National Nuclear Security Administration

Sandia National Laboratories is a multimission laboratory managed and operated by National Technology and Engineering Solutions of Sandia, LLC., a wholly owned subsidiary of Honeywell International, Inc., for the U.S. Department of Energy's National Nuclear Security Administration under contract DE-NA0003525.

Acknowledgements

- Suzy Vitale
- Warren York
- Li-ion Batteries:
  - MSU: Prof. Wei Lai and his research group
  - Stanford: Prof. William Chueh
  - SNL: Kevin McCarty, Anthony McDaniel, Farid El Gabaly, Kyle Fenton, John Sullivan, Mark Homer, Norm Bartelt
  - Gatan: Ray Twesten, Bernhard Shaffer
  - Lehigh University: Prof. Masashi Watanabe
- Nanoporous Pd/Rh and bubbles
  - Norm Bartelt
  - SNL: David Robinson, Patrick Cappillino, Markus Ong, Paul Kotula
  - Protochips: Ben Jacobs
- Electronic Components
  - Danny Dominguez
  - Bonnie Antoun
  - Kevin Connelly

Sandia National Labs Sites: National Security Complex

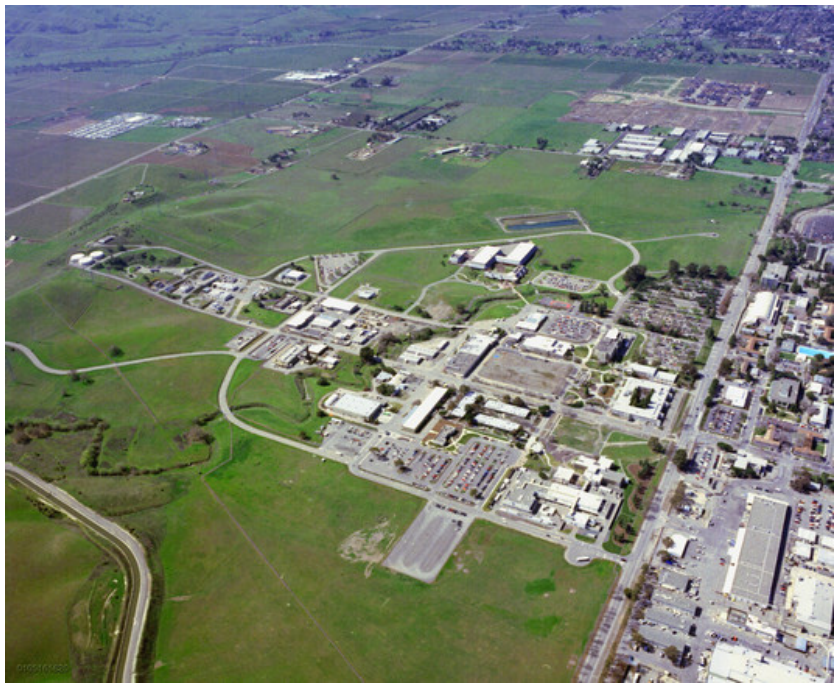

Livermore, CA

Albuquerque, NM

Available Signals for Microstructural Analysis

- Elastically Scattered Electrons
  - Energy is not lost from scattering process
  - Microstructural information from images
  - Crystallographic information from diffraction patterns
  - Atomic number (HAADF STEM)
- Inelastically Scattered Electrons
  - Energy is lost and converted into photons
  - Compositional and bonding/electronic structure information
    - Energy Dispersive Spectroscopy (EDS)
    - Electron Energy Loss Spectroscopy (EELS)

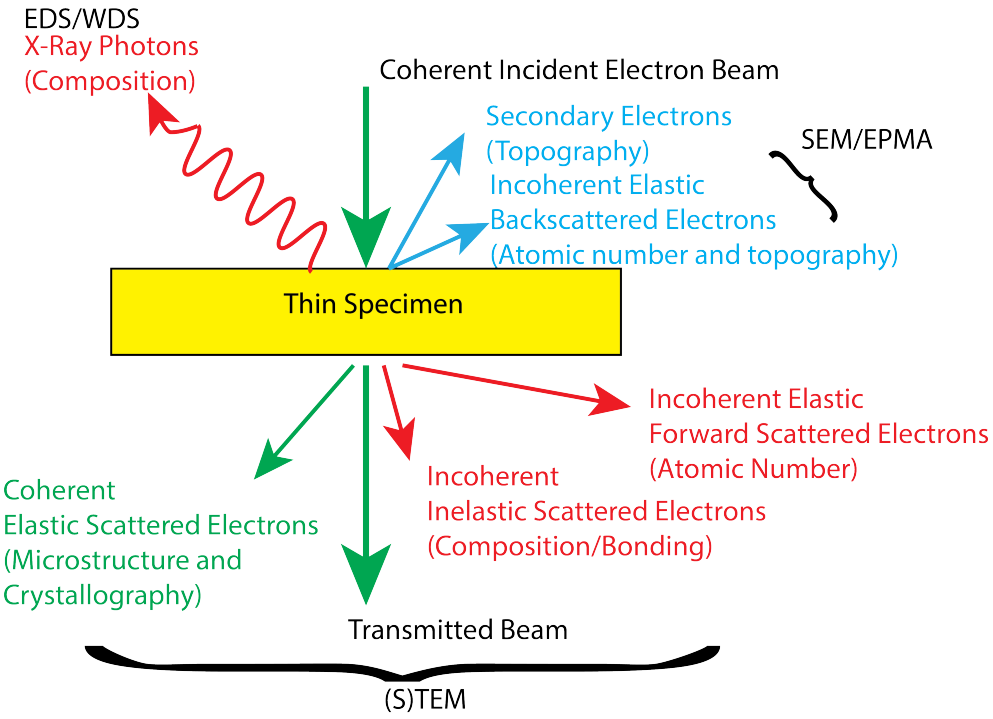

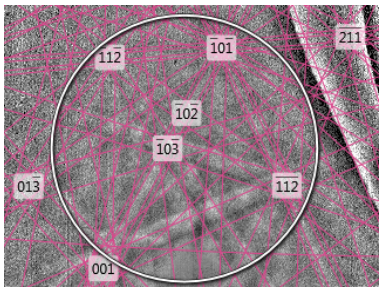

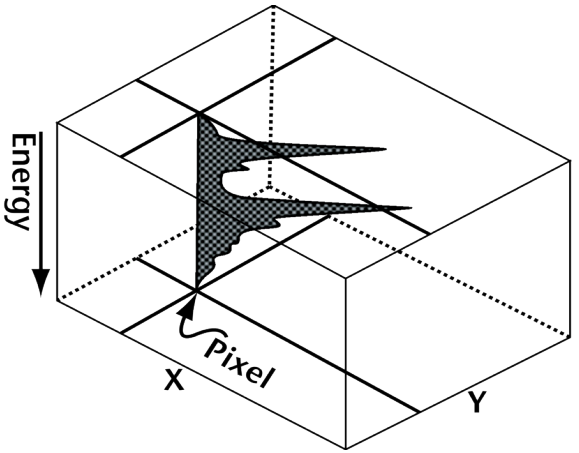

How do we use this information to understand materials synthesis and properties?

Spectrum Image Data is 3-D: Spectrum at every pixel

Sandia National Laboratories

- Generally, 1000s of spectra to analyze
- Need to get physically meaningful information
- Would like a compact representation
- Analogy to RGB images
  - Each RGB color is like an energy channel
  - Perhaps RGB is not the most compact, chemically relevant representation of the data

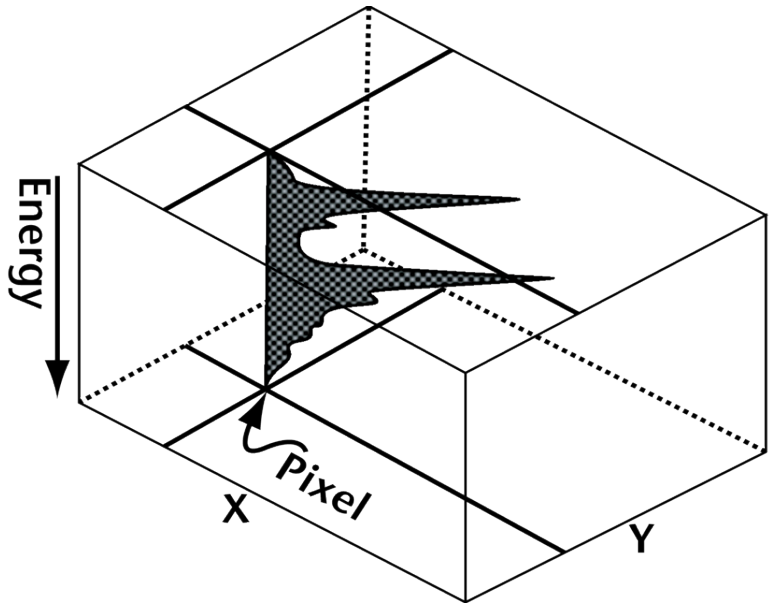

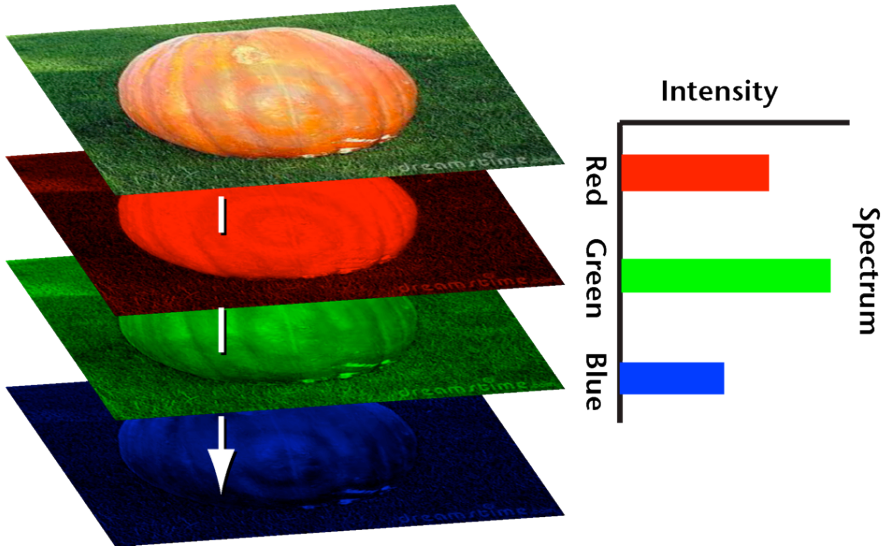

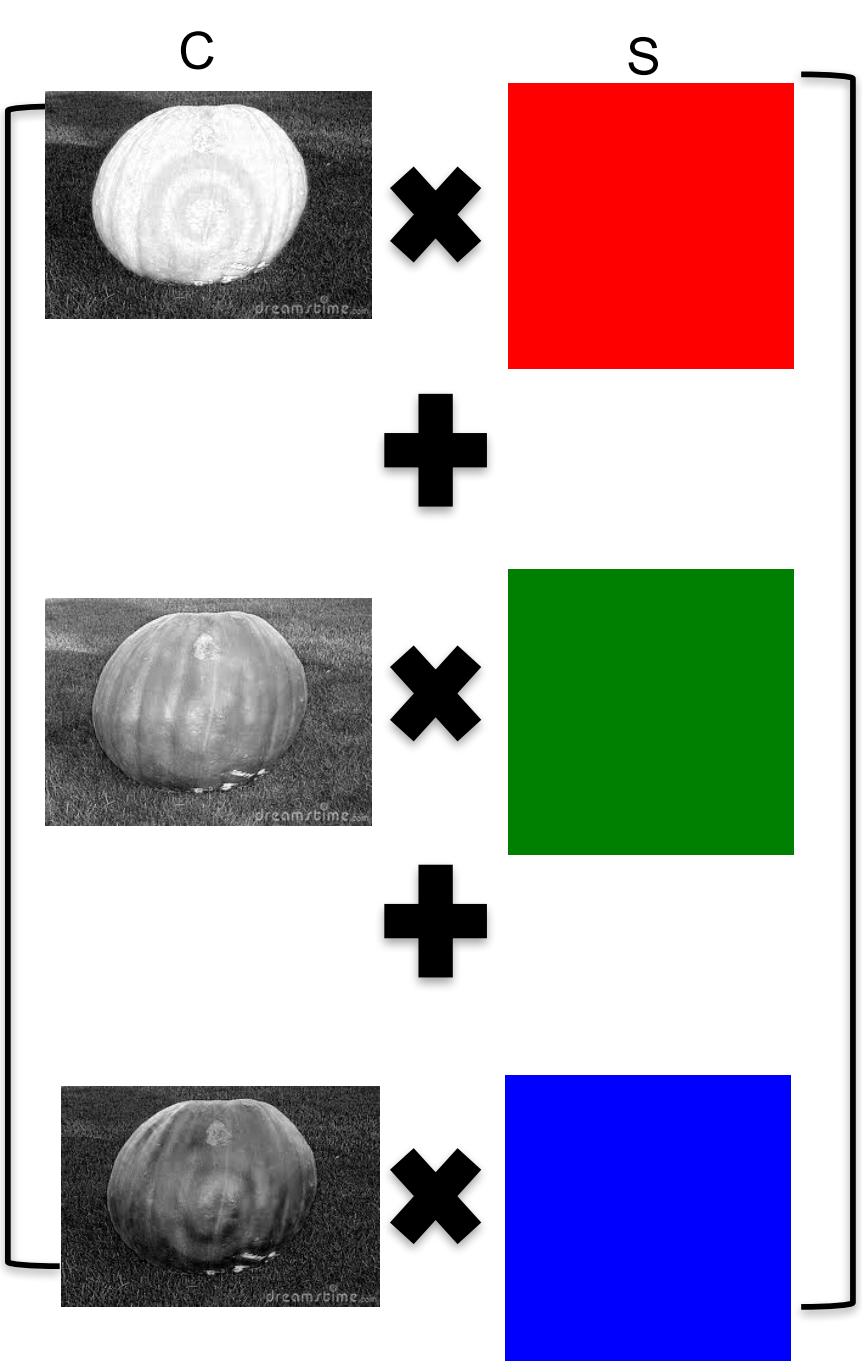

Original Data : RGB Space $D=C*S^T$

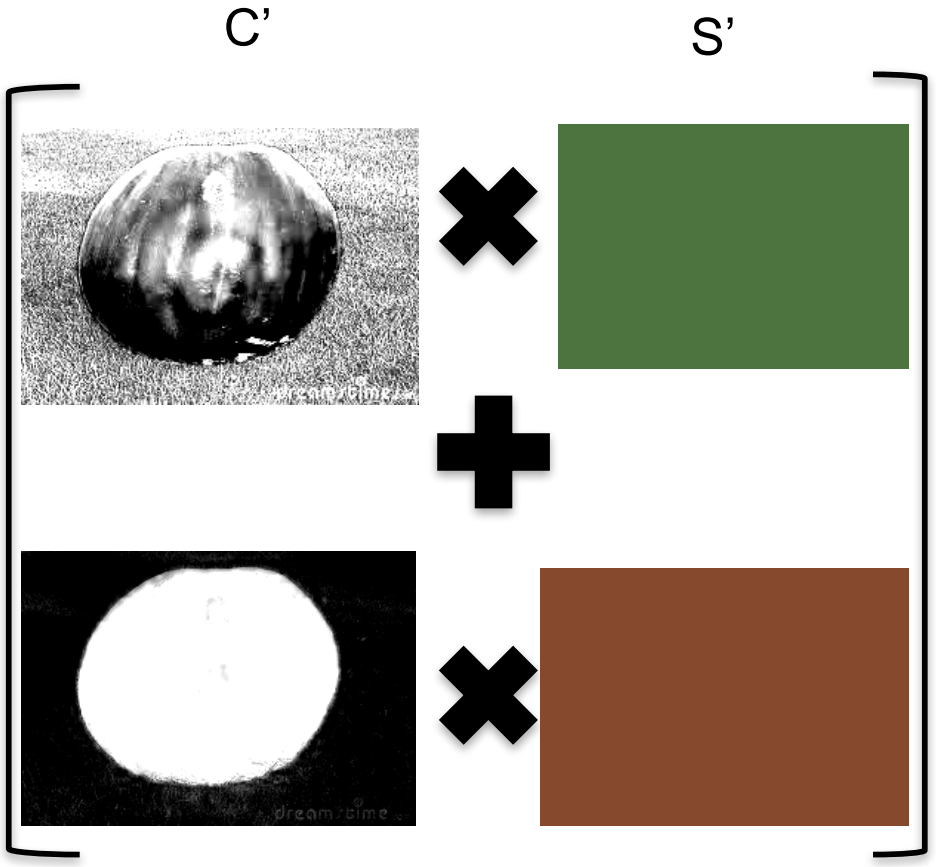

MSA Processed Data: Grass and Pumpkin Space $D'=C'S'^T$

Kotula et al. *Microsc Microanal* **9**[1] (2003) 1-17
Keenan et al. *Surf Int Anal* **36** (2004) 203-212
Keenan. *Surf Int Anal* **41** (2009) 79-87

D≅D’

Sandia National Laboratories

RGB image

Brown-Green image

- Decomposed data into components that are physically meaningful (grass and pumpkin)
- Can apply the same routine to 2048 channels of spectral data (EDS or EELS) to reduce data to a set of physically meaningful factors

Linking Microstructural Measurements to Transport Phenomena

Sandia National Laboratories

- Helium bubbles formed by ^{3}H β decay, α decay, neutron (n, α) reactions
- Rh-ion transport during fabrication of nanoporous hydrogen storage materials
- Li-ion transport during charge/discharge of $LiFePO_4$ electrodes
- Reliability of aged electronic components with variability in manufacturing process

Find Meaningful Factors to Solve $D=C*S^T$

(Data/Color Image) = (Concentration) * (Spectral Component)

Sandia National Laboratories

- Assume data follow a linear additive model
- Multivariate Statistical Analysis (MSA) routines to solve the matrix decomposition problem $D=C*S^T$ based on
  - Principal Component Analysis (PCA)
  - Multivariate Curve Resolution (MCR)
  - Singular Value Decomposition (SVD)
- Scale the data to account for Poisson noise
  - Throw away noise components
- Factor rotation for orthogonal C or S (Varimax)
  - 2-D histogram of data shows that S_1-S_2 space is not simple
  - Rotated axes S_1'-S_2' more simply represent the data

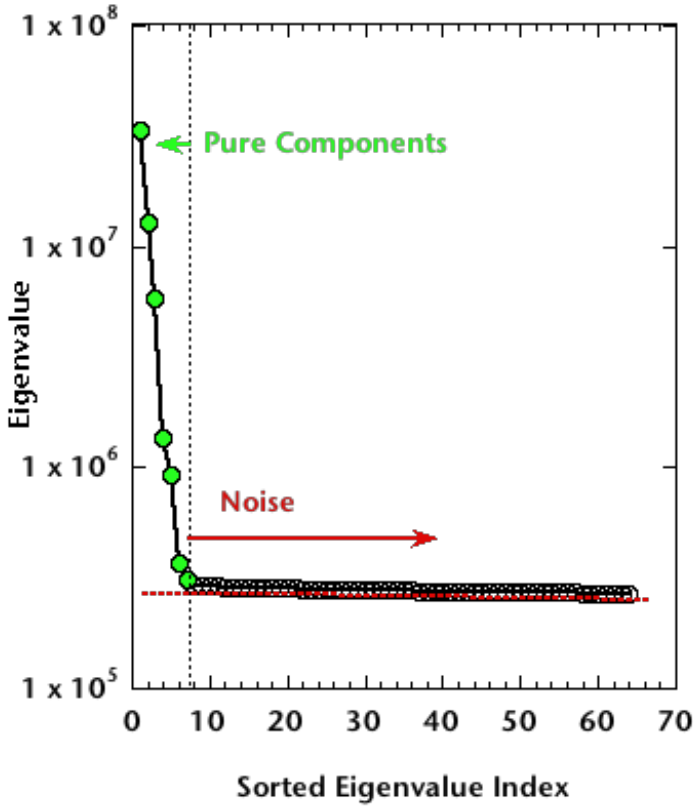

- Implemented using AXSIA (Sandia Software)
  - Kotula et al. *Microsc Microanal* **9**[1] (2003) 1-17
  - Keenan et al. *Surf Int Anal* **36** (2004) 203-212
  - Keenan. *Surf Int Anal* **41** (2009) 79-87

Find Meaningful Factors to Solve $D=C*S^T$

(Data/Color Image) = (Concentration) * (Spectral Component)

Sandia National Laboratories

- Assume data follow a linear additive model
- Multivariate Statistical Analysis (MSA) routines to solve the matrix decomposition problem $D=C*S^T$ based on
  - Principal Component Analysis (PCA)
  - Multivariate Curve Resolution (MCR)
  - Singular Value Decomposition (SVD)
- Scale the data to account for Poisson noise
  - Throw away noise components
- Factor rotation for orthogonal C or S (Varimax)
  - 2-D histogram of data shows that S_1-S_2 space is not simple
  - Rotated axes S_1'-S_2' more simply represent the data

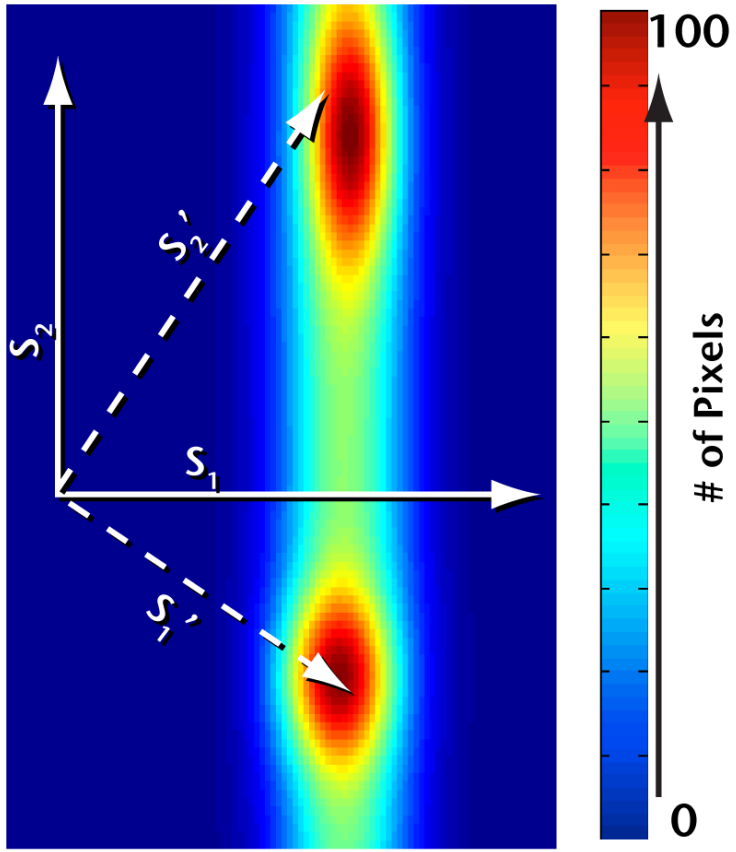

- Implemented using AXSIA (Sandia Software)
  - Kotula et al. *Microsc Microanal* **9**[1] (2003) 1-17
  - Keenan et al. *Surf Int Anal* **36** (2004) 203-212
  - Keenan. *Surf Int Anal* **41** (2009) 79-87

Under and Overfocus

Sandia National Laboratories

Fresnel fringe of bubbles is bright when underfocused (left) and dark when overfocused (right), confirming presence of void spaces, and not other types of crystal defects

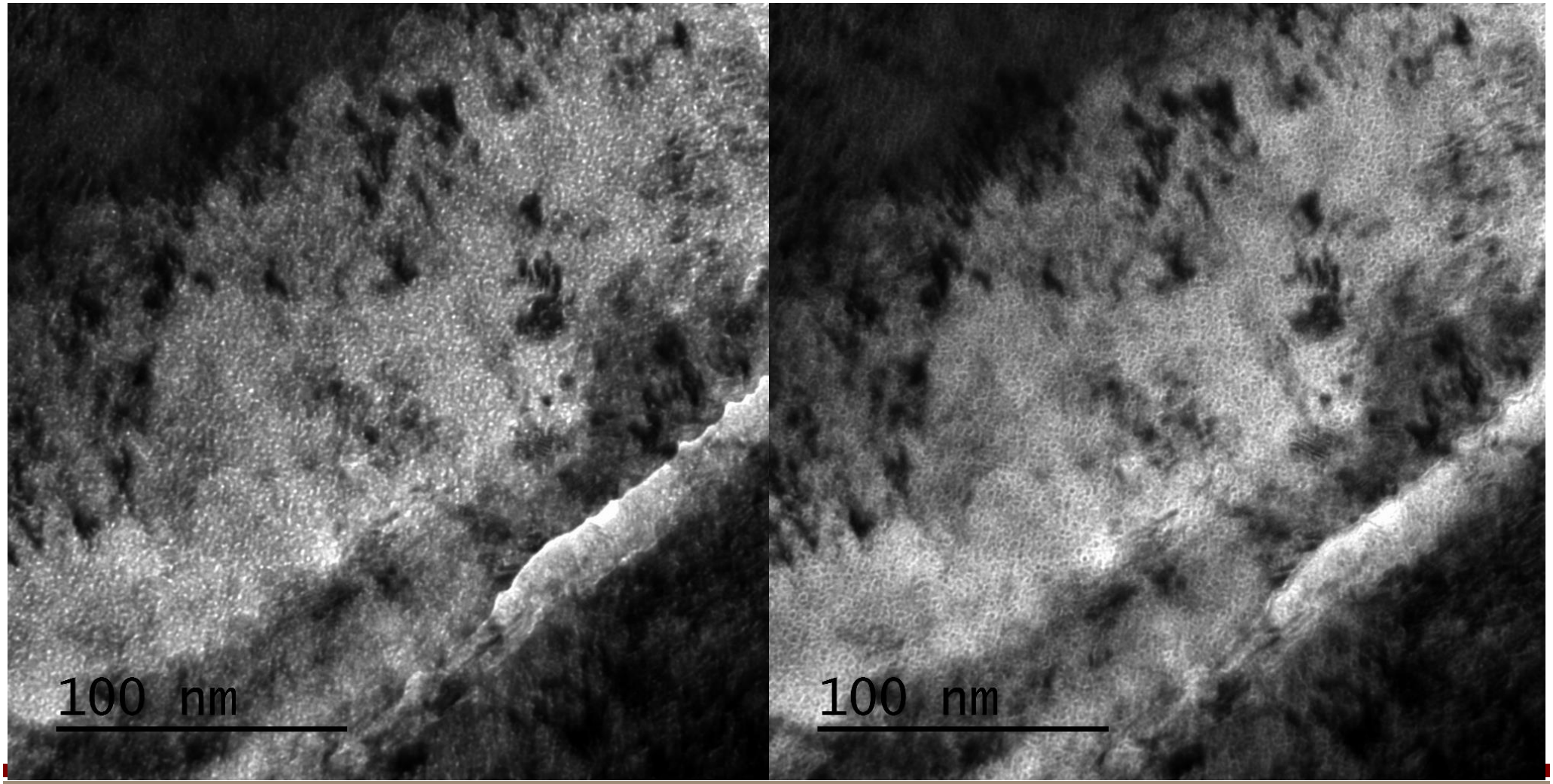

^{3}He causes bubbles in metal tritides

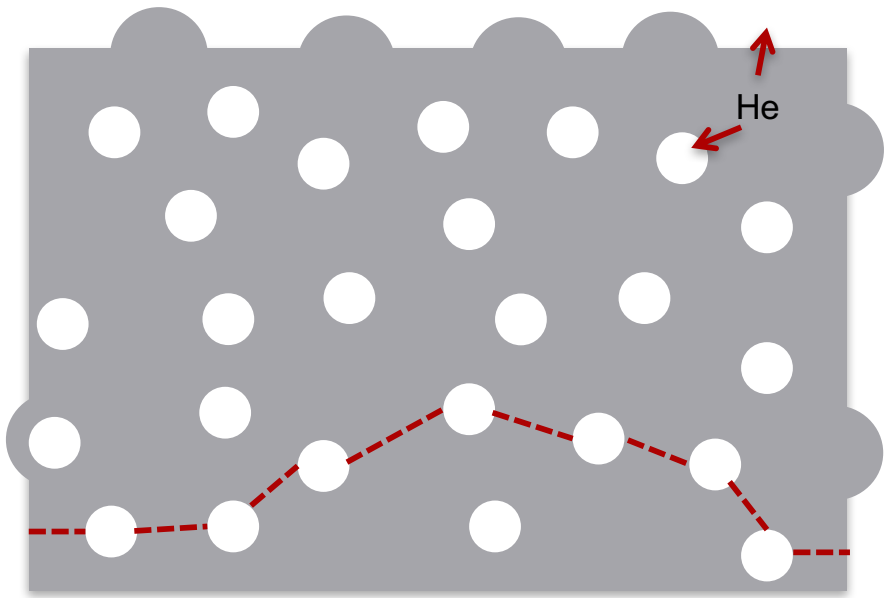

- ^{3}H decays to insoluble ^{3}He.
- ^{3}He clusters push metal atoms, forming bubbles.
- Bubbles create fracture paths, swelling/deformation.
- ^{3}He may escape at surfaces (and fracture surfaces), through grain boundary paths.
- Properties are believed to depend on size and spacing distribution of bubbles

Early nucleation process is conventionally thought to define distributions, property evolution

D.F. Cowgill, Fusion Sci. Tech. 28 539 (2005)
J.H. Evans, J. Nuc. Mater. 68 129 (1977)
F. Montheillet et al., Mat. Sci. Eng. A 494 407 (2008)

Helium Bubbles in Metals

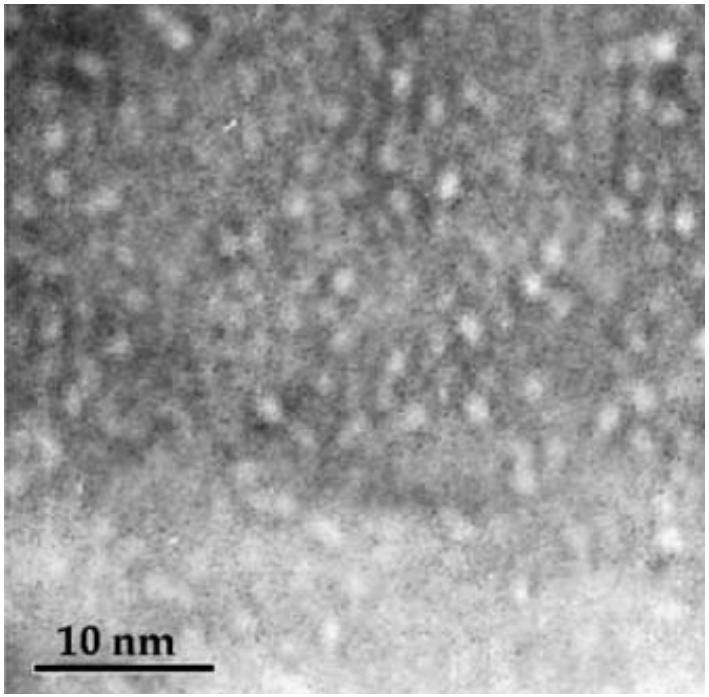

A. Fabre et al., 8-month Pd tritide
J. Nuc. Mater. 342 101 (2005)

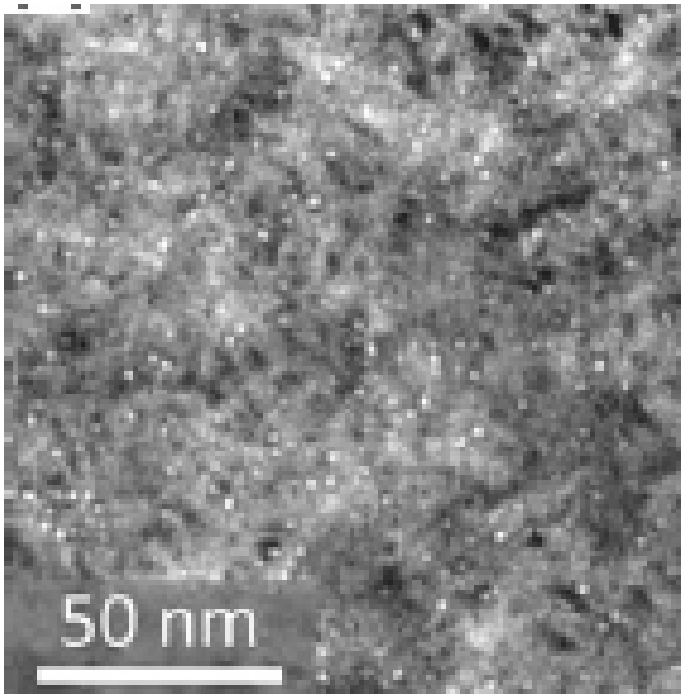

J. R. Jeffries et al., Pu-Ga alloy
J. Nuc. Mater. 410 84 (2011)

- Bubbles are a few nm diameter, tens of nm apart.

2D TEM Images

- No information on bubble spacing in z direction.
- Large bubbles may obscure small bubbles, skewing distribution.
- Smallest bubbles may be difficult to observe.

Capture Volume Theory

Sandia National Laboratories

- If all bubbles nucleate at a same early time and their growth is diffusion limited, then they should contain the He generated in a capture region geometrically nearest each bubble.

- Capture volume is described by Voronoi tessellation.

2D Voronoi tessellation

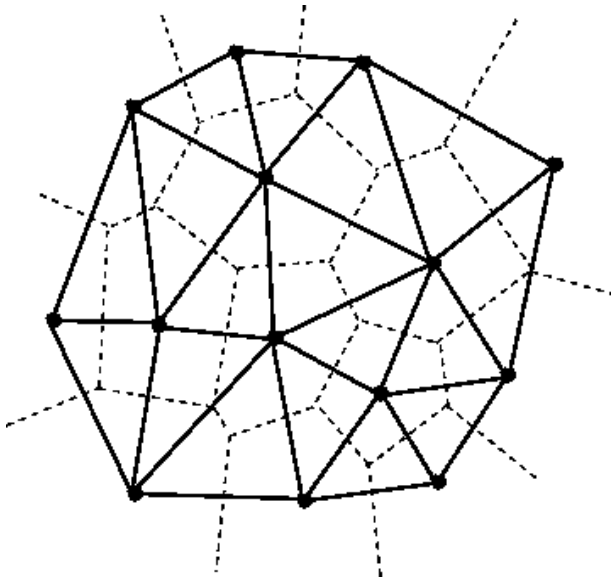

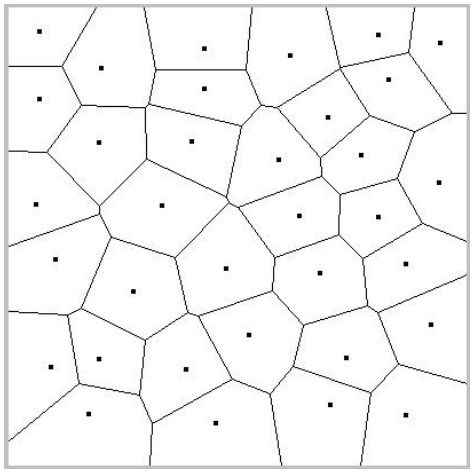

small capture area $\Rightarrow$ small bubble?

What if bubble locations are random?

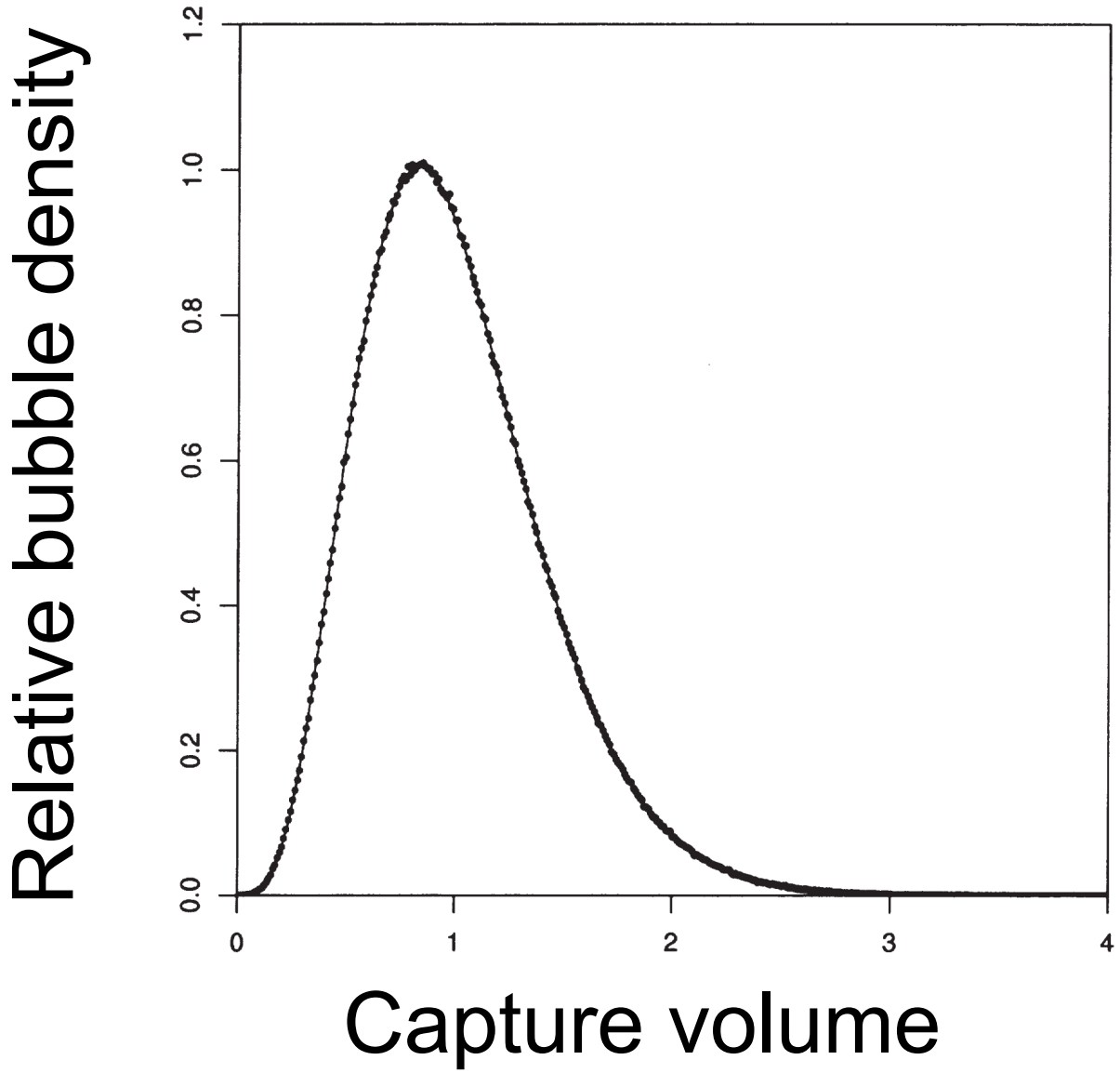

Capture volume of randomly nucleated bubbles satisfies log normal distribution.

From M. Tanemura, Forma 18, 221-247 (2003)

Questions and Solutions

- Can the early nucleation, diffusion limited growth, and capture volume theory be validated?
- We aim to generate three dimensional images of bubble configurations and use them to answer this question directly from experiments.

Answering this question allows us to develop improved models of helium bubble nucleation and growth, and better predict swelling, fracture, and ^{3}He release.

Electron Tomography

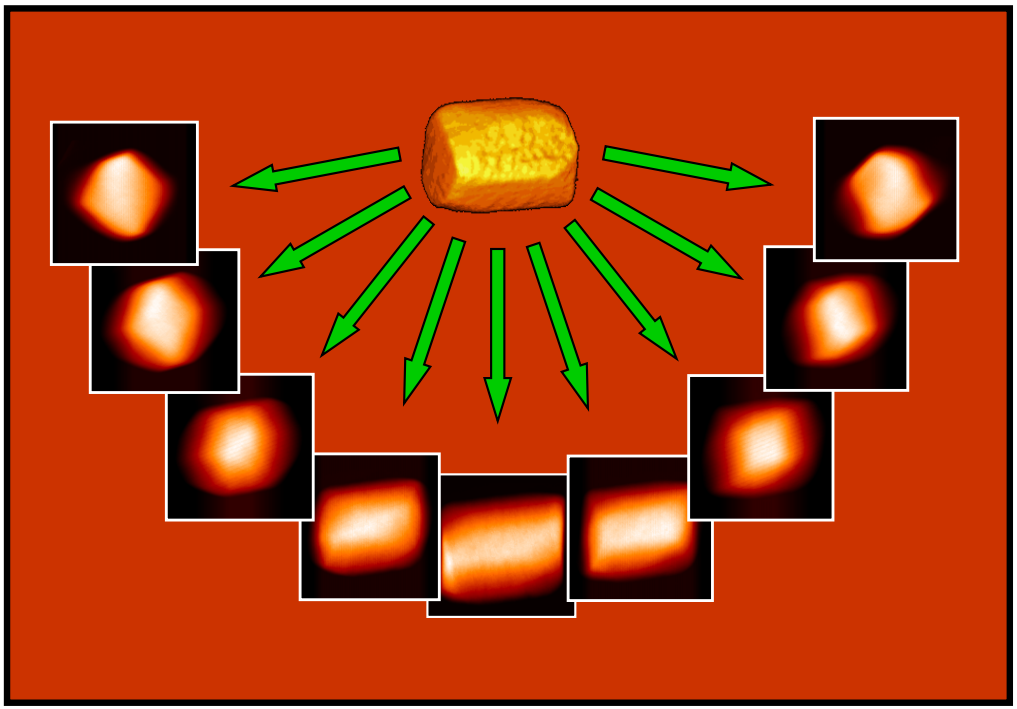

Sample images are recorded in a transmission electron microscope at many angles.

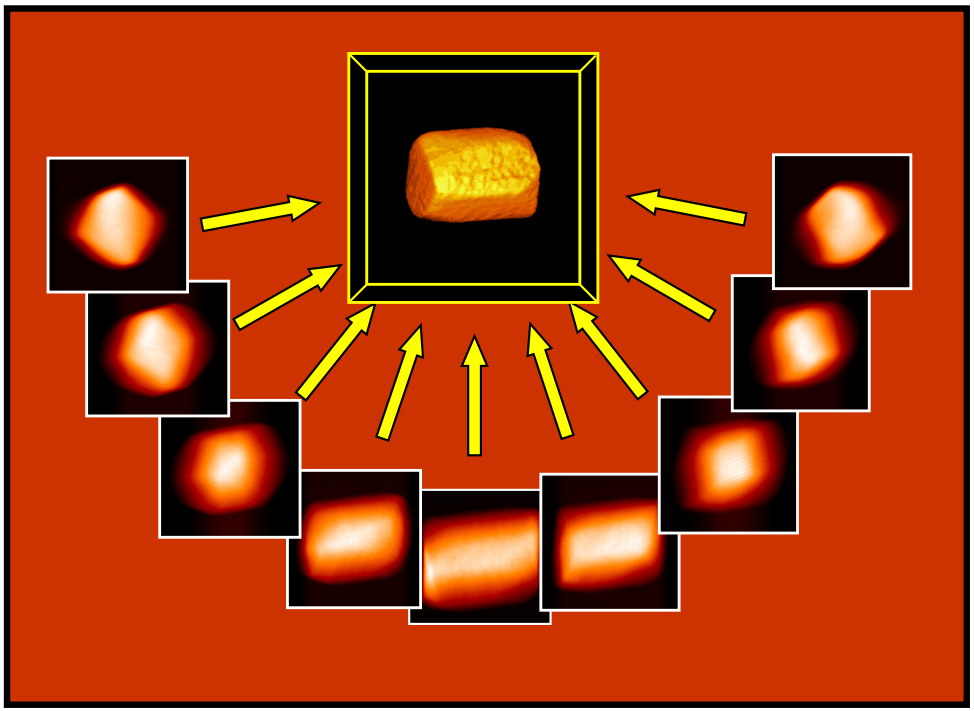

Image data are used to reconstruct a 3D representation of the sample.

Figure prepared by Ilke Arslan

FIB-SEM sample for tomography

Sandia National Laboratories

Tip geometry allows imaging at many angles

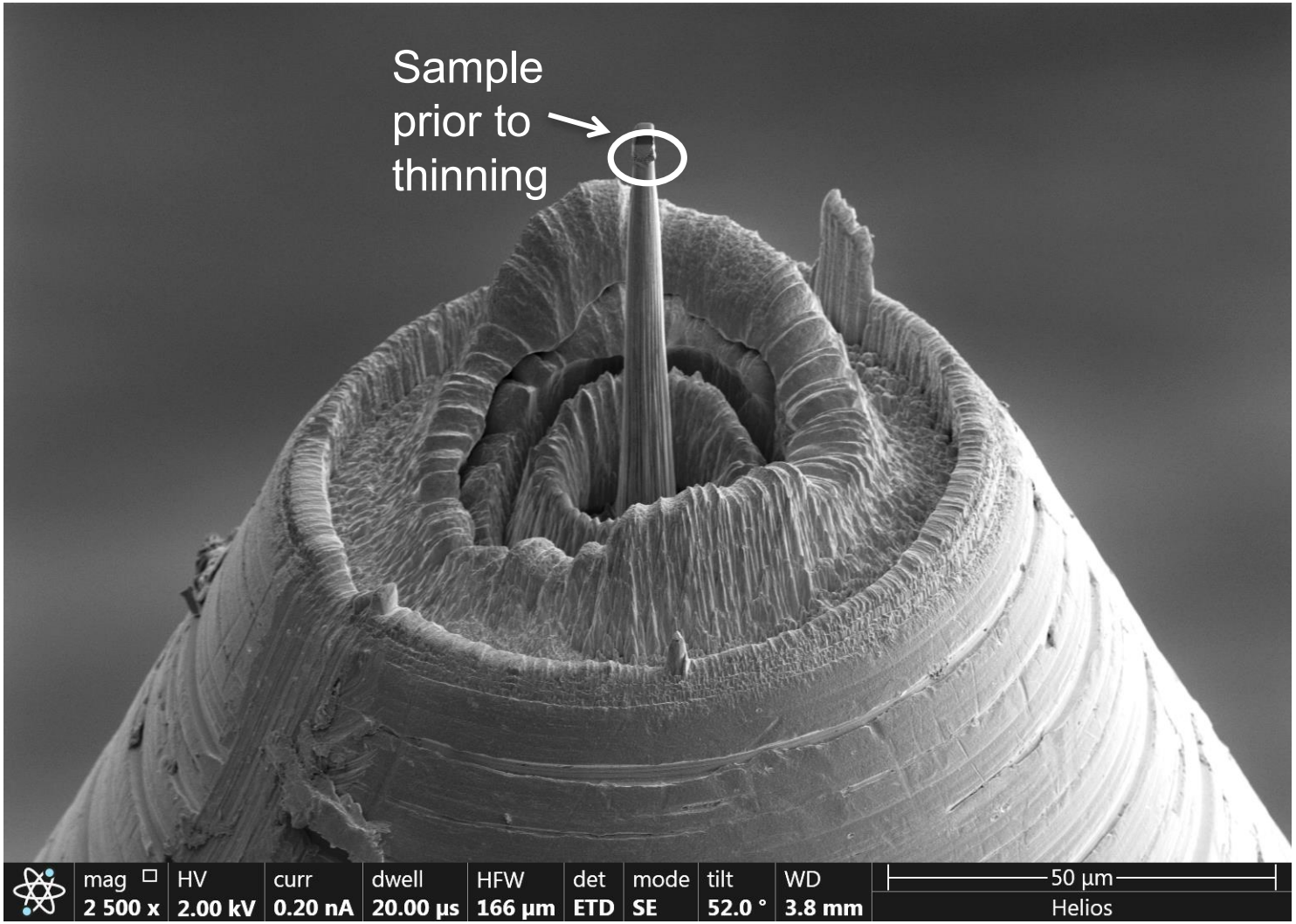

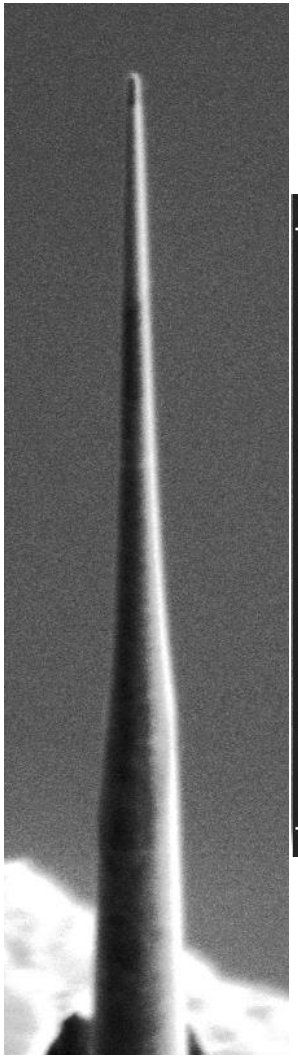

Nearly finished sample

Dark field (HAADF) TEM Images

- Tritided for 3.8 years (from a SRNL Pd-5 at.% Ni ribbon).
- Single crystal (estimated He/Pd = 0.12).
- Bubbles are dark, ~2 nm diameters.
- Images taken from -70^{o} to 70^{o} (increment 1^{o}).

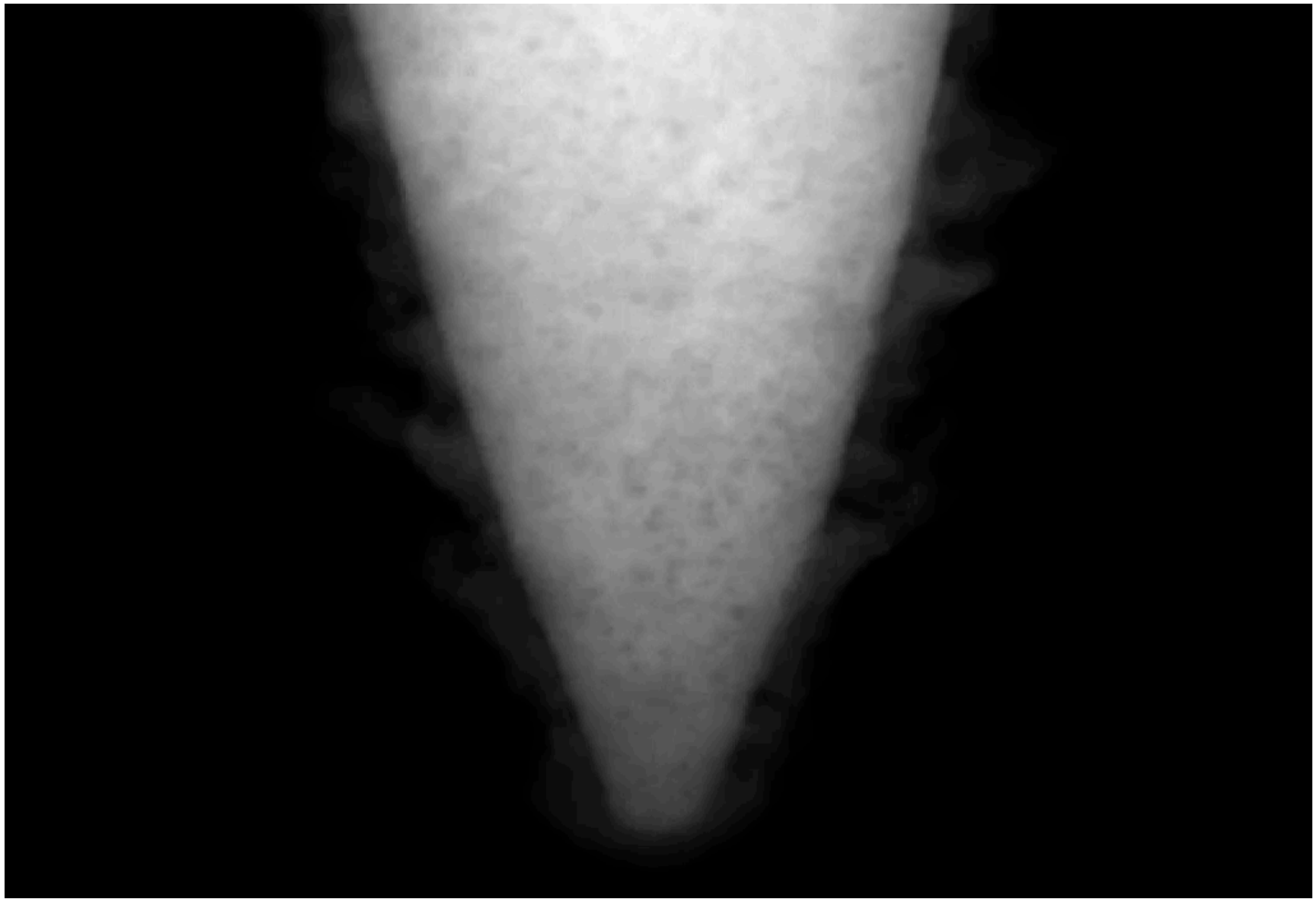

Reconstruction of the 3D Bubbles

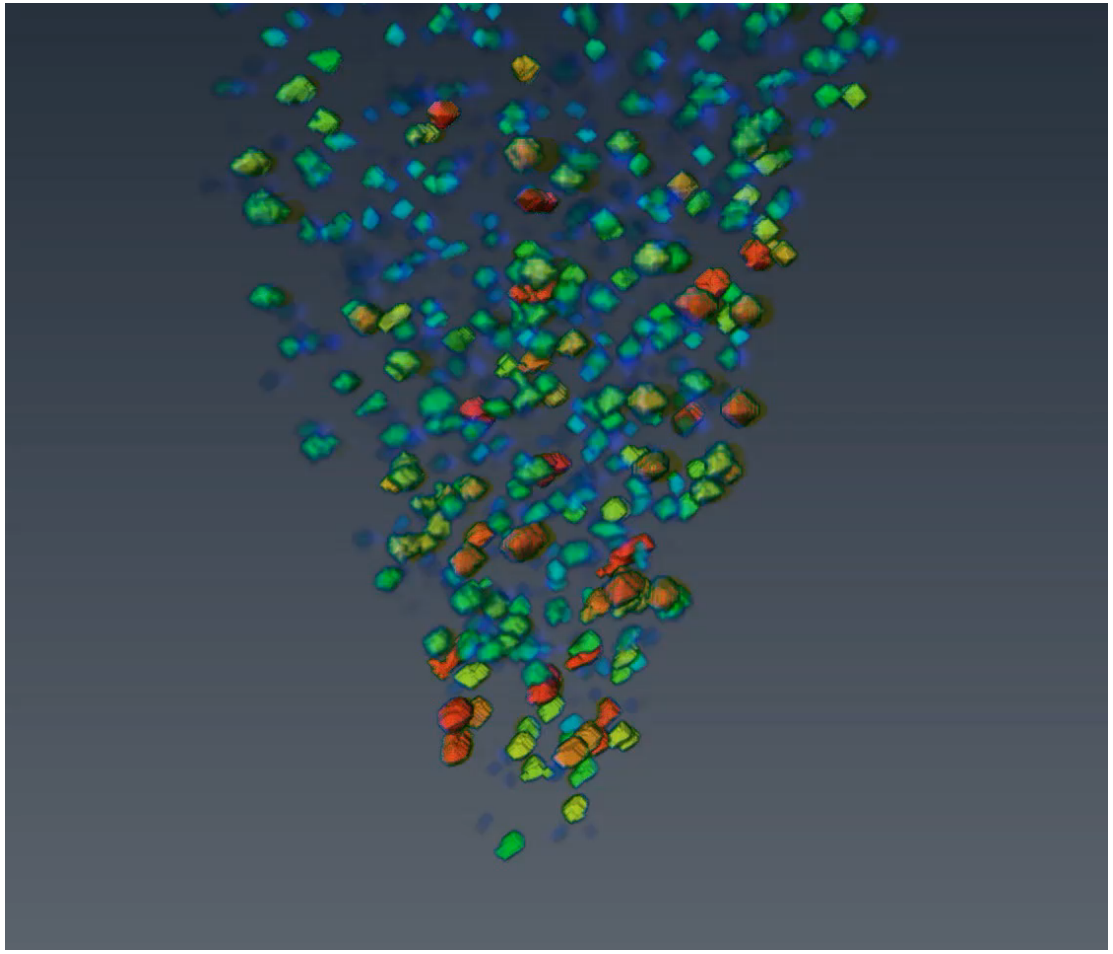

- 3D bubbles are iteratively matched to 2D experimental images using the "*Simultaneous Iterative Reconstruction Technique.*"
- ~1000 bubbles with average diameter 2 nm
- Bubbles can be elongated due to reconstruction artifacts
- Red bubbles are large, blue bubbles are small.

Reconstruction of capture volumes

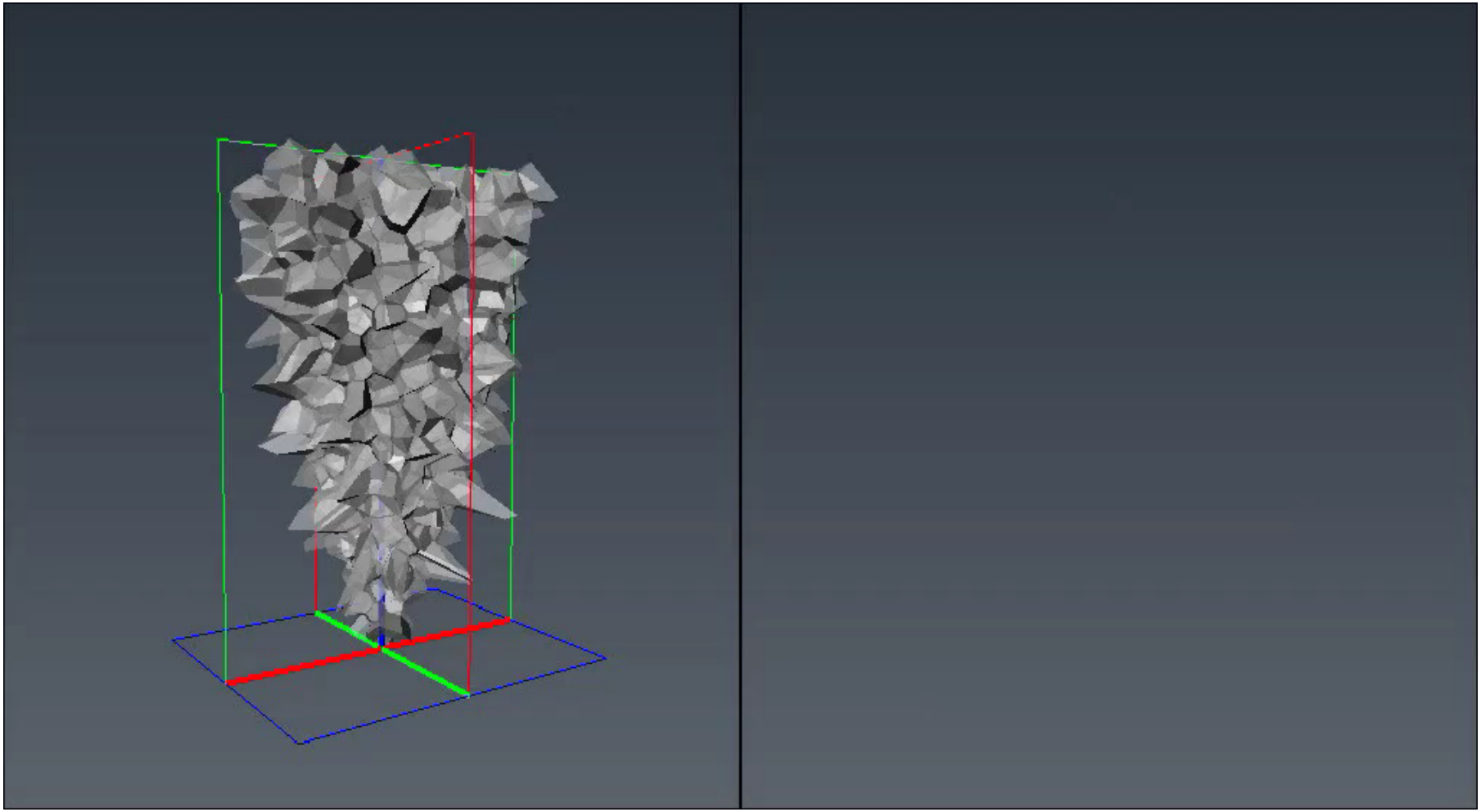

- Determined by 3D Voronoi tessellation of bubbles
- Outer layer of surface-crossing volumes is omitted from further analysis

Histograms of particle size and capture volume

Sandia National Laboratories

Capture Volume Distribution

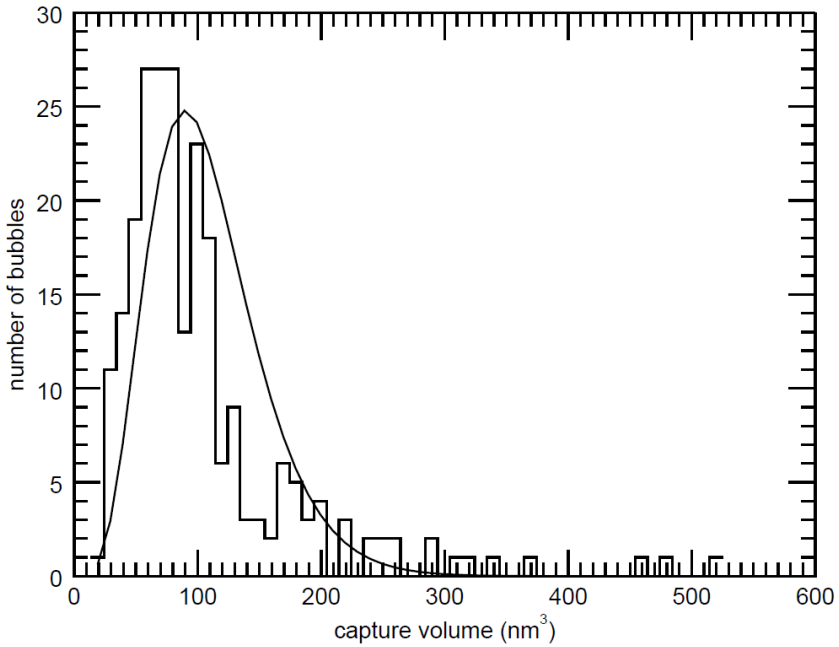

Bubble Volume Distribution

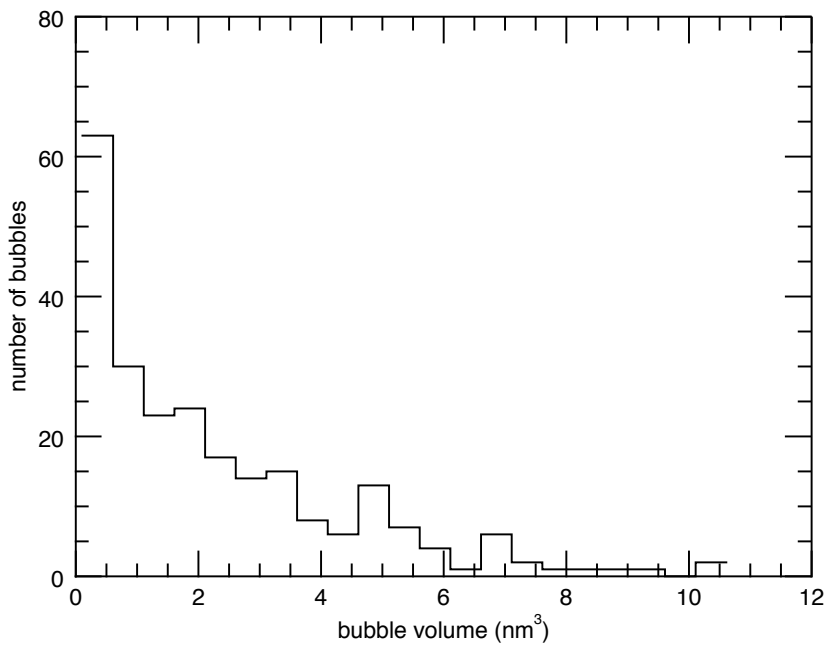

- Capture volume distribution is consistent with log normal distribution, but bubble volume distribution is not
- Large number of small bubbles $\Rightarrow$ Late nucleation?

Bubble and Capture Volume Correlation

Sandia National Laboratories

Individual Capture Volume

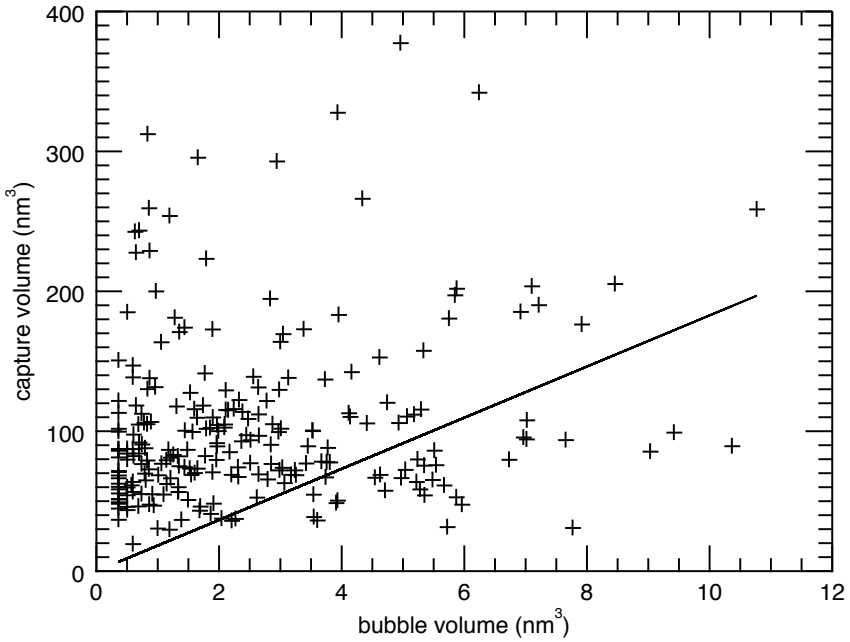

Solid line: expected for 3.8 year of tritium decay (He/Pd = 1.2) if bubbles have 5GPa pressure based on the loop punching growth

No bubble and capture volume correlation is found!

What If Small Bubbles Are Excluded?

Perhaps small bubbles nucleated late or reconstruction algorithm was inaccurate for small bubbles ⇒ excluding from the analysis all bubbles smaller than 3 nm^3

Individual Capture Volume

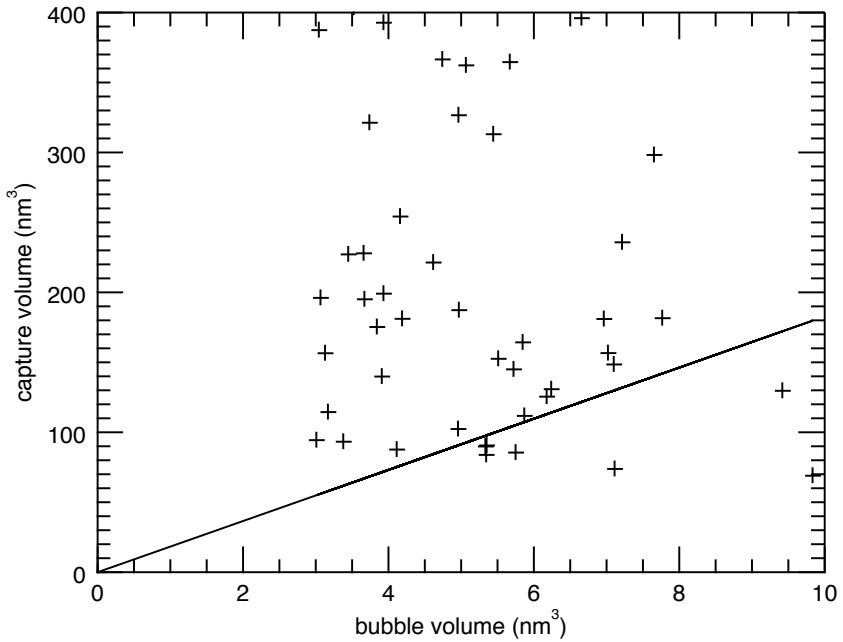

Still no correlation!

Tentative Conclusions

- Bubble size and spacing are uncorrelated
- Model assuming early nucleation, diffusion limited growth of He bubbles does not explain all observations
- Are bubbles mobile?
- Lack of environmental dependence of growth rate suggests that there exists a barrier to bubble growth
- He atoms can escape capture volume

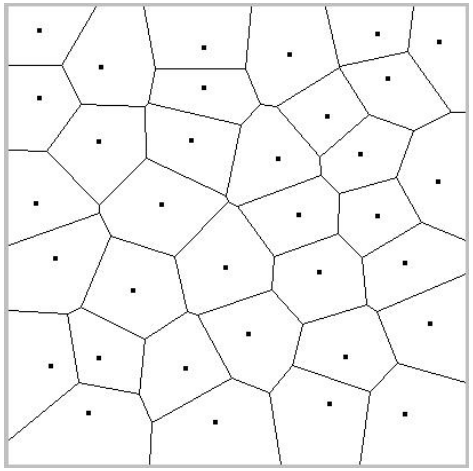

Linking Microstructural Measurements to Transport Phenomena

Sandia National Laboratories

- Helium bubbles formed by ^{3}H β decay, α decay, neutron (n, α) reactions
- Rh-ion transport during fabrication of nanoporous hydrogen storage materials
- Li-ion transport during charge/discharge of $LiFePO_4$ electrodes
- Reliability of aged electronic components with variability in manufacturing process

Pd Materials With Large Surface Area

- Nanoporous materials have high surface areas
  - High surface area can improve surface-limited reaction rates
  - Provides an escape path for helium decay product
    - He bubbles can cause stiffening of bulk Pd

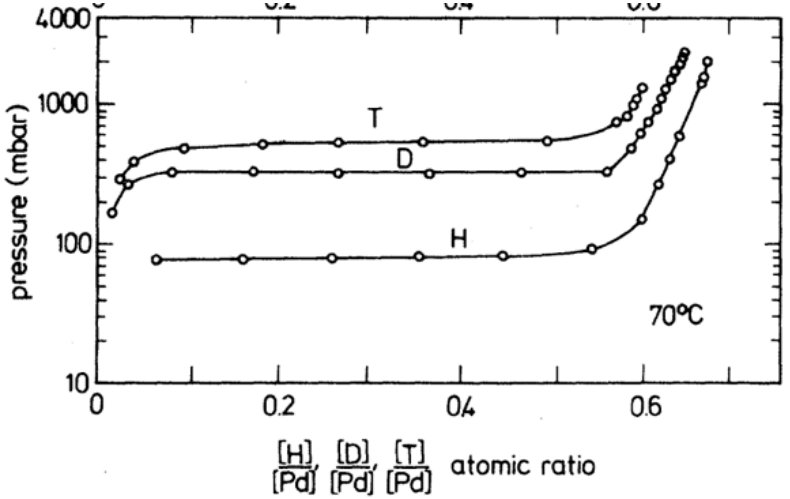

Lässer, *PRB*, **26(6)**, 1982

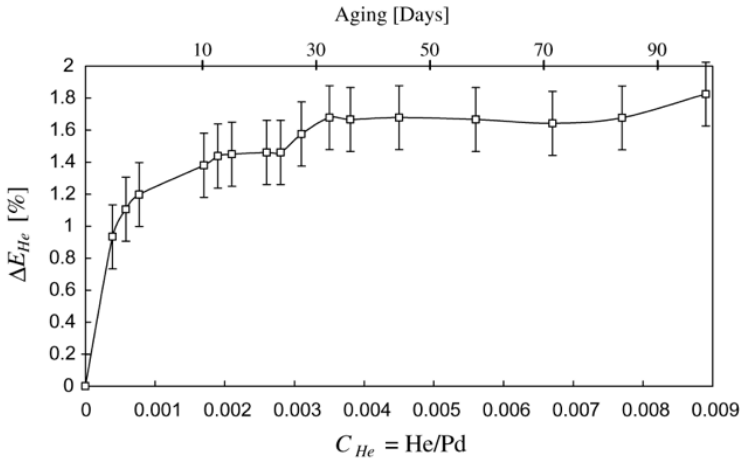

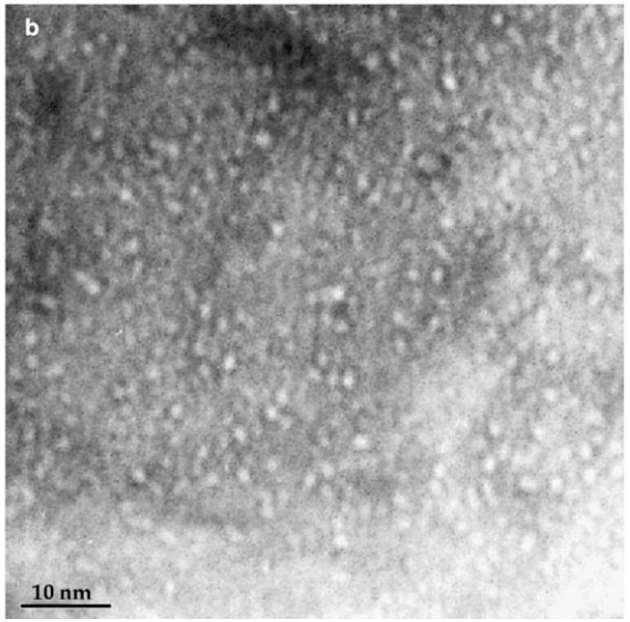

Fabre et al., *J Nuc Mat*, **342**, 2005

Pd Materials With Large Surface Area

- Nanoporous materials have high surface areas
  - High surface area can improve surface-limited reaction rates
  - Provides an escape path for helium decay product
    - He bubbles can cause stiffening of bulk Pd
- Goals
  - Uniform pore structure homogeneously distributed in material
  - Stable pore structure over wide T range

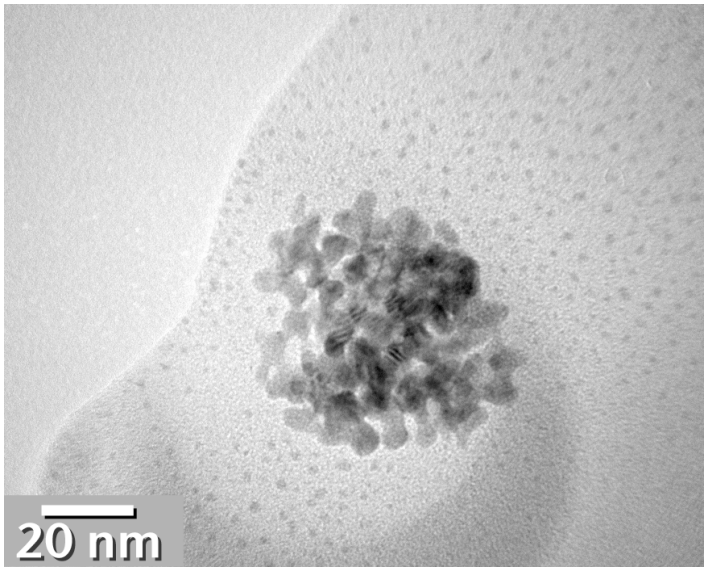

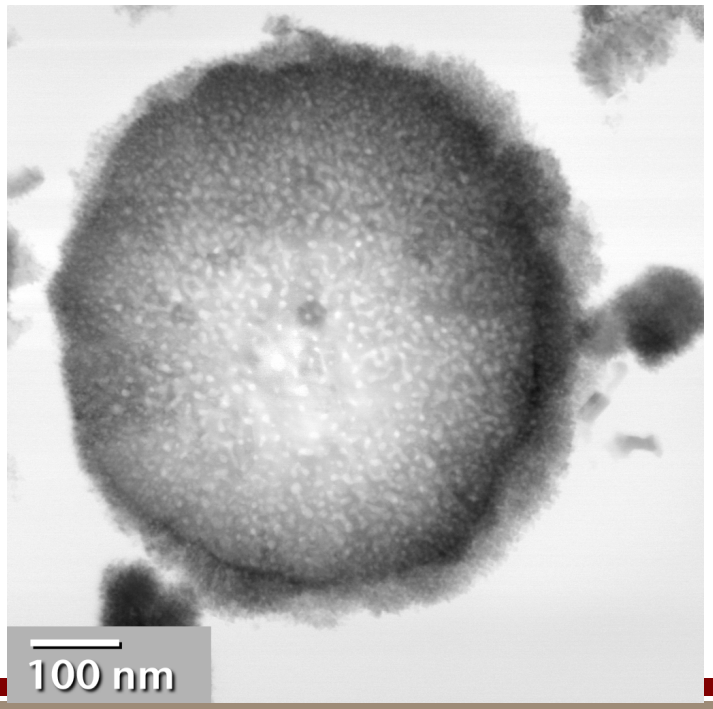

Nanoporous Pd/Rh alloys for H Storage

- Nanoporous Pd shows reduced capacity
- Nanoporous Pd has poor elevated temperature stability

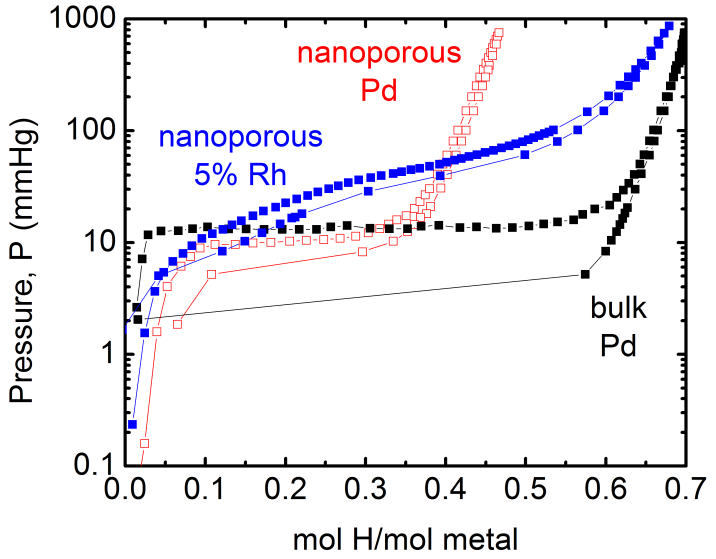

200 ° C
12 min

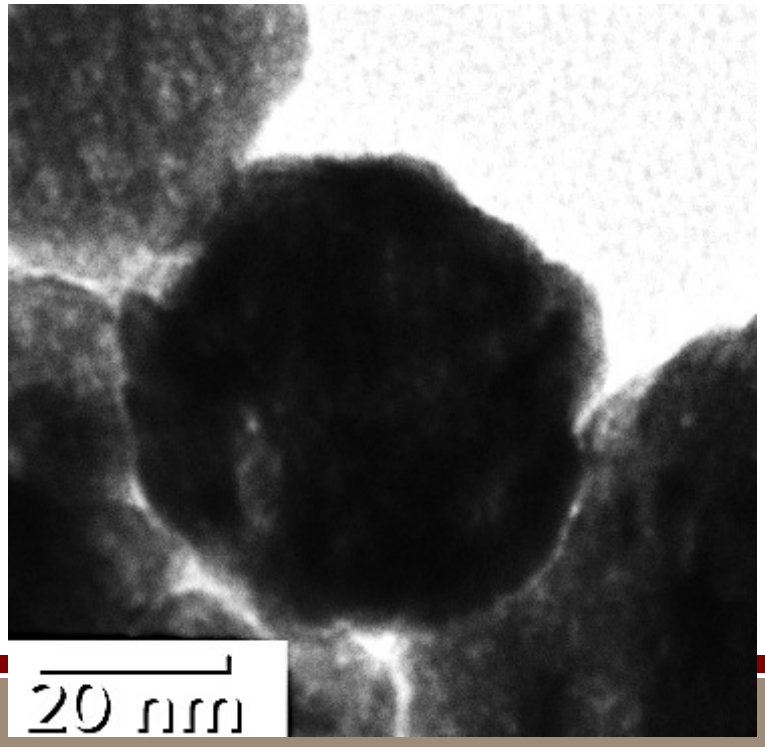

Nanoporous Pd/Rh alloys for H Storage

- Addition of Rh improves temperature stability
  - 10 at. % Rh-Pd has more stable pores
    - Stable up to 300° C
- Where is the Rh and is it uniform?
  - Pd/Rh overlap
  - Compositional variation at small length scales
  - Low count rates
  - How do we prepare different forms?
    - nm to micron particles

200 ° C
12 min
Pure Pd

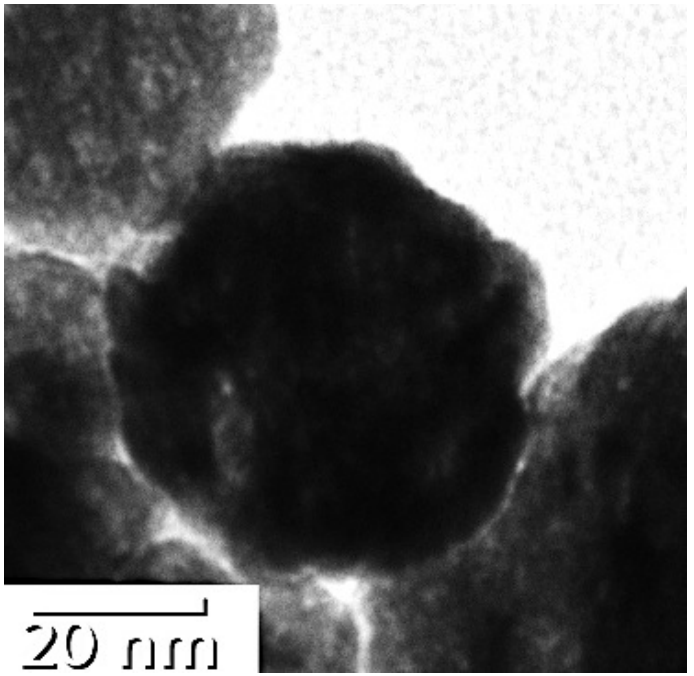

200 ° C
30 min
10 at.% Rh-Pd

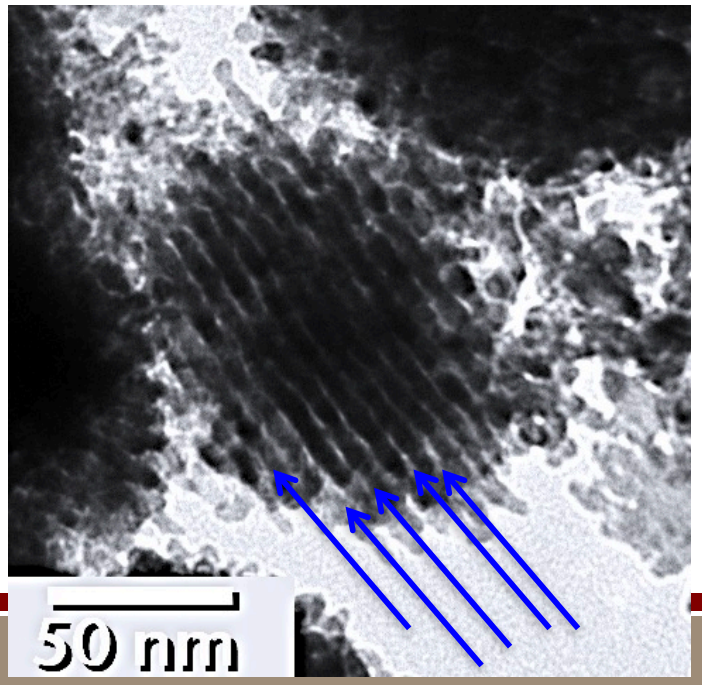

STEM-EDS Quantification

- EDS spectrum imaging
  - Spectrum at every pixel
  - Overlap of PdL and RhL

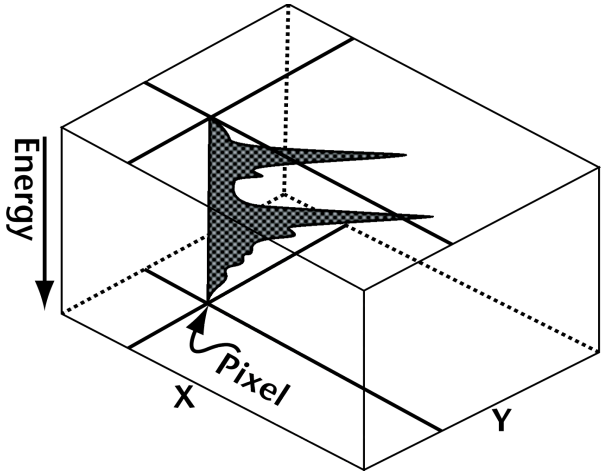

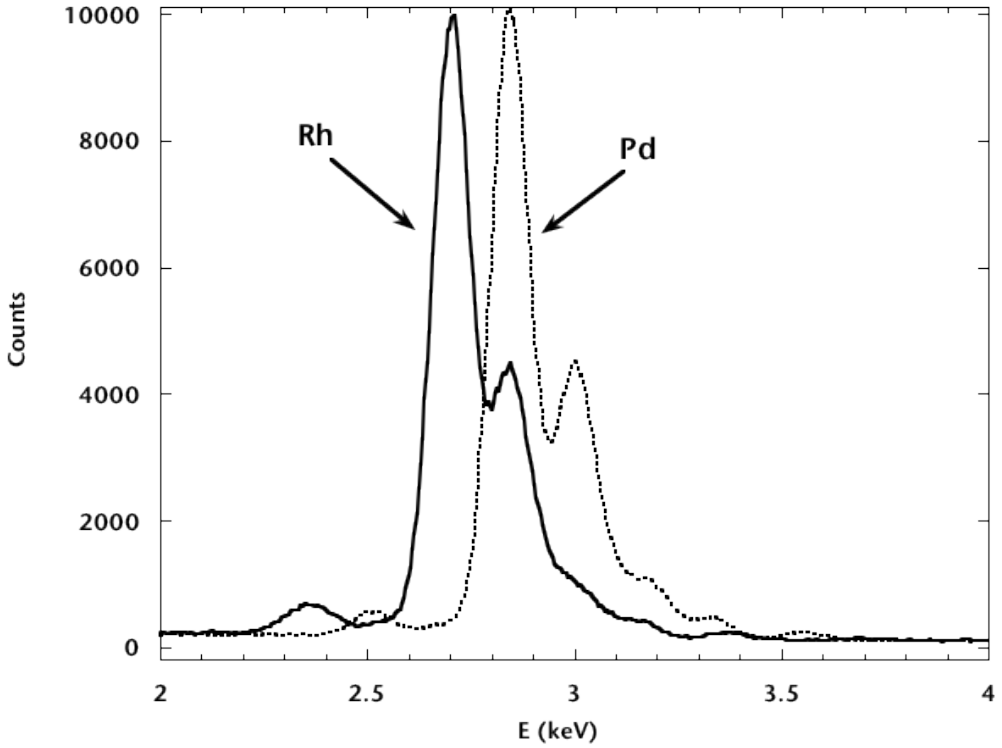

STEM-EDS Quantification

- EDS spectrum imaging
  - Spectrum at every pixel
  - Overlap of PdL and RhL
- Multivariate Statistical Analysis: AXSIA
  - Decomposition of data matrix
    - $D=C*S^T$
      - C is a matrix of spectral weight at each pixel
      - S are “pure” component spectra
    - Weighted for Poisson Statistics
    - Rotated for spectral simplicity
      - Kotula PG, et al. Microsc Miroanal 2003;9:1.
      - Keenan MR. Surf Interface Anal 2009;41:79.
  - Reconstruct the denoised data matrix D
  - Quickly identify Rh uniformity

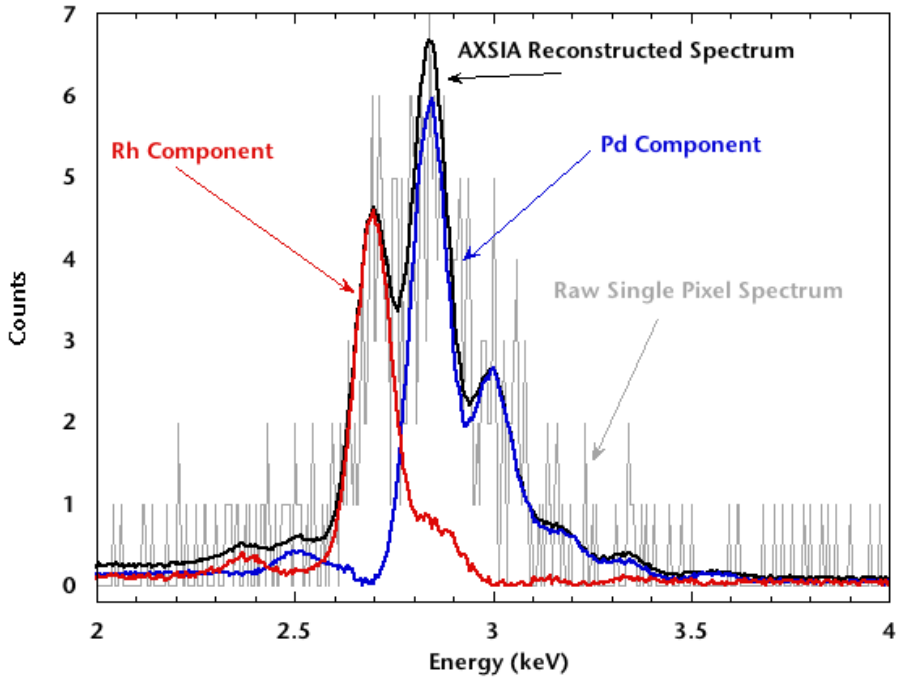

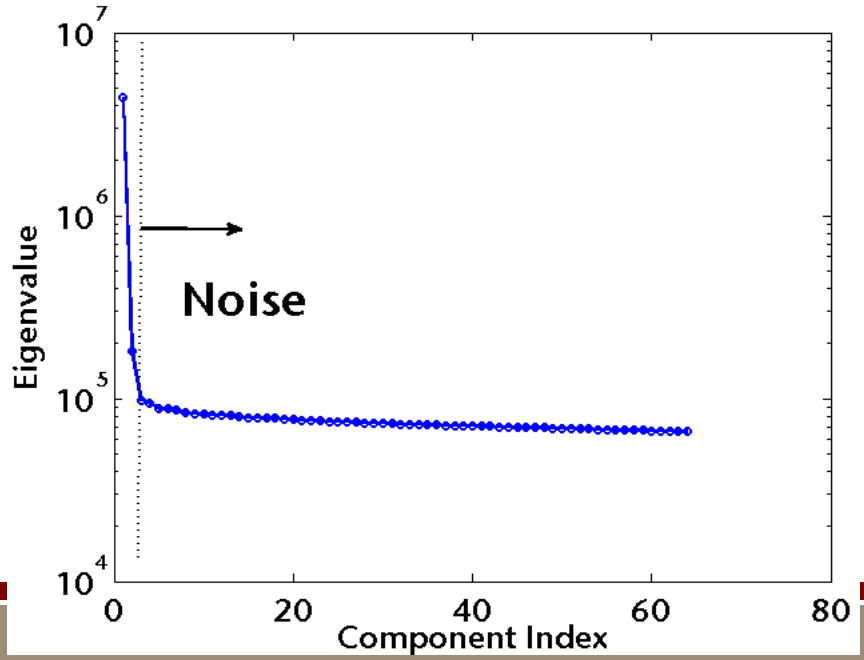

STEM-EDS Quantification

- EDS spectrum imaging
  - Spectrum at every pixel
  - Overlap of PdL and RhL
- Multivariate Statistical Analysis
  - Decomposition of data matrix
    - $D=C*S^T$
      - C is a matrix of spectral weight at each pixel
      - S are "pure" component spectra
    - Weighted for Poisson Statistics
    - Rotated for spectral simplicity
      - Kotula PG, et al. Microsc Miroanal 2003;9:1.
      - Keenan MR. Surf Interface Anal 2009;41:79.
  - Reconstruct the denoised data matrix D
  - Quickly identify Rh uniformity
- Multiple Least Squares Fit-MLSQ
- Cliff-Lorimer Ratio
  - Cliff G, Lorimer GW. *J Microsc-Oxford* 1975;103:203.
  - From pure references and calibrated known standard (8 at.% Rh-Pd foil)

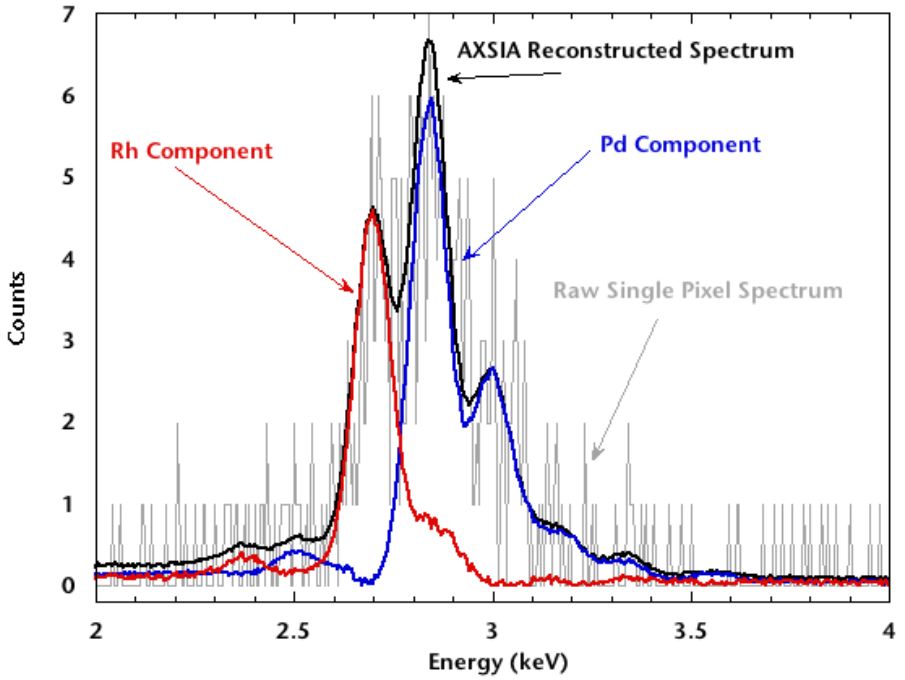

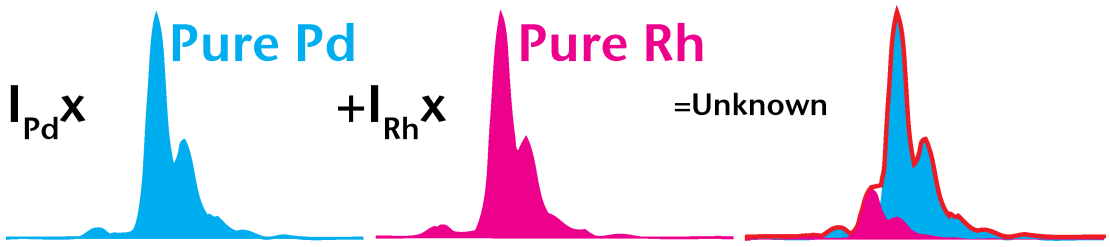

$$\frac{C_{Pd}}{C_{Rh}} = k_{Pd-Rh}\frac{I_{Pd}}{I_{Rh}}$$

$$C_{Pd} + C_{Rh} = 1$$

$$k_{\text{JEOL2010F}-200\,kV} = 0.99$$

$$k_{\text{Titan-200kV}} = 0.96$$

$$k_{\text{Titan-80kV}} = 1.11$$

EDS Quant: Background Subtraction

- EDS Background Empirical Formula

Lifshin, E. (1974). In *Proc. 9th Ann. Conf. Microbeam Analysis Soc.*, Ottawa, Canada, p. 53.

$$N(E) = f_E P_E \bar{Z}\left[a\left(\frac{E_0 - E}{E}\right) + b\frac{(E_0 - E)^2}{E}\right]$$

f_E = absorption

P_E = detector efficiency

$\bar{Z}$ = average atomic number

  - Computationally not straight forward
  - Difficult for 1000s of spectra

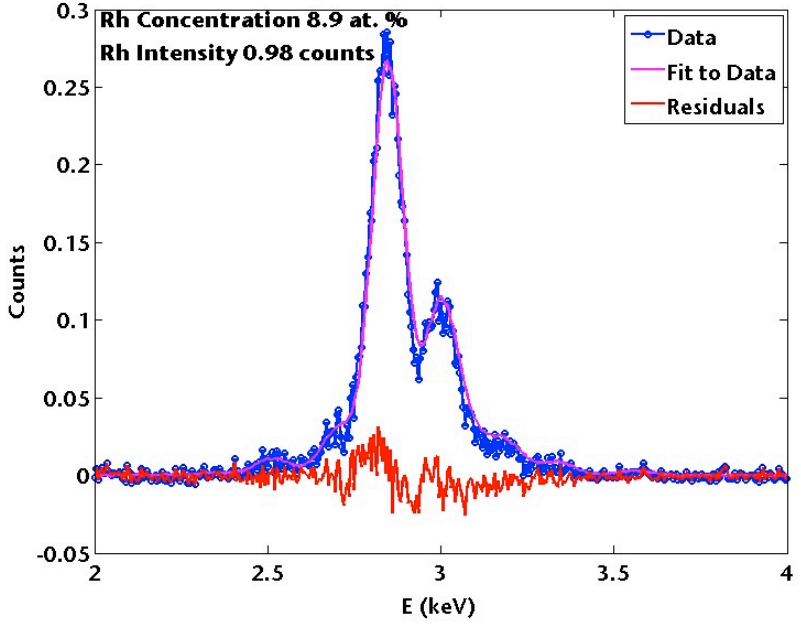

- Top-Hat Filtering

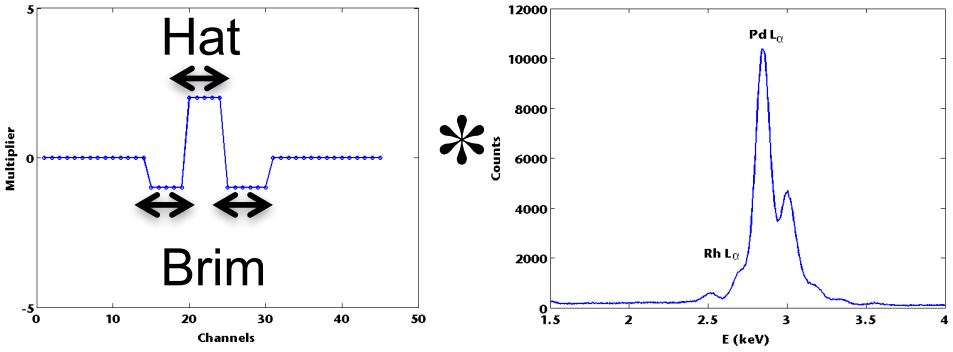

- Linear Interpolation

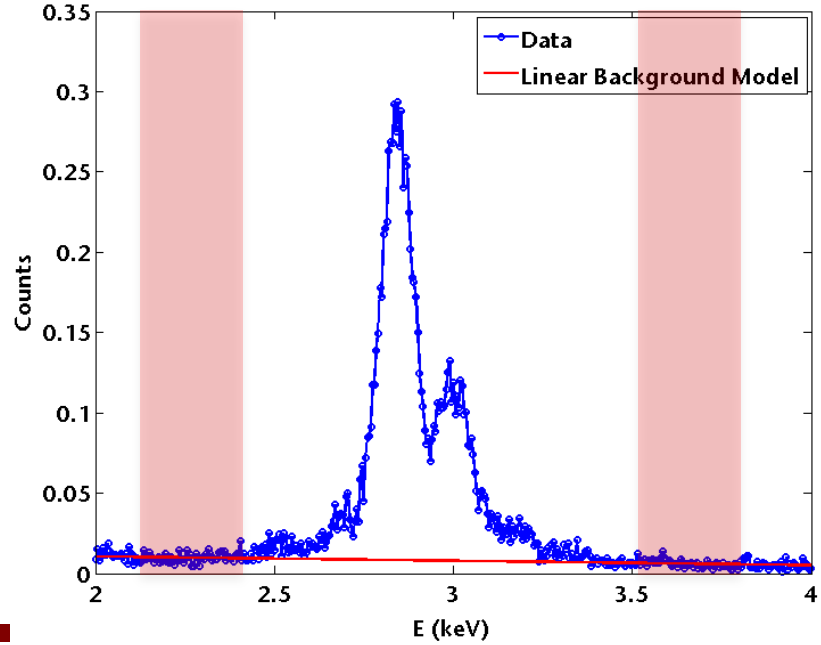

Method 1: Dendrimer-Encapsulated Nanoparticle Consolidation

- Pd/Rh Alloy particles: $Pd_{0.9}Rh_{0.1}$
  - Metal salts mixed with dendrimer and reduced together
- Pd/Rh Core/Shell particles: $Pd_{0.9}@Rh_{0.1}$
  - Pd salt reduced in first step
  - Rh salt reduced in second step
- Agglomerates of particles ~5 nm in diameter with pores between particles range in size (1 nm – 100 nm)

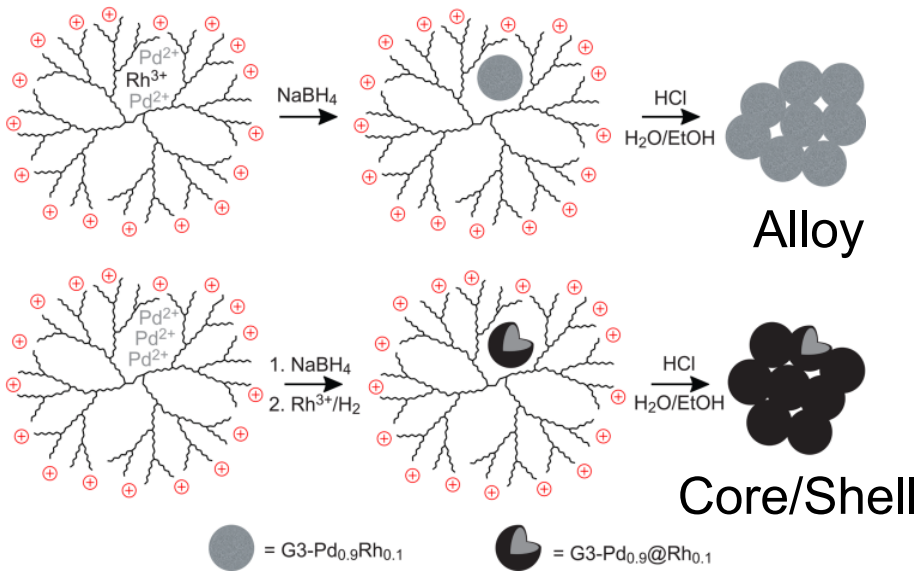

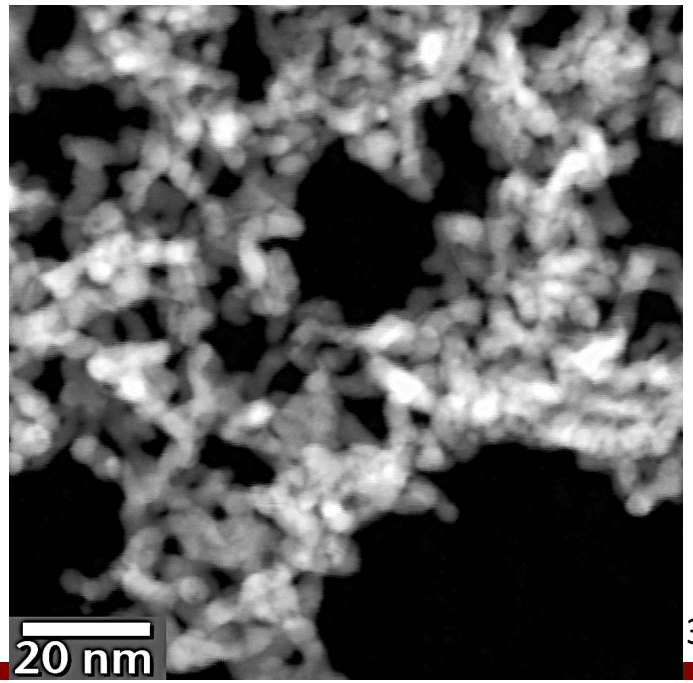

P.J. Cappillino, et al., *Journal of Materials Chemistry* **22** (2012)

Large Solid Angle Detector Finds Rh Shell

- FEI Probe-Corrected Titan G2 80-200 with 0.7 sr SDD detector array at 200 kV

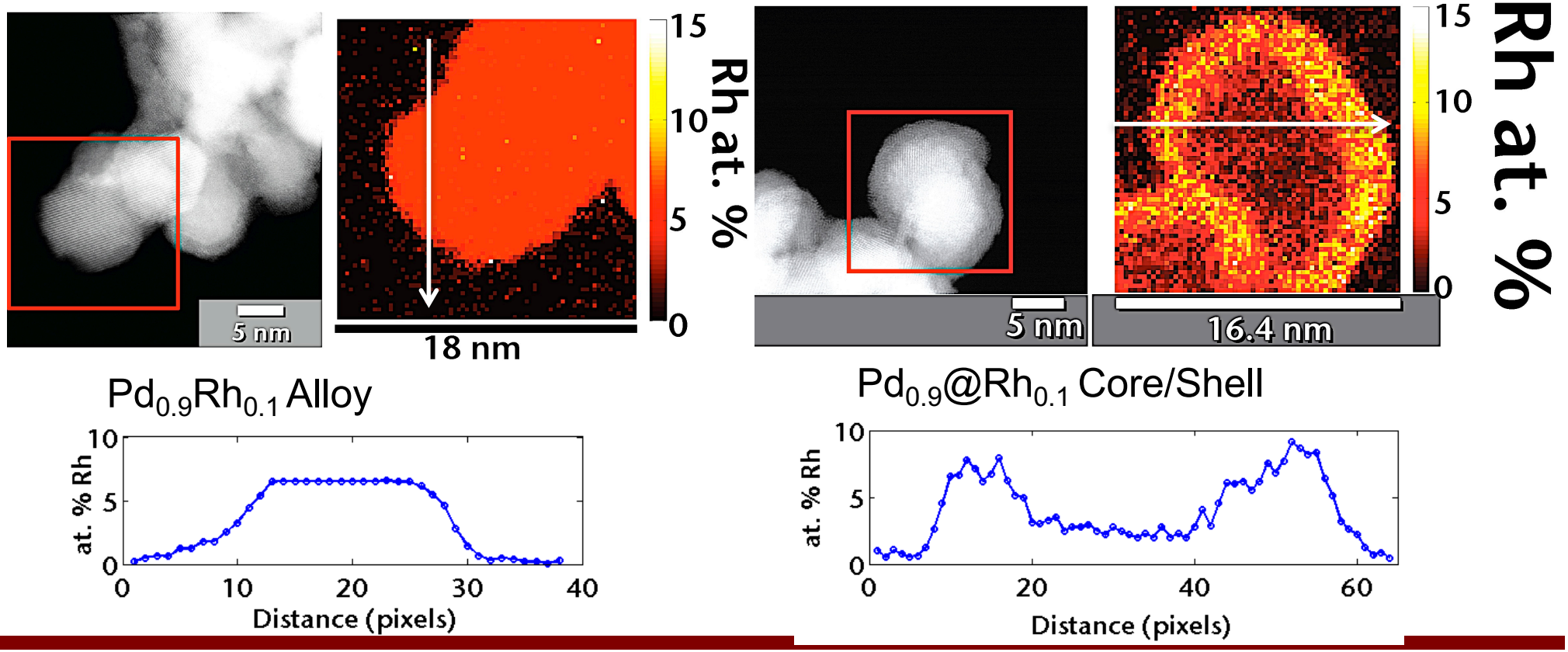

P.J. Cappillino, et al., *Journal of Materials Chemistry* **22** (2012)

Method 2: Surfactant Template Fabrication

- Organic molecule, Brij 56, forms cylindrical micelle in water
  - Hydrophobic center
  - Solution of metal salts

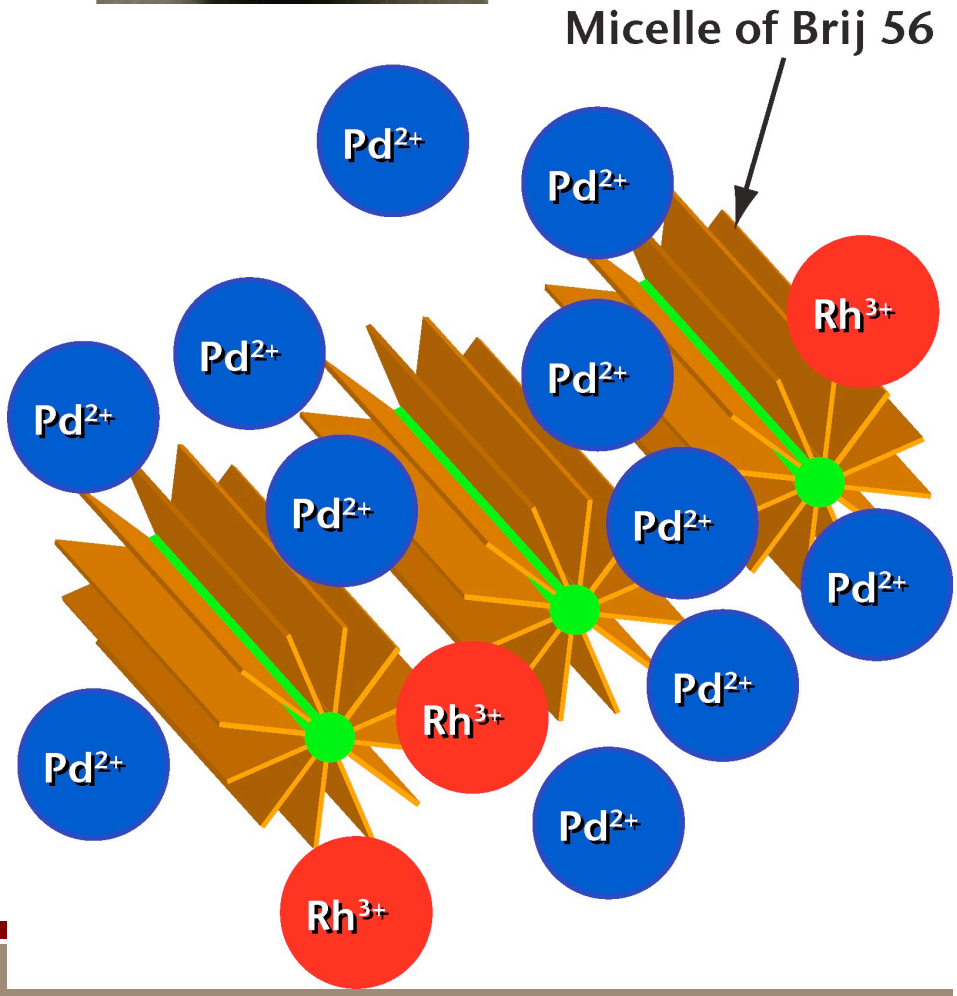

Robinson, D. et al., *IJHE*, **35** (2010).

Method 2: Surfactant Template Fabrication

Sandia National Laboratories

- Organic molecule, Brij 56, forms cylindrical micelle in water
  - Hydrophobic center
  - Solution of metal salts
- Reduce the metal salts in flowing gas
  - $(NH_4)PdCl_4 + H_2 \rightarrow Pd + NH_4Cl + 2HCl$
  - $2Na_3RhCl_6 + 3H_2 \rightarrow 2Rh + 6NaCl + 6HCl$
- Rinse off organic residue
- Nanoporous material
- Did it work?

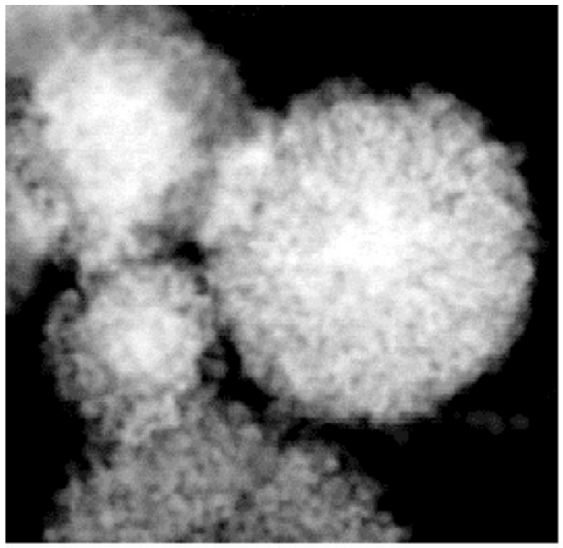

100 nm

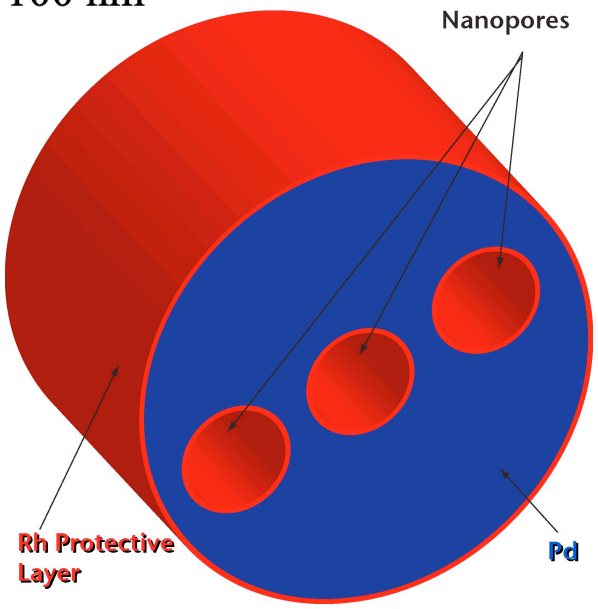

Core/Shell Compositional Distribution

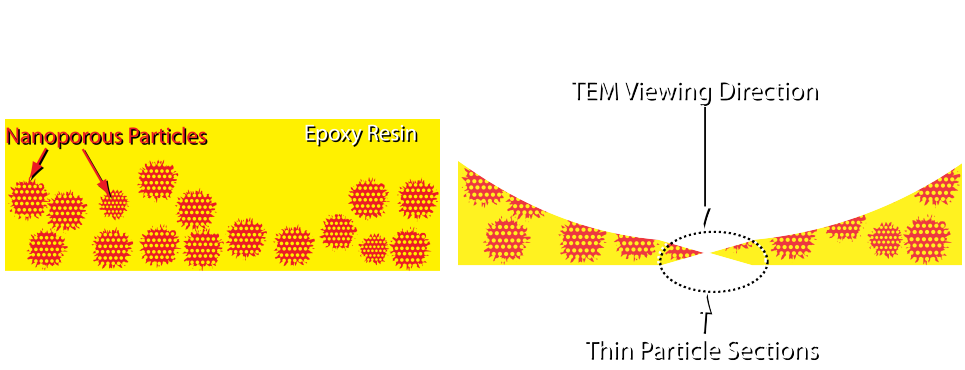

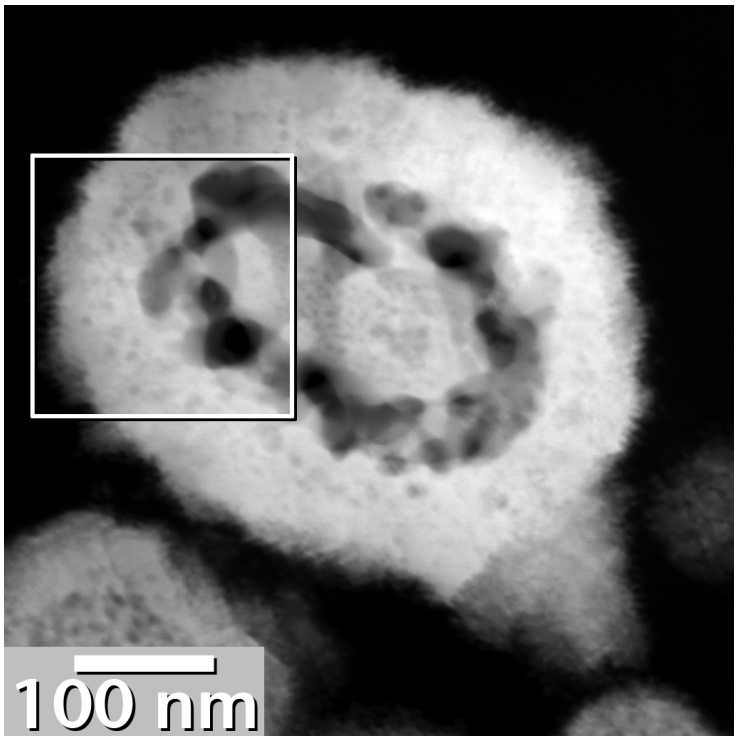

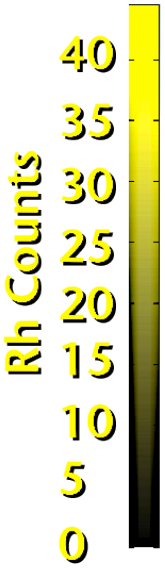

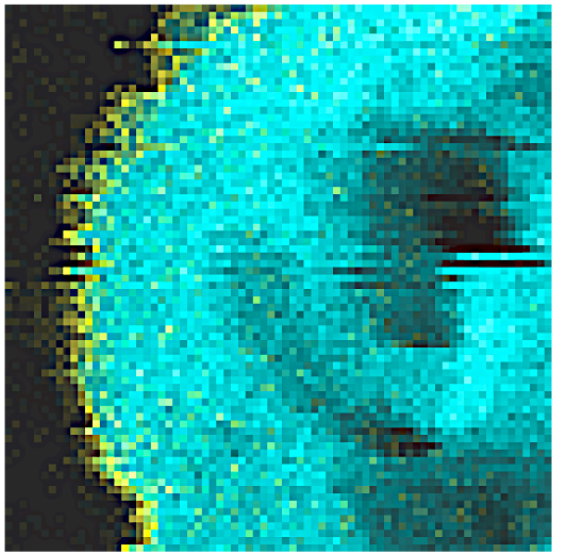

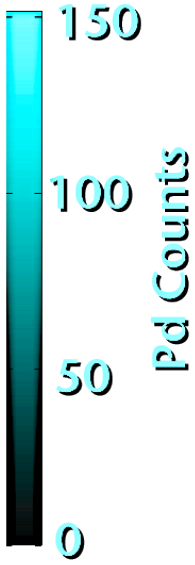

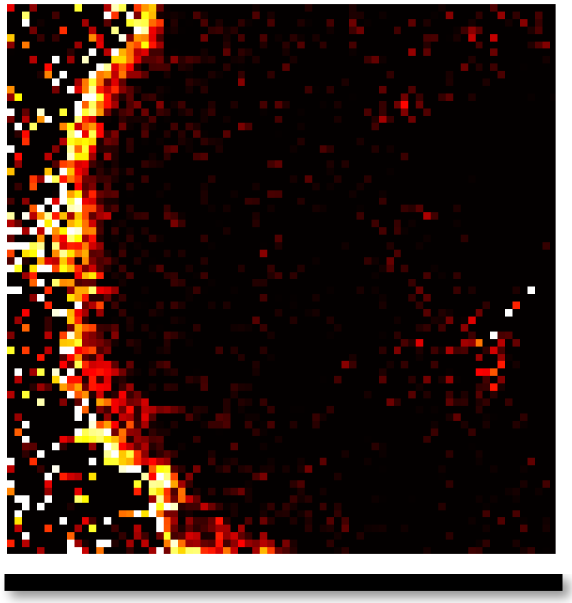

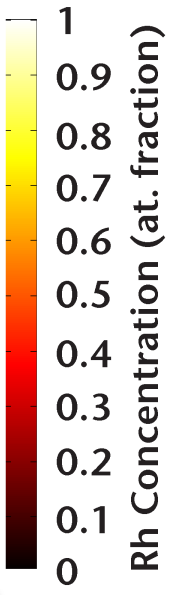

M.D. Ong, et al., *Chemistry of Materials* **24** (2012)

Core/Shell Compositional Distribution

- Rh-rich shell
- Smaller (~100 nm diameter) particles have Rh concentration that is higher than the nominal concentration during synthesis
- Higher Rh content produces more uniform pore sizes

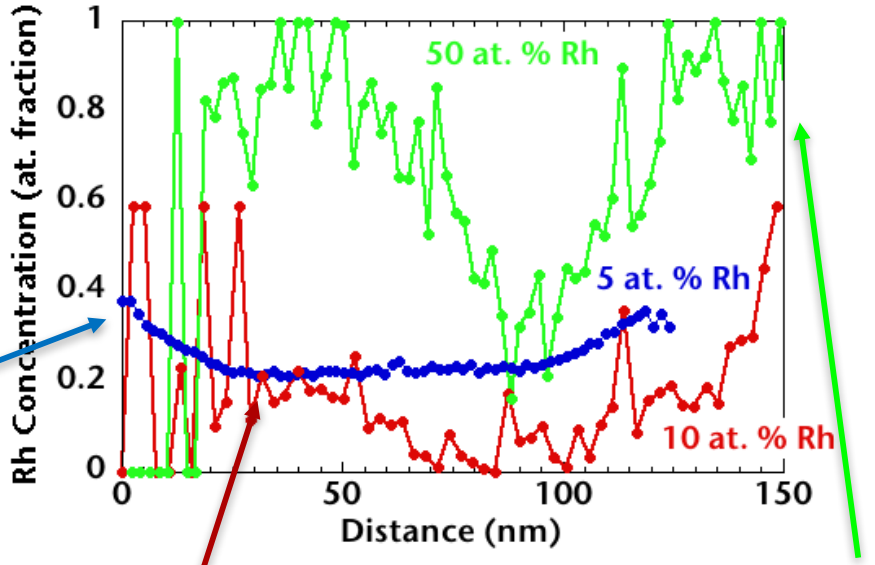

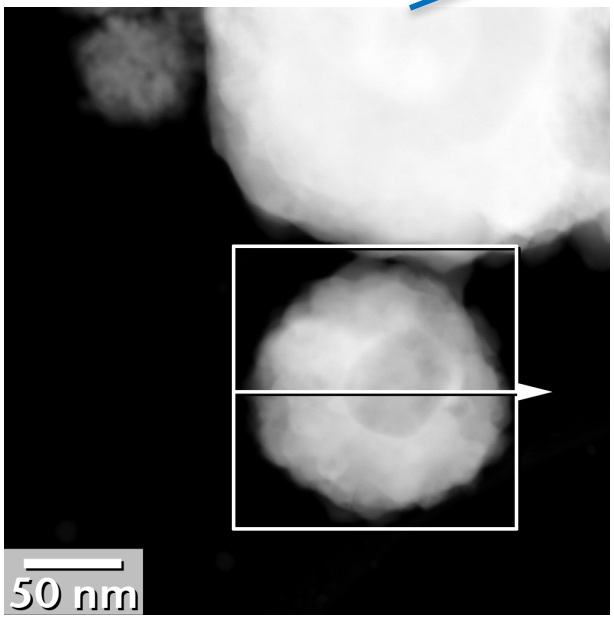

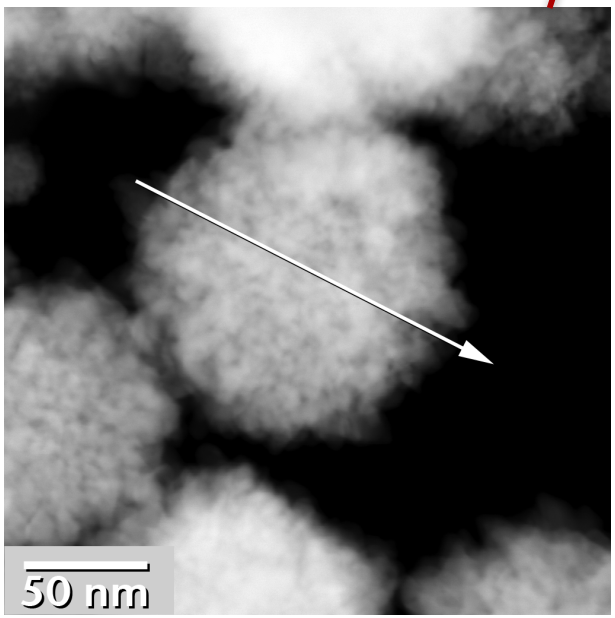

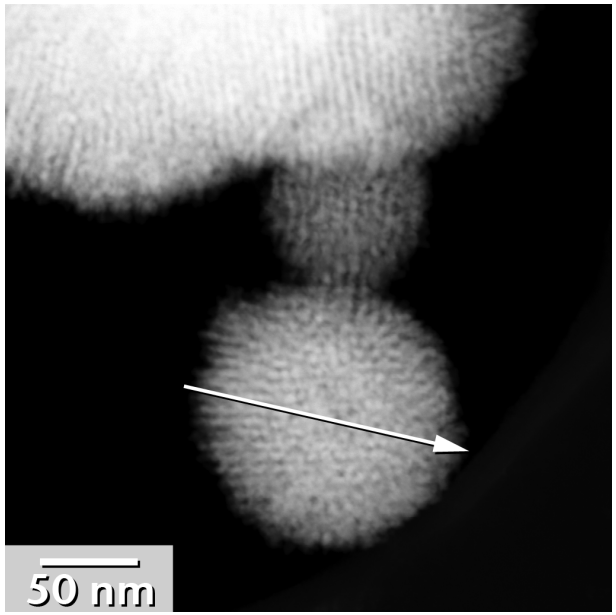

Kinetics Dictate Rh Distribution

- Pd reduction faster than Rh
- Nucleation occurs throughout the reaction duration
- Large particles nucleate early in a Pd-rich environment
  - Creates a Pd-depleted zone

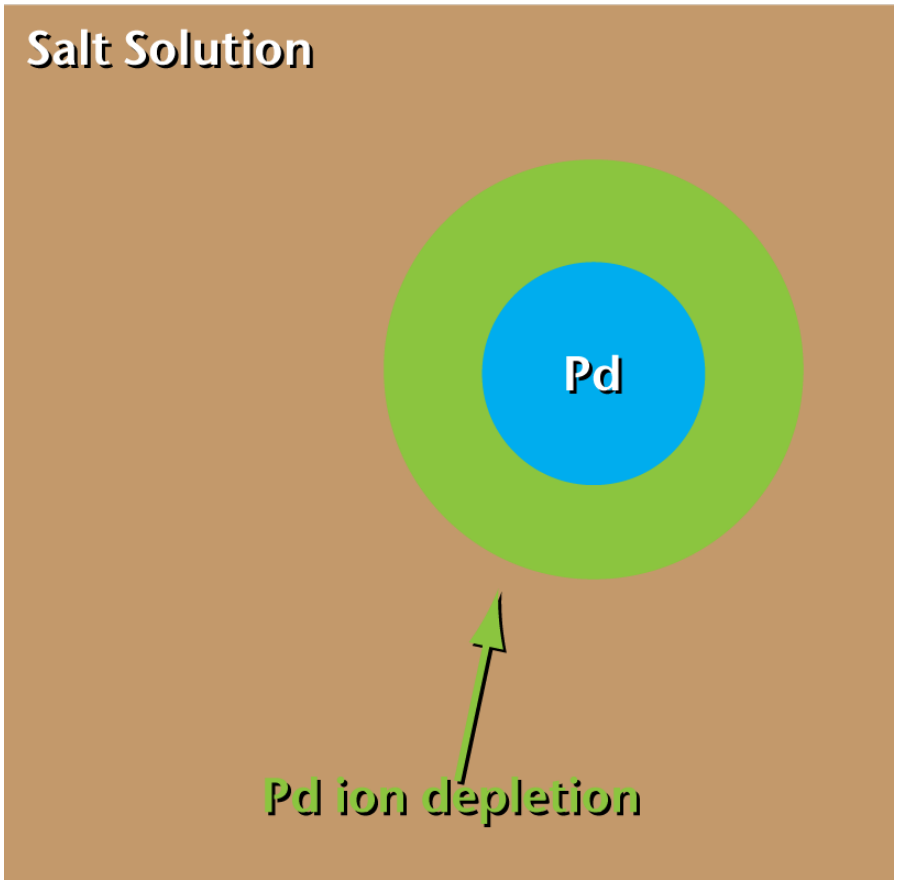

Kinetics Dictate Rh Distribution

- Pd reduction faster than Rh
- Nucleation occurs throughout the reaction duration
- Large particles nucleate early in a Pd-rich environment
  - Creates a Pd-depleted zone
- All the Pd is consumed and reacted
  - Rh-rich shell on large particles then forms
- Rh is distributed less uniformly than desired

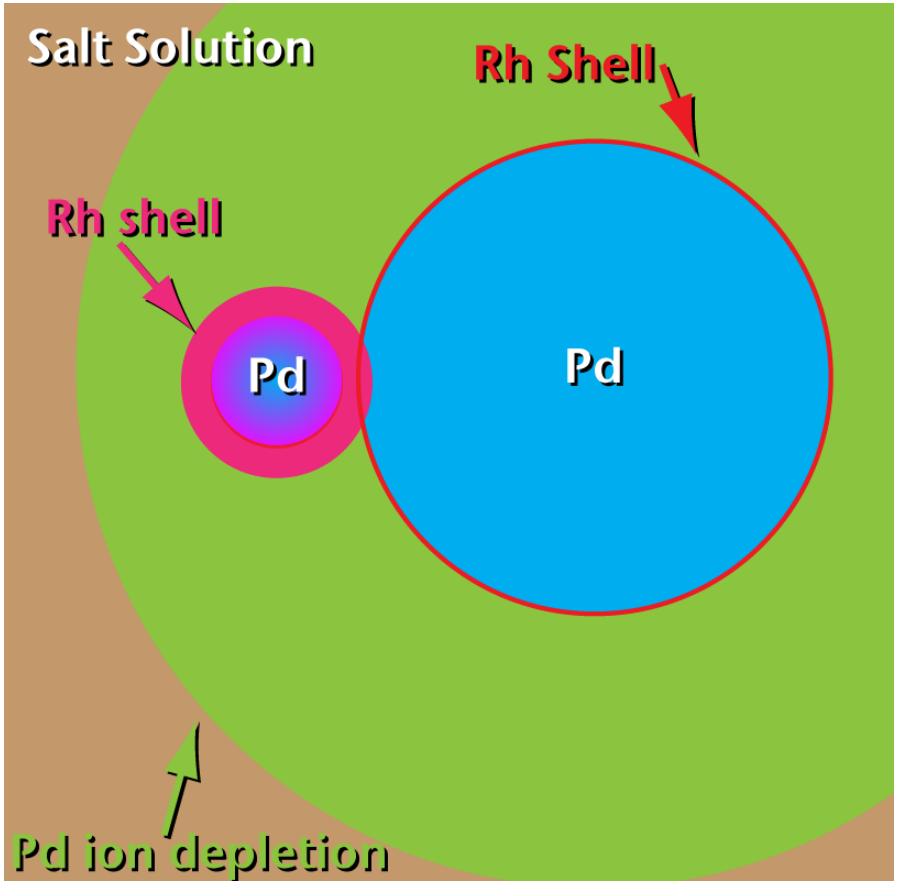

Method 3: Atomic Layer Electroless Deposition

Sandia National Laboratories

- Precise control of thickness based on number of electrochemical cycles
- Deposition on high-aspect ratio structure
- Microtomed thin sections

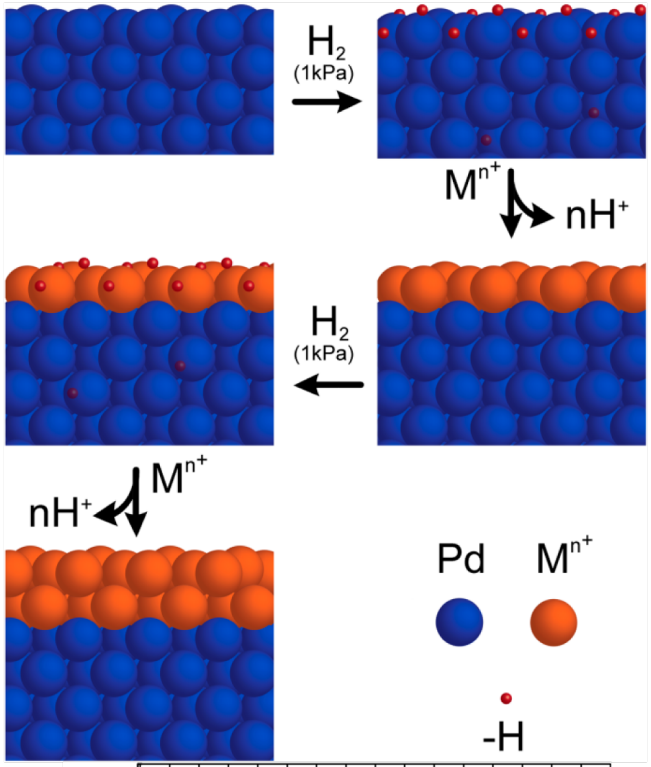

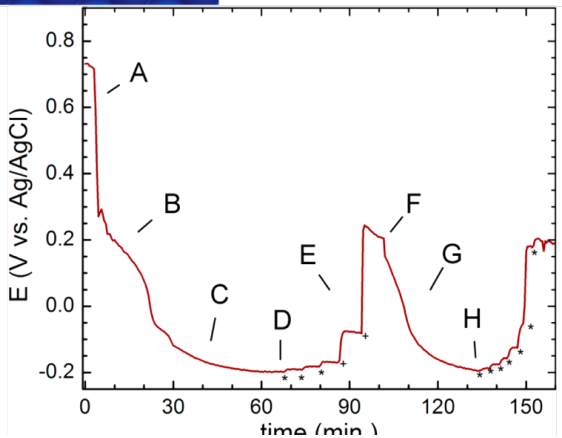

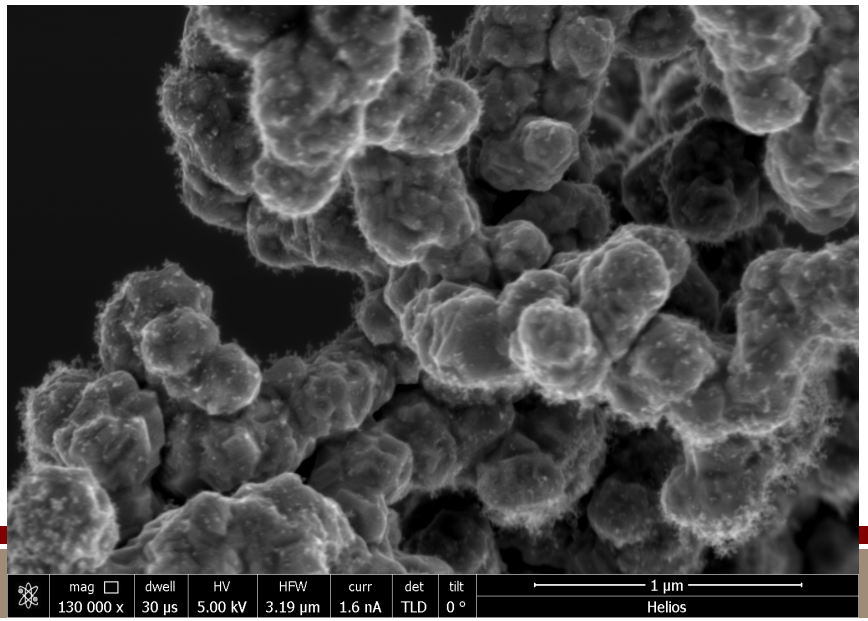

Cappillino, P. J., et al. (2014). "Atomic-Layer Electroless Deposition: A Scalable Approach to Surface-Modified Metal Powders." Langmuir **30**(16): 4820-4829.

8 Electrochemical cycles Pd/Rh

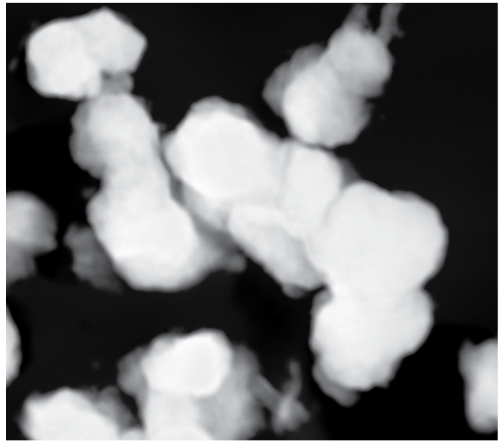

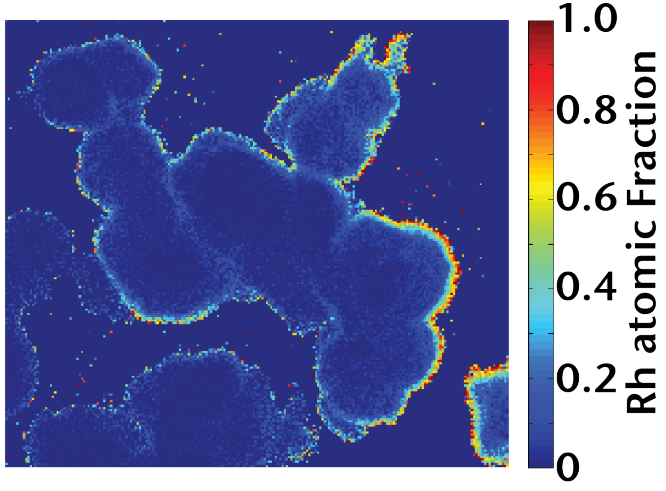

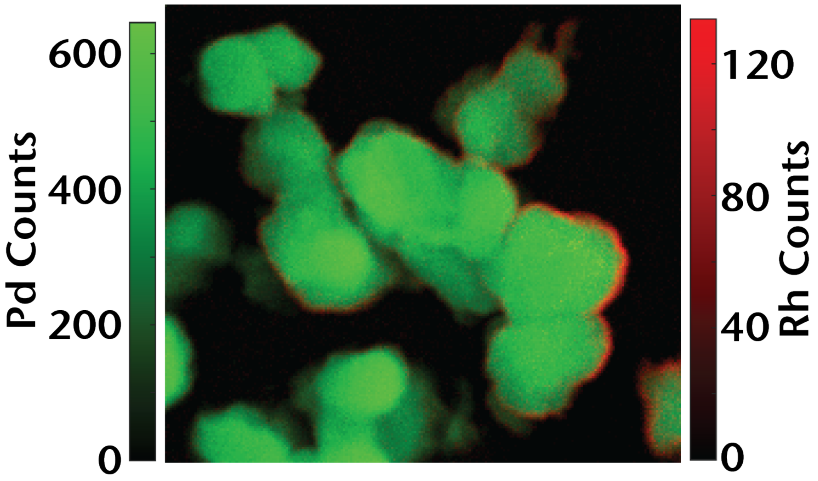

20-30 nm of Rh enrichment at particle surface

1 Electrochemical cycle Pd/Rh

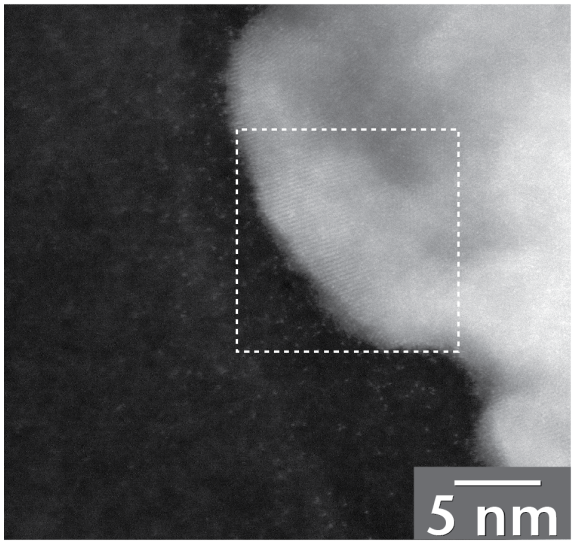

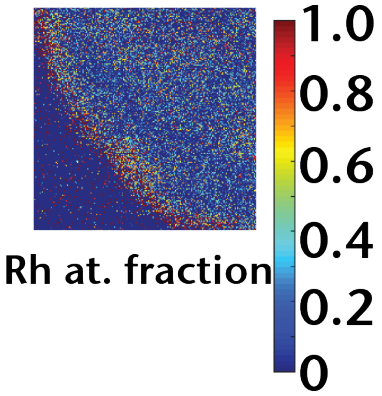

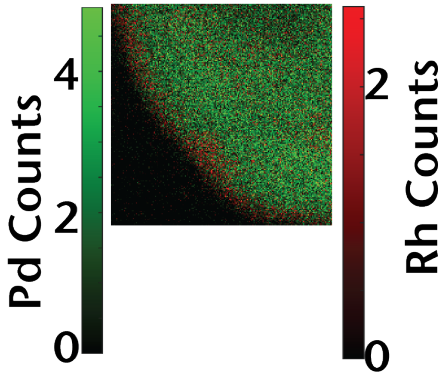

1 nm of Rh enrichment at particle surface

Pt Surface Coatings

- Normalization Window for reference shapes is same energy width
- Cliff-Lorimer k-factor=0.96
- Electrochemically deposited Pt approximately 10 nm thick

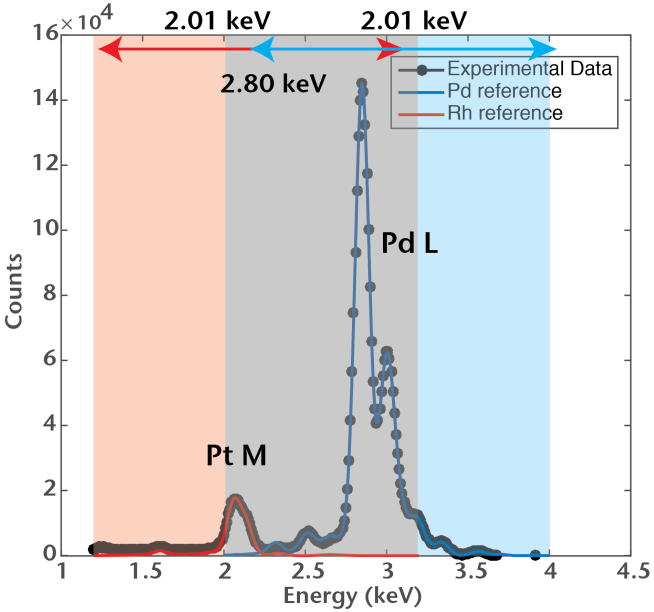

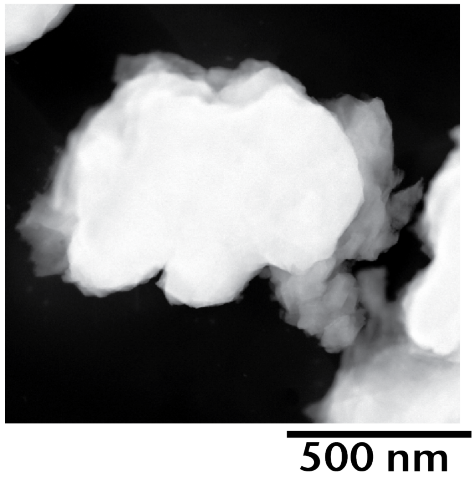

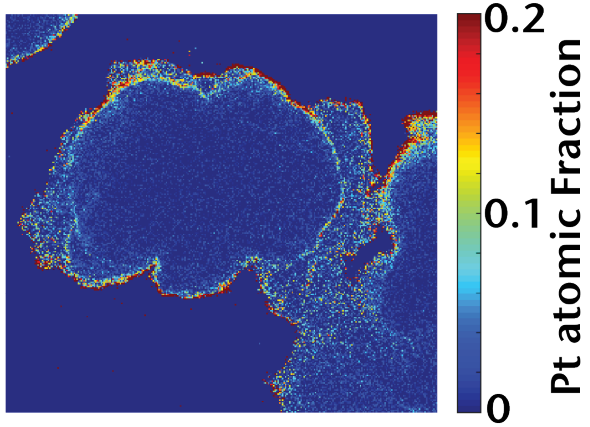

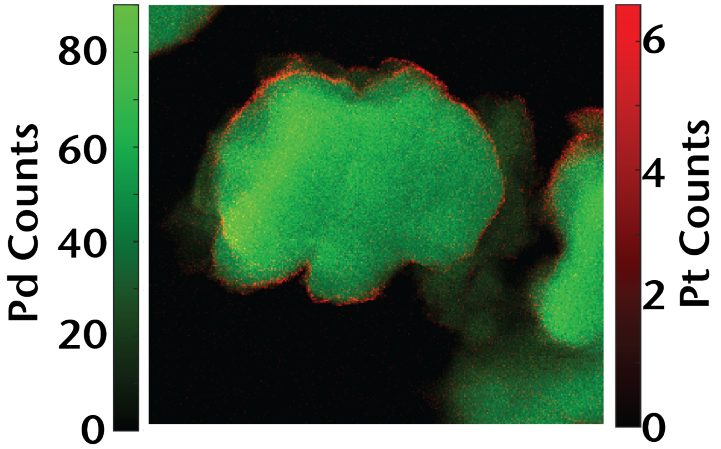

Can We Reproduce Clean Data with Newer Modern Methodologies

Sandia National Laboratories

Can we FIB these particles and get equivalent chemical information?

- Higher ionization cross-section at 30 kV

$$Q \propto \frac{\ln\left(E_0 / E_c\right)}{E_0 \; E_c}$$

Q = ionization cross section

E_0 = Accelerating Voltage

E_c = Ionization Energy for the shell in keV

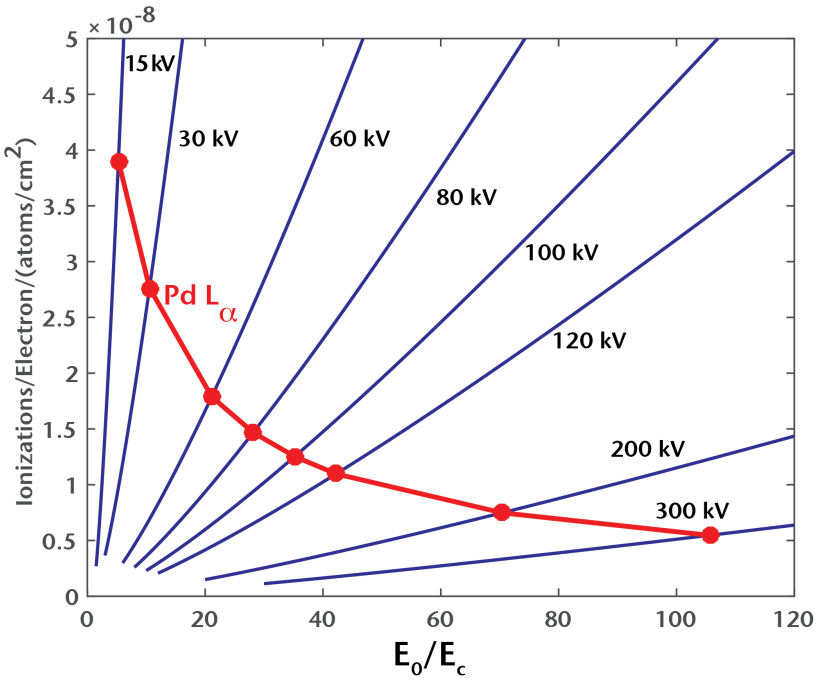

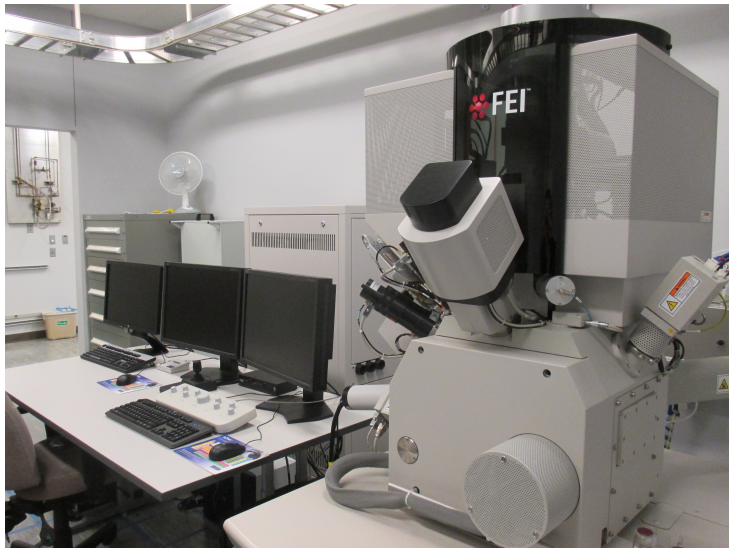

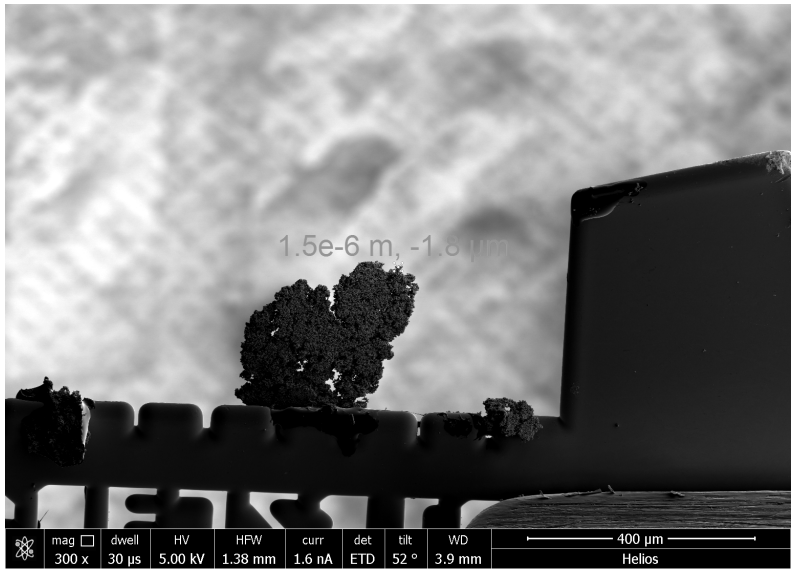

Surrounding Epoxy Causes Mixing in MSA

- Elements in surrounding epoxy resin mix with elements in coating layer
- Analysis using only MLLS yields the expected results
- Can we measure this material using FIB where no epoxy is required?

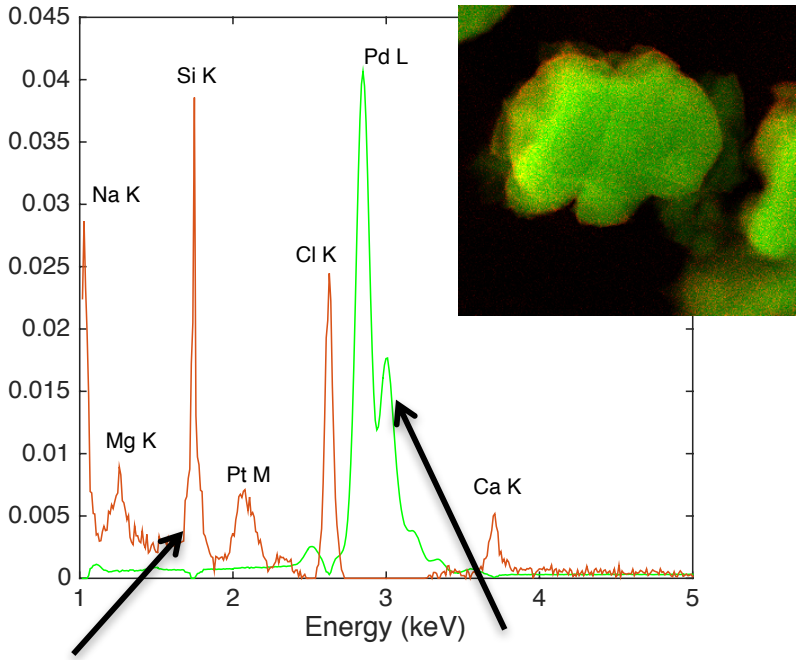

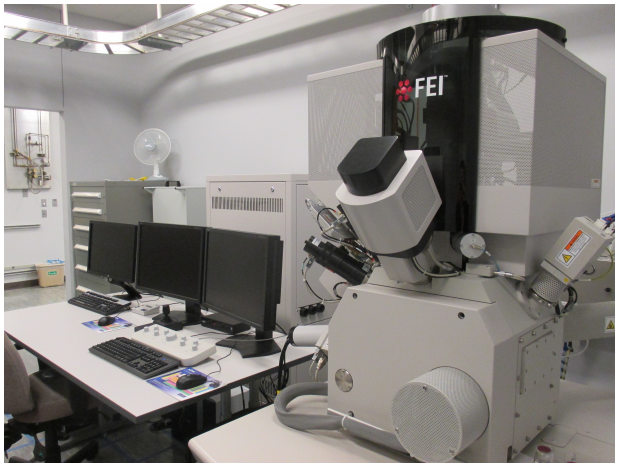

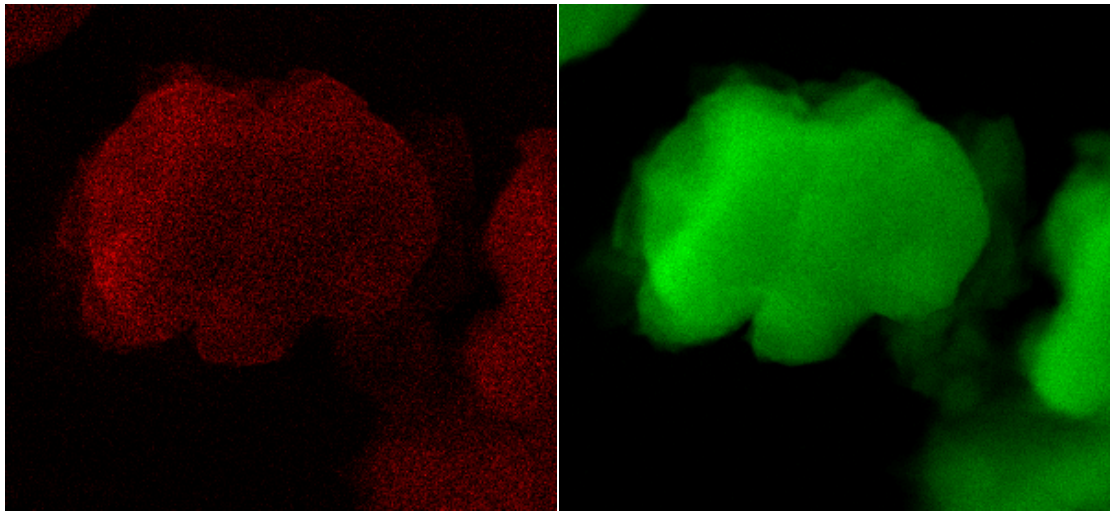

FEI Helios 660

Are Thin Layers Observable at 30 kV

Sandia National Laboratories

- Higher ionization cross-section at 30 kV

$$Q \propto \frac{\ln\left(E_0 / E_c\right)}{E_0 \, E_c}$$

Q = ionization cross section

E_0 = Accelerating Voltage

E_c = Ionization Energy for the shell in keV

- Small interaction volume for thin samples
- FIB-thinned specimens

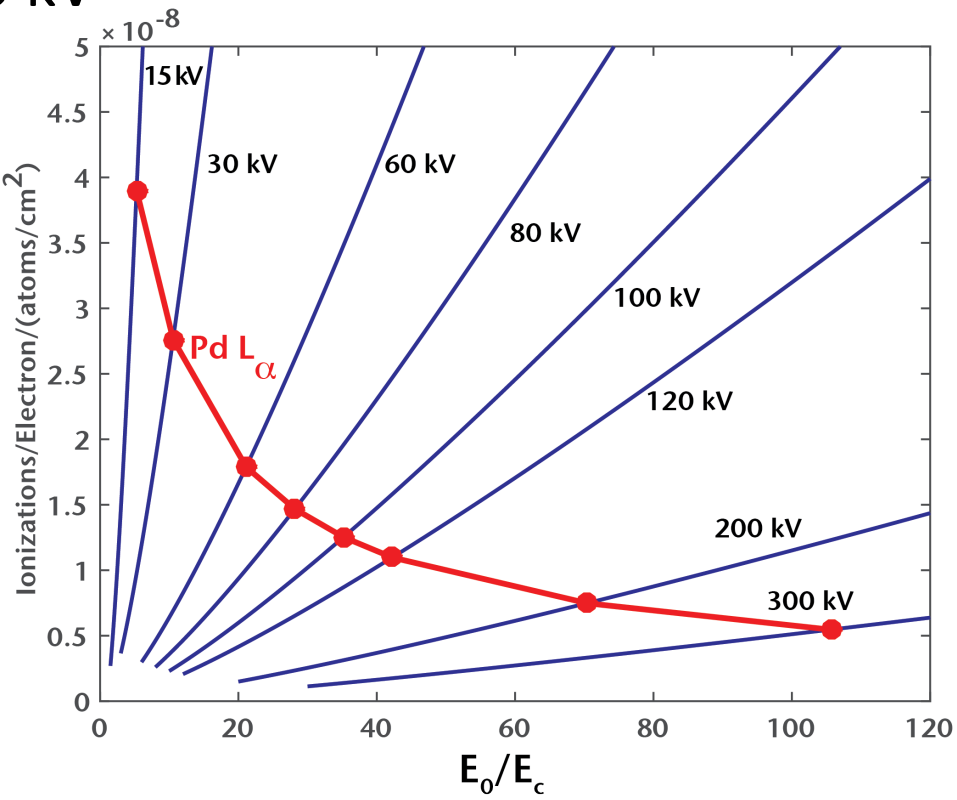

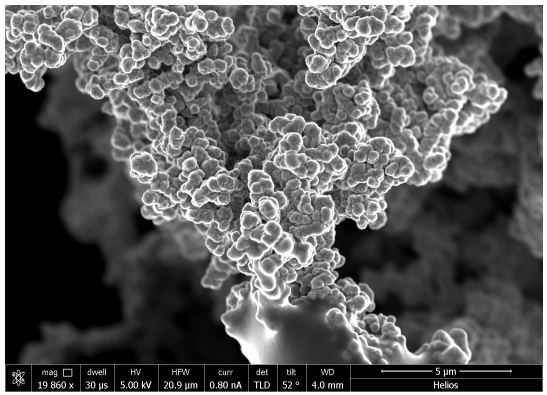

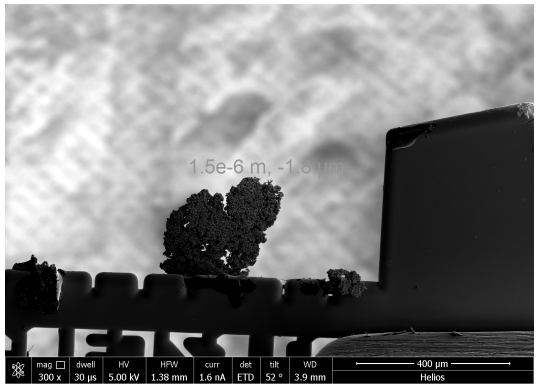

200 kV STEM on FEI Probe-corrected G2 Titan with Chemistem SDD large angle detector (20 nm coating)

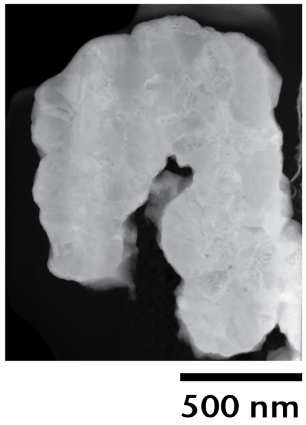

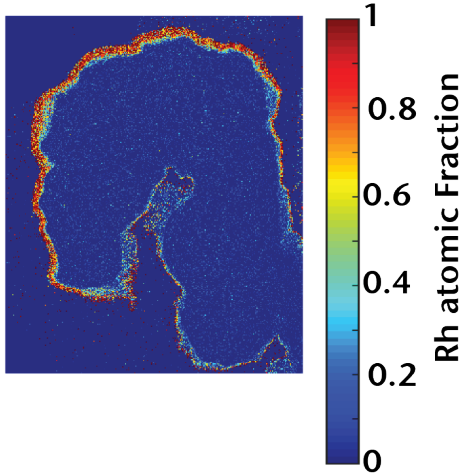

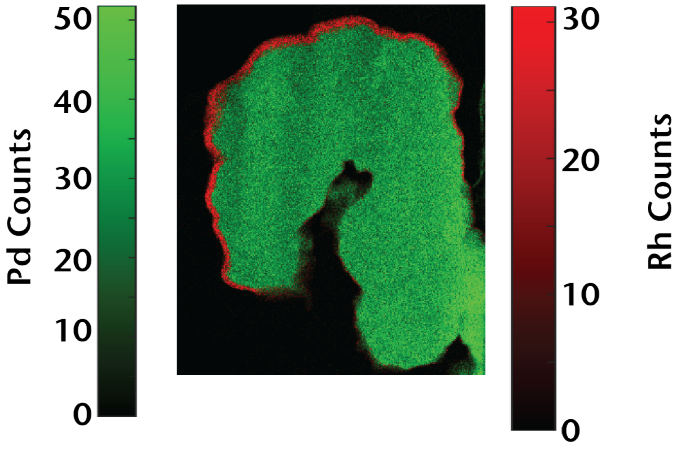

30 kV STEM on FEI Helios 660 with Oxford XmaX 80 SDD EDS Detector (assumed k-factor 1)

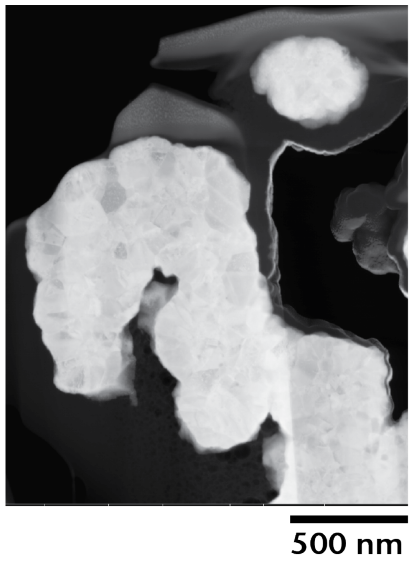

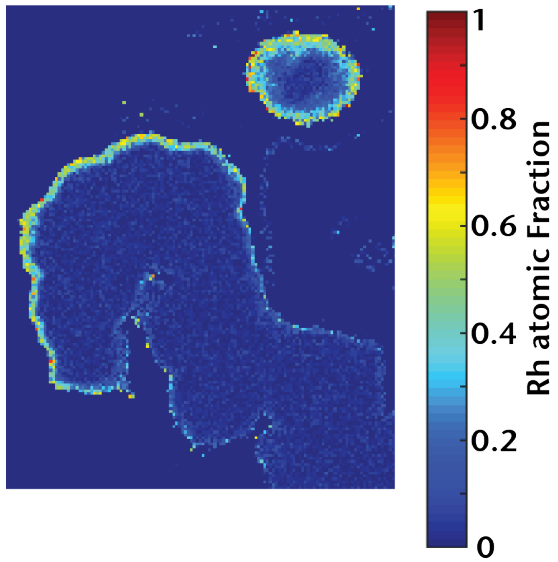

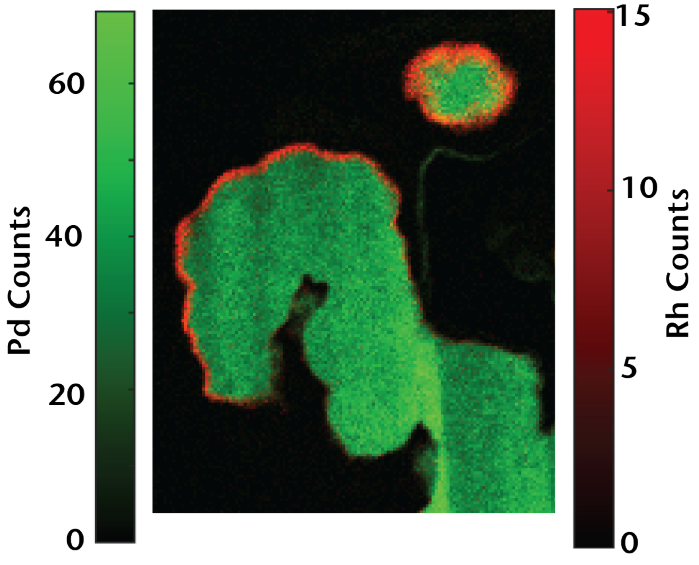

Thin (<5 nm) Layers at 200 kV Microtome

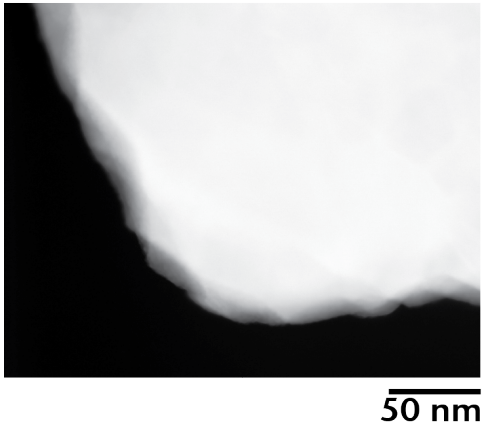

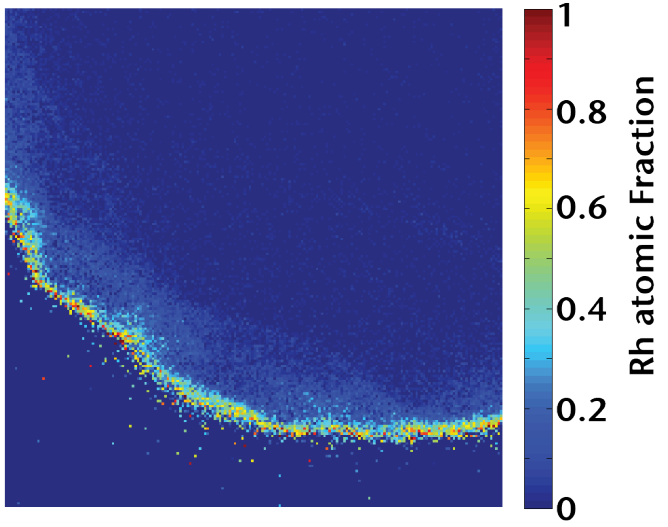

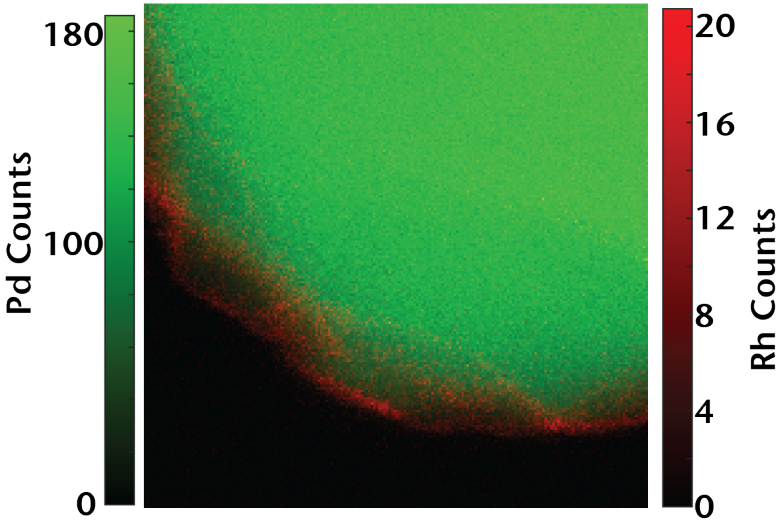

Thin (<5 nm) Layers at 30 kV FIB

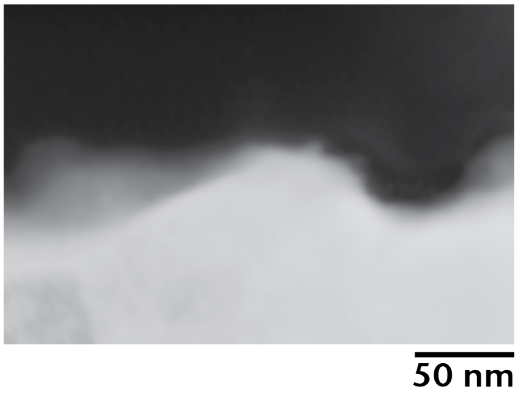

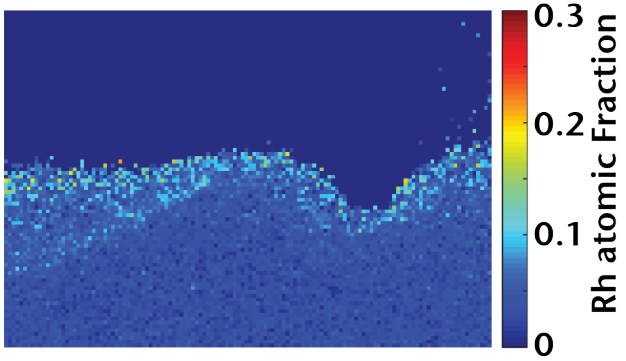

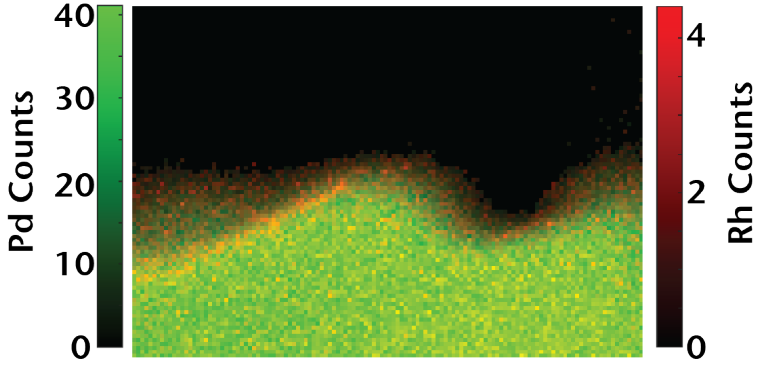

Linking Microstructural Measurements to Transport Phenomena

Sandia National Laboratories

- Helium bubbles formed by ^3H β decay, α decay, neutron (n, α) reactions
- Rh-ion transport during fabrication of nanoporous hydrogen storage materials
- Li-ion transport during charge/discharge of $LiFePO_4$ electrodes
- Reliability of aged electronic components with variability in manufacturing process

Electrochemical Energy Storage for Transportation

- Do particles charge at the same time?
- What limits the charging rate?

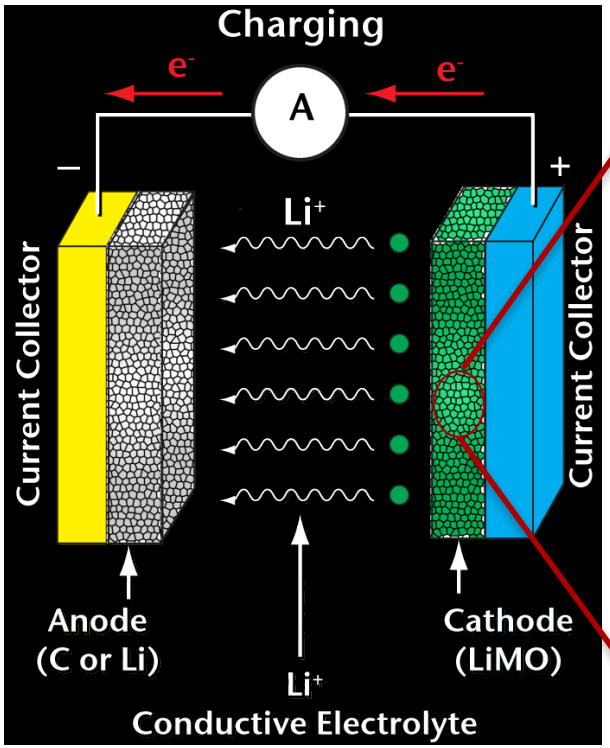

How Does it Charge?

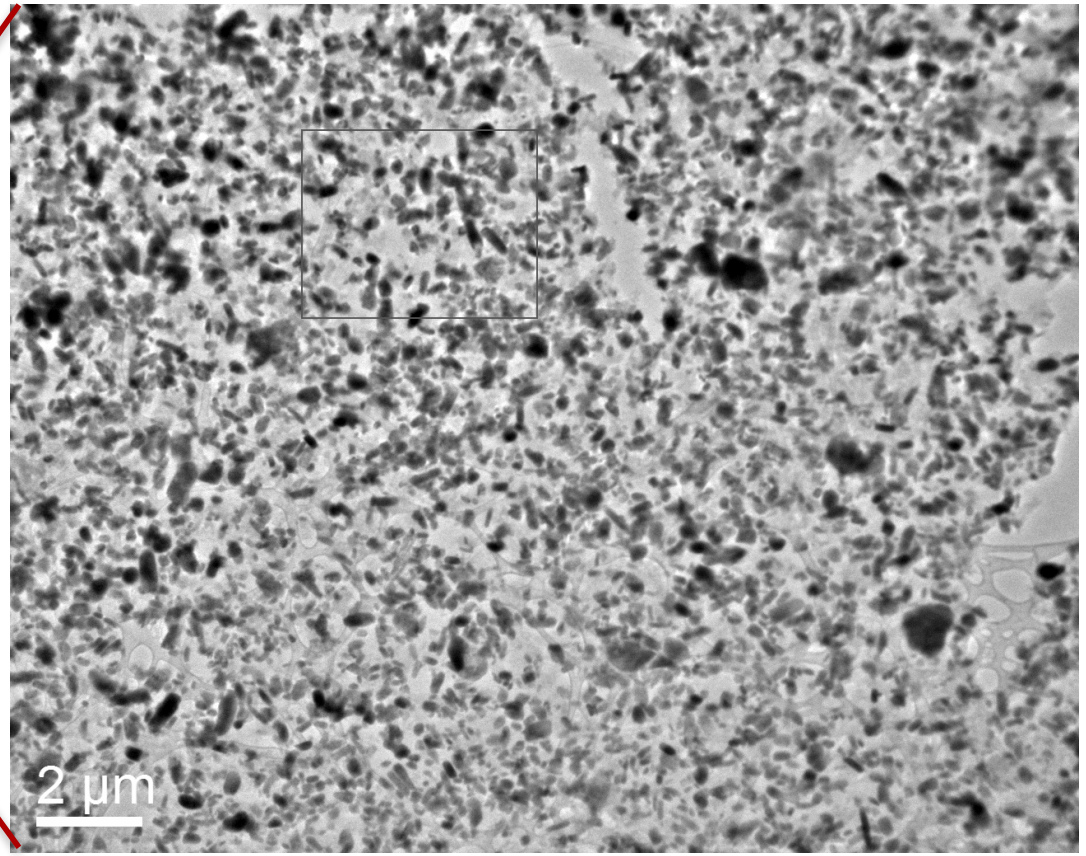

We need a tool to be able to measure this

Understanding Li-ion Transport in Li-ion Batteries

Sandia National Laboratories

- What mechanisms control the intercalation reactions in real battery electrodes?
  - Charge/Discharge rate
  - Efficiency
  - Degradation

Intercalation in a single particle

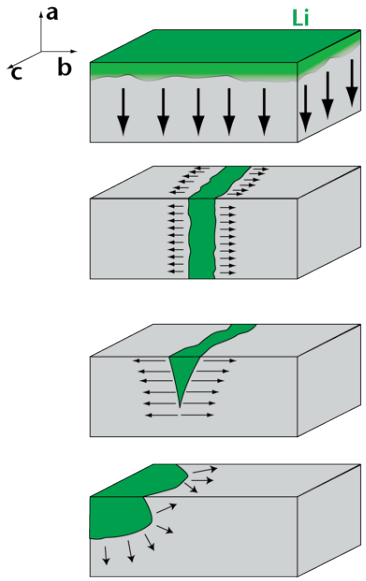

Chen et al. ECSSL, 2006

Laffont et al. Chem Mater, 2006

Intercalation in many particle systems

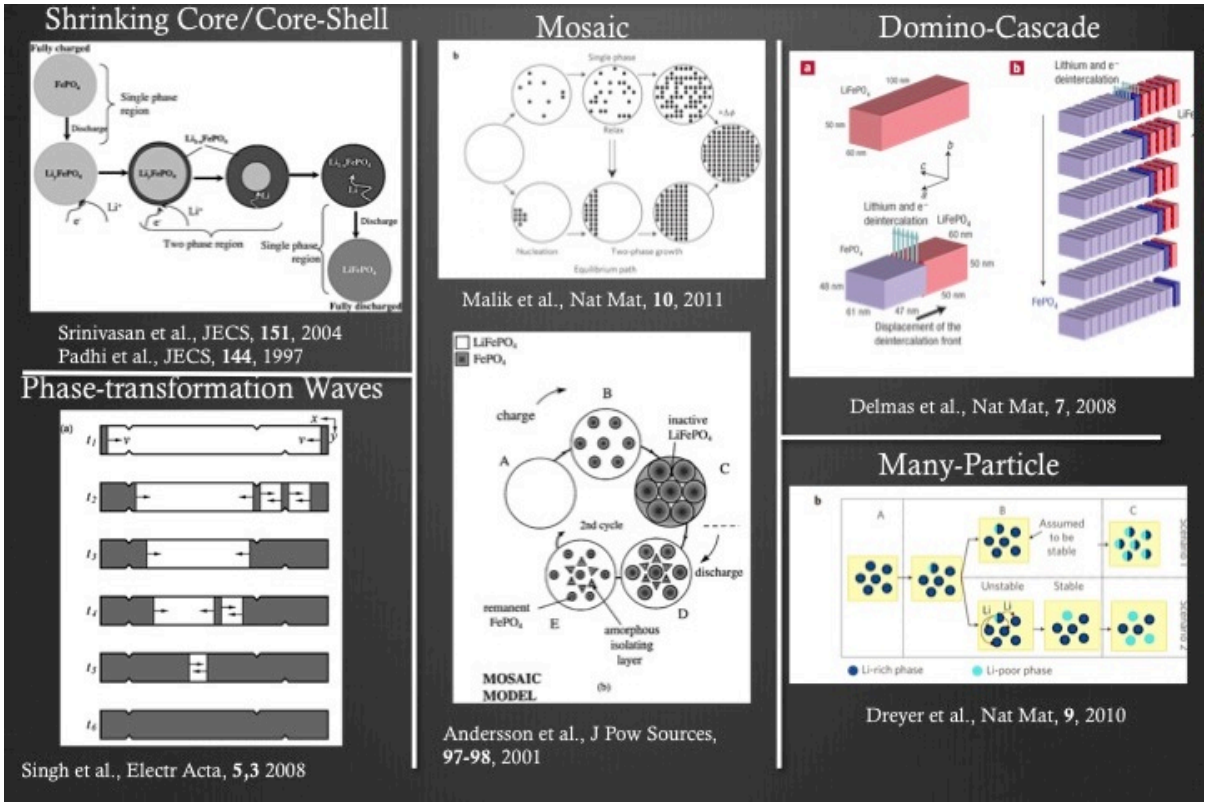

How to image Li at different times

Sandia National Laboratories

- In Situ experiments
  - Liquid environments under vacuum
  - Electrical biasing in the microscope
  - Volatile electrolytes
- Ex Situ forensic analysis on a batteries cycled to several states of charge
  - Standard Coin Cell
    - 35-µm thick carbon coated LFP (d_{ave}~220nm)/graphite composite cathode
    - Li anode
    - 1.2 M $LiPF_6$/ethylene carbonate/ethyl methyl carbonate electrolyte
    - Charged to 50 % state of charge (75 mAg g^{-1}) at 1 C
    - Rapidly disassembled and rinsed with excess dimethyl carbonate (<4 min)

Imaging Li Distribution

- Direct: Li is a light element
  - Z-contrast will not work
  - X-ray emission line is too low for EDS
  - Absorption edge is at 55 eV
    - Ni: 68 eV
    - Co: 60 eV
    - Fe: 54 eV
    - Mn: 49 eV
- Indirect: Fe change of valence
  - Less Signal at higher energy
  - $LiFe^{2+}PO_4$ vs. $Fe^{3+}PO_4$
  - 2 eV is close to resolution limit of common spectrometers

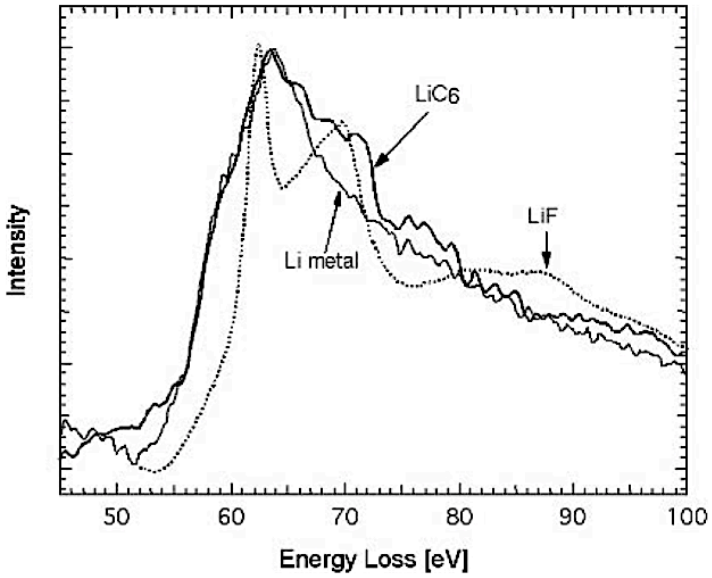

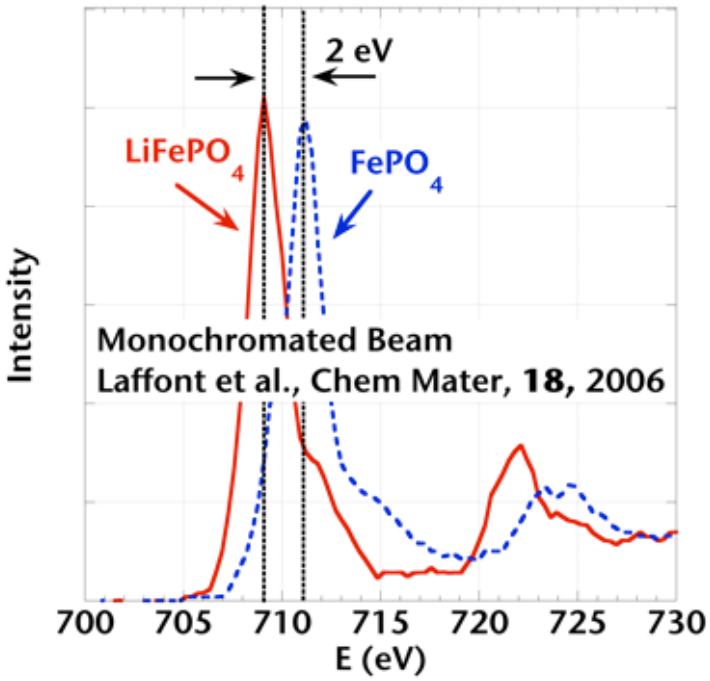

Focused Electron Beam Causes Damage

- Fe shift is visible in a non-monochromated system

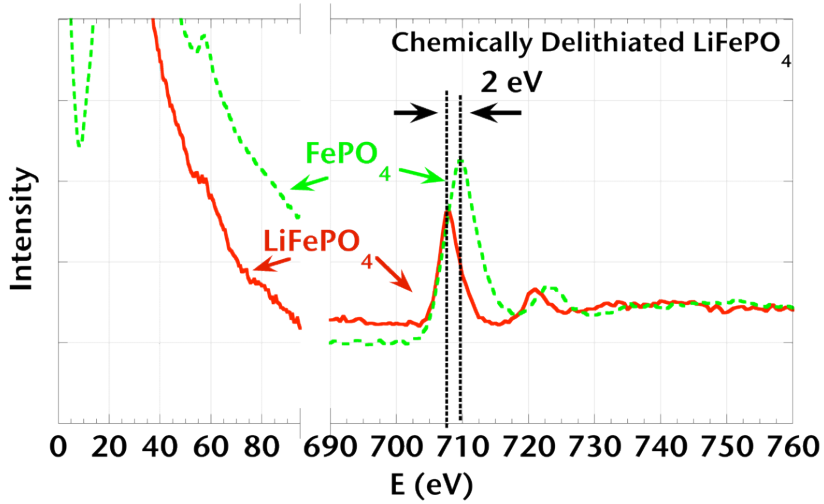

- Electron-beam induced Fe reduction
  - 1 s/pixel
  - 50 sec total

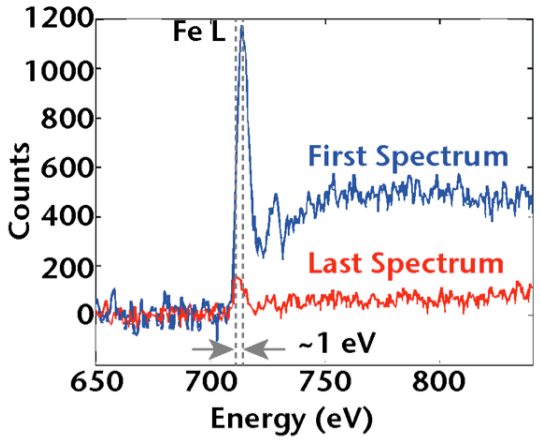

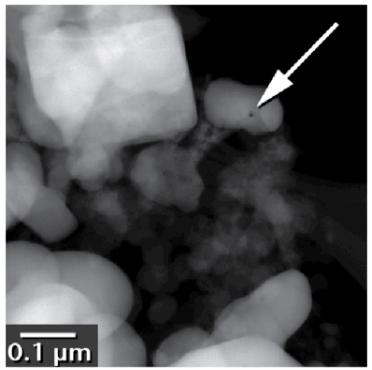

Reduced Dose Analytical Microscopy

- Focused probe causes damage in seconds: STEM-EELS

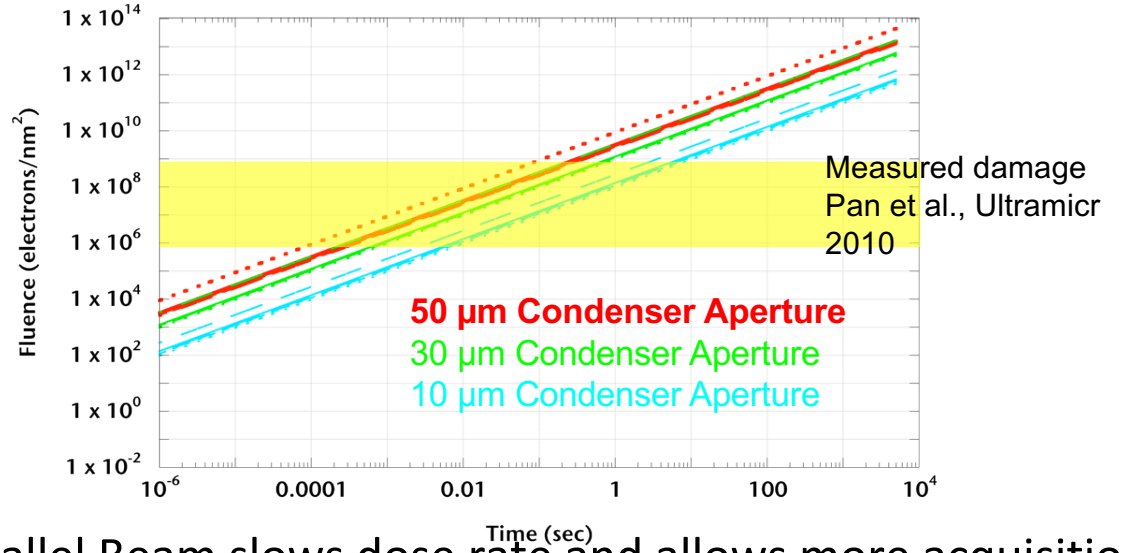

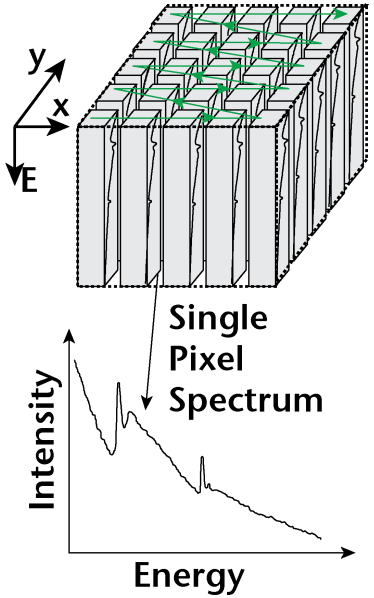

- Parallel Beam slows dose rate and allows more acquisition time: EFTEMSI

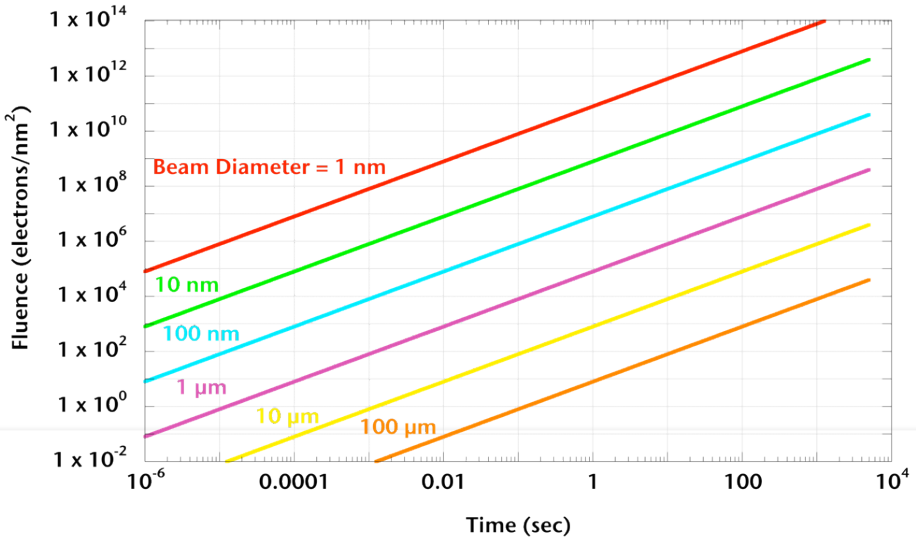

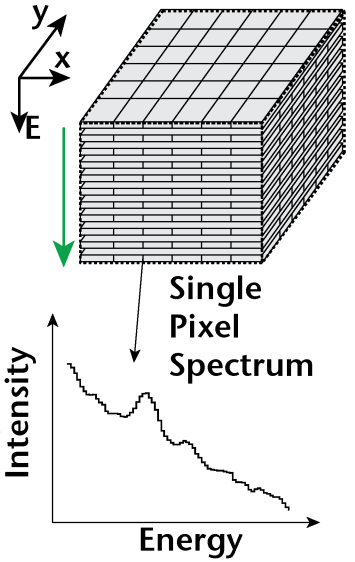

Extracted Particles on SiN Support

- Particles are extracted from a real battery: Spatial Simplicity Analysis

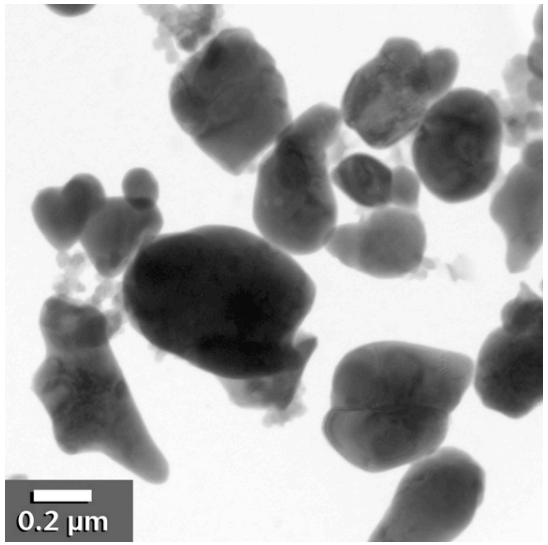

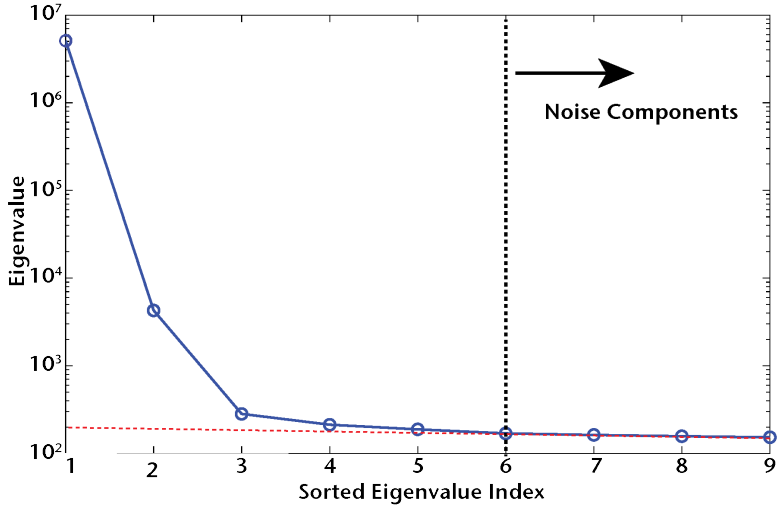

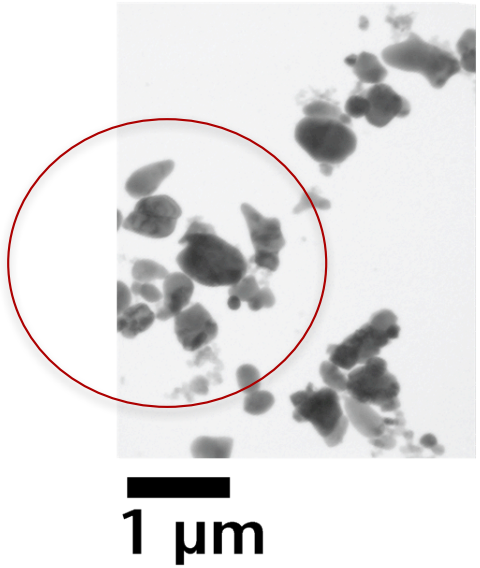

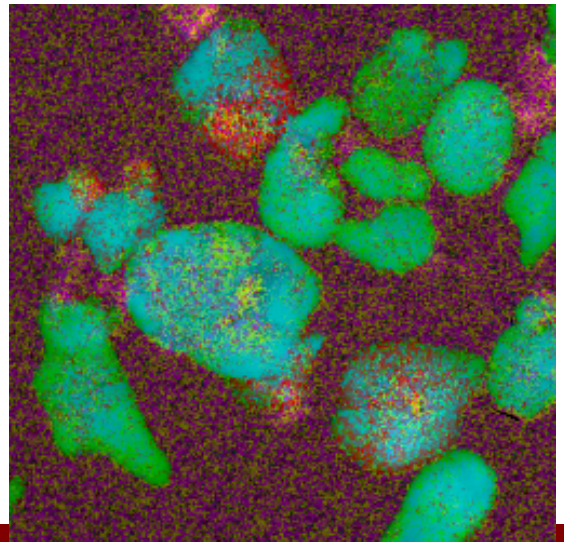

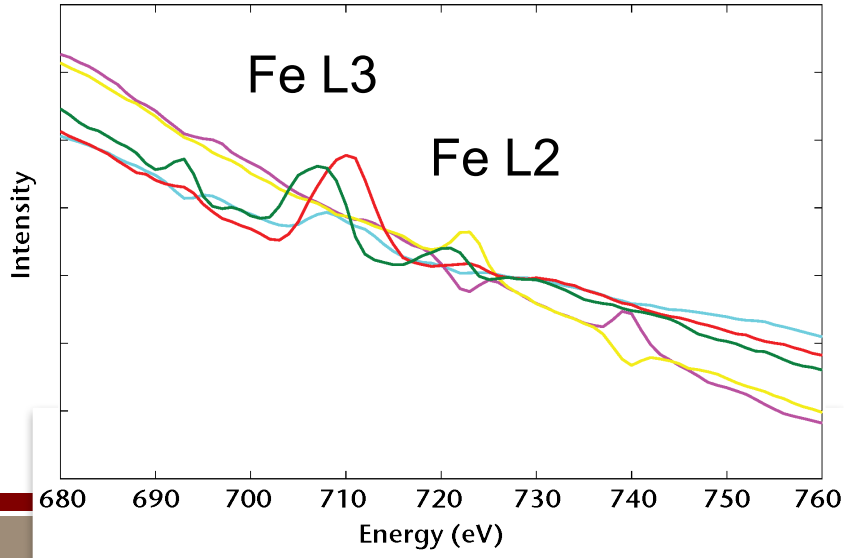

Extracted Particles on SiN Support

- Particles are extracted from a real battery

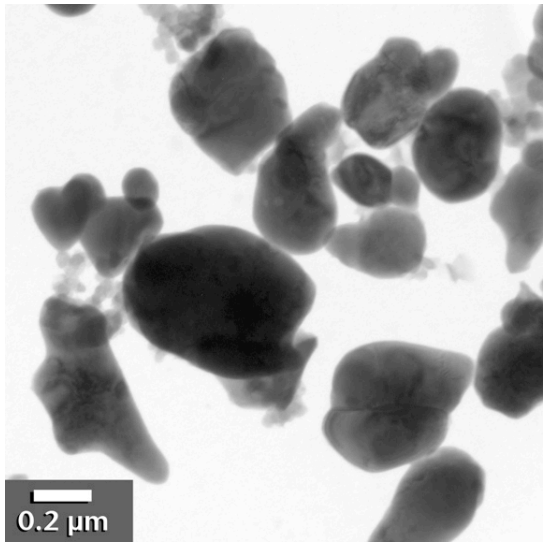

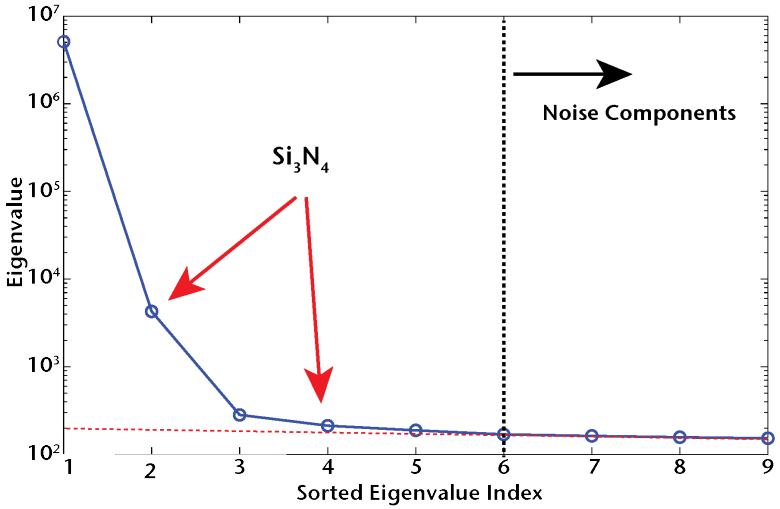

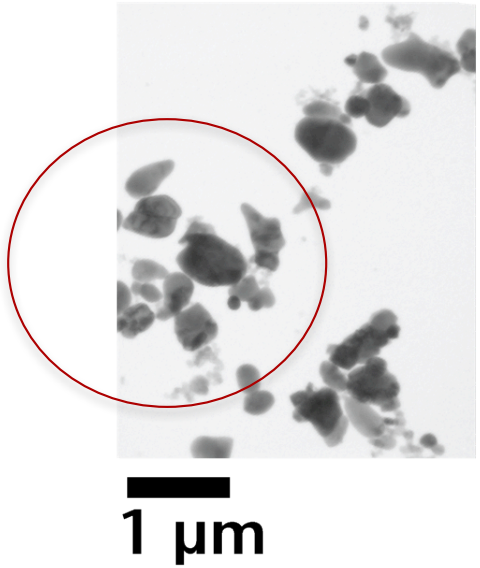

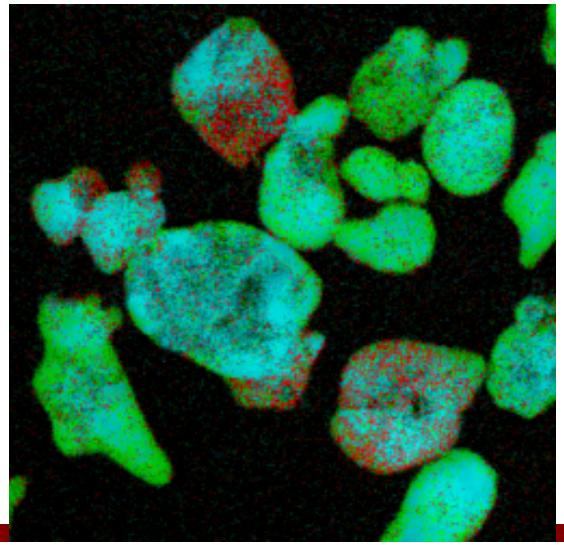

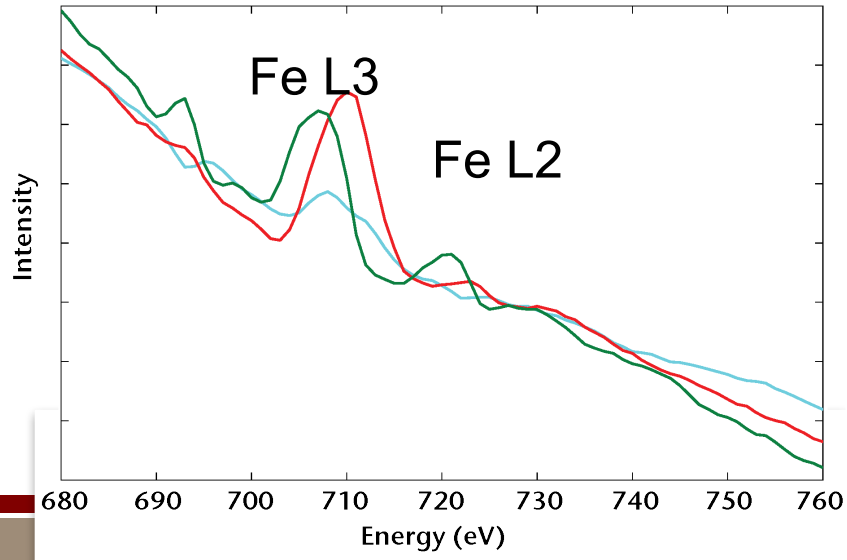

Extracted Particles on SiN Support

- Particles are extracted from a real battery

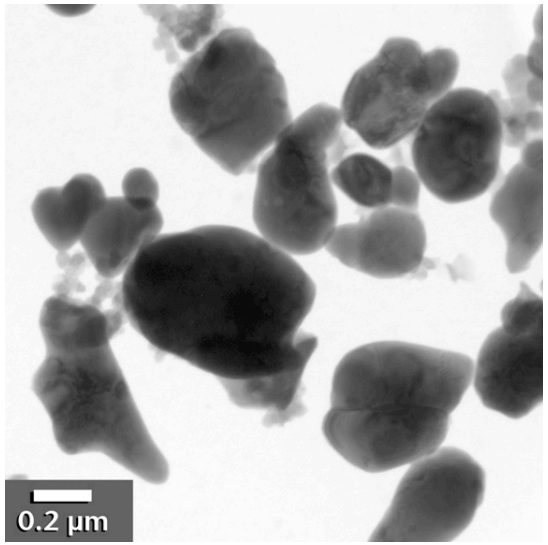

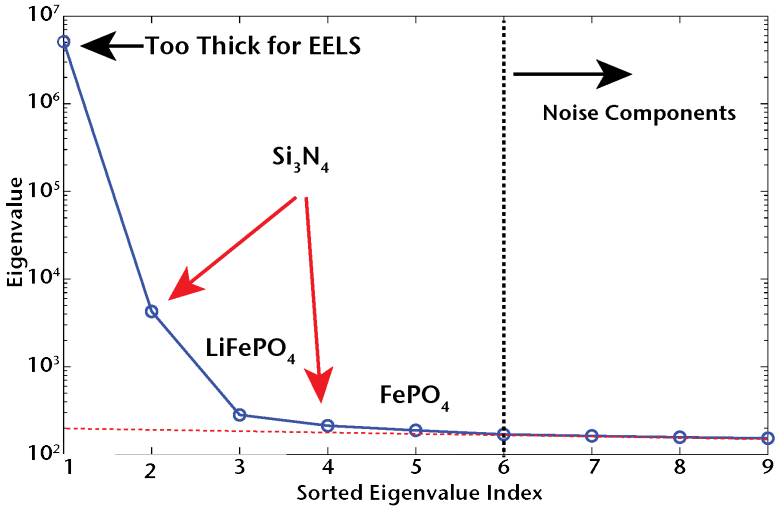

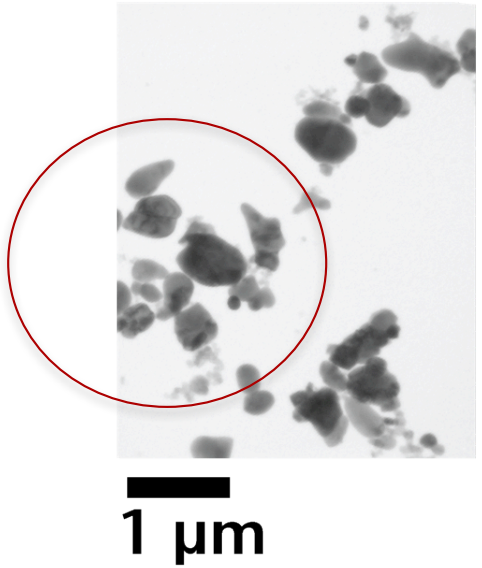

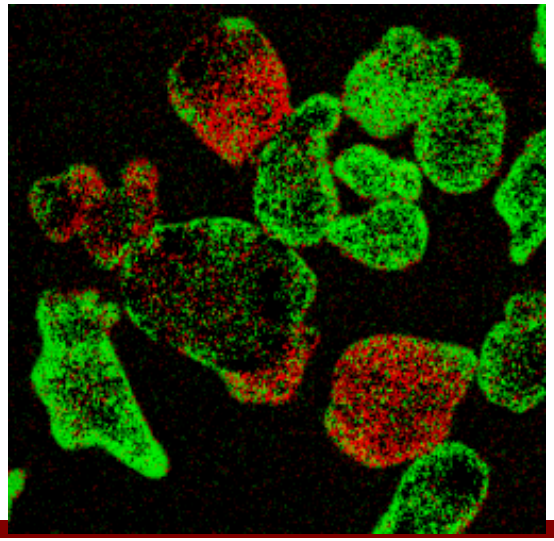

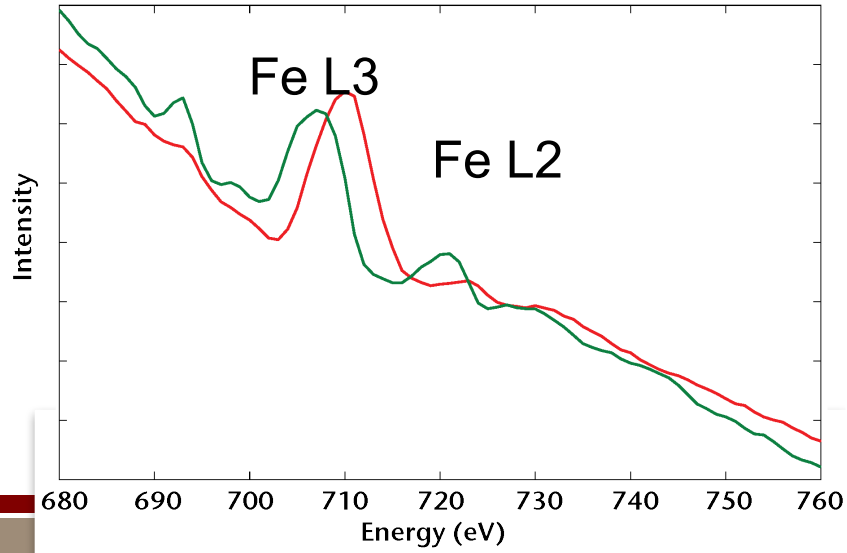

Extracted Particles on SiN Support

- Particles are extracted from a real battery

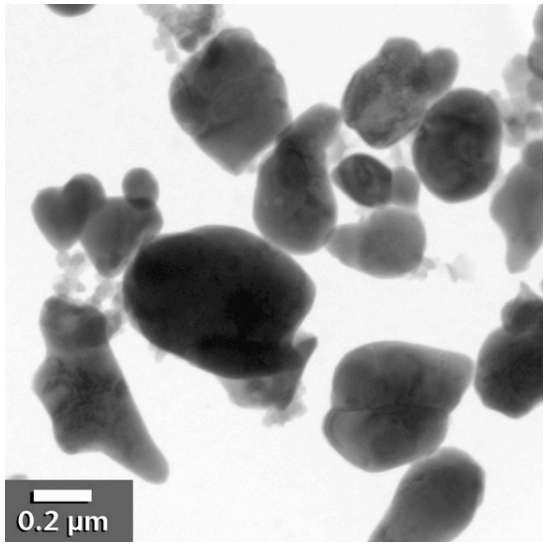

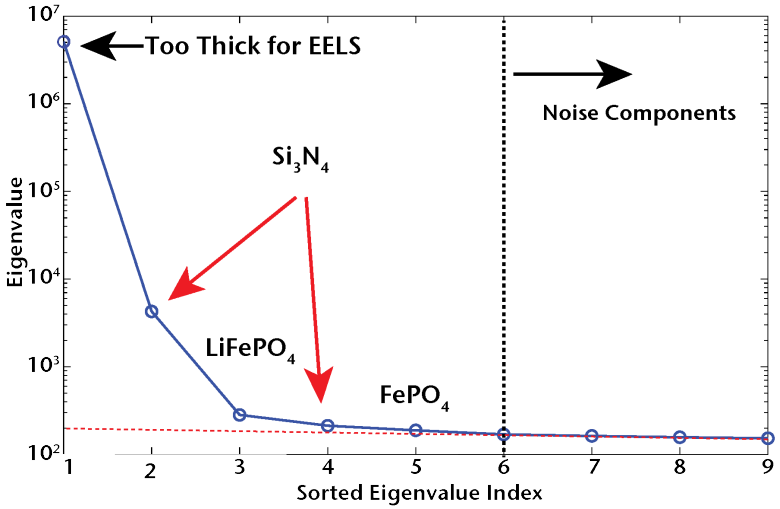

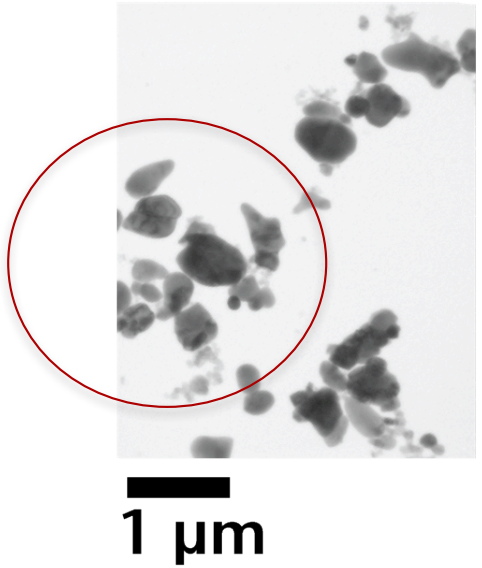

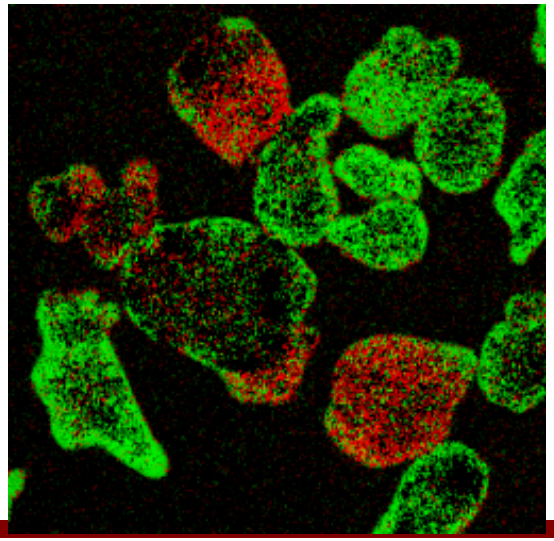

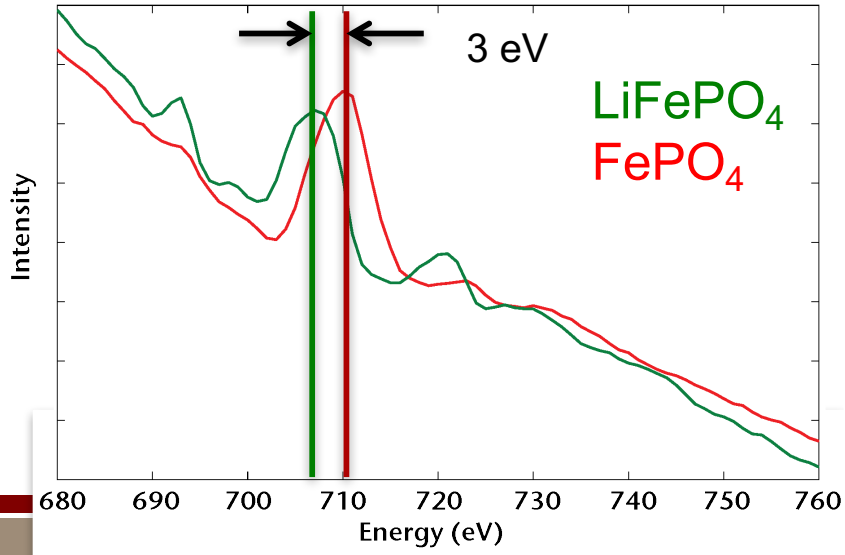

Validating the Spectroscopy

- Use Scanning Transmission X-ray Microscopy (STXM) at the Advanced Light Source to verify our results

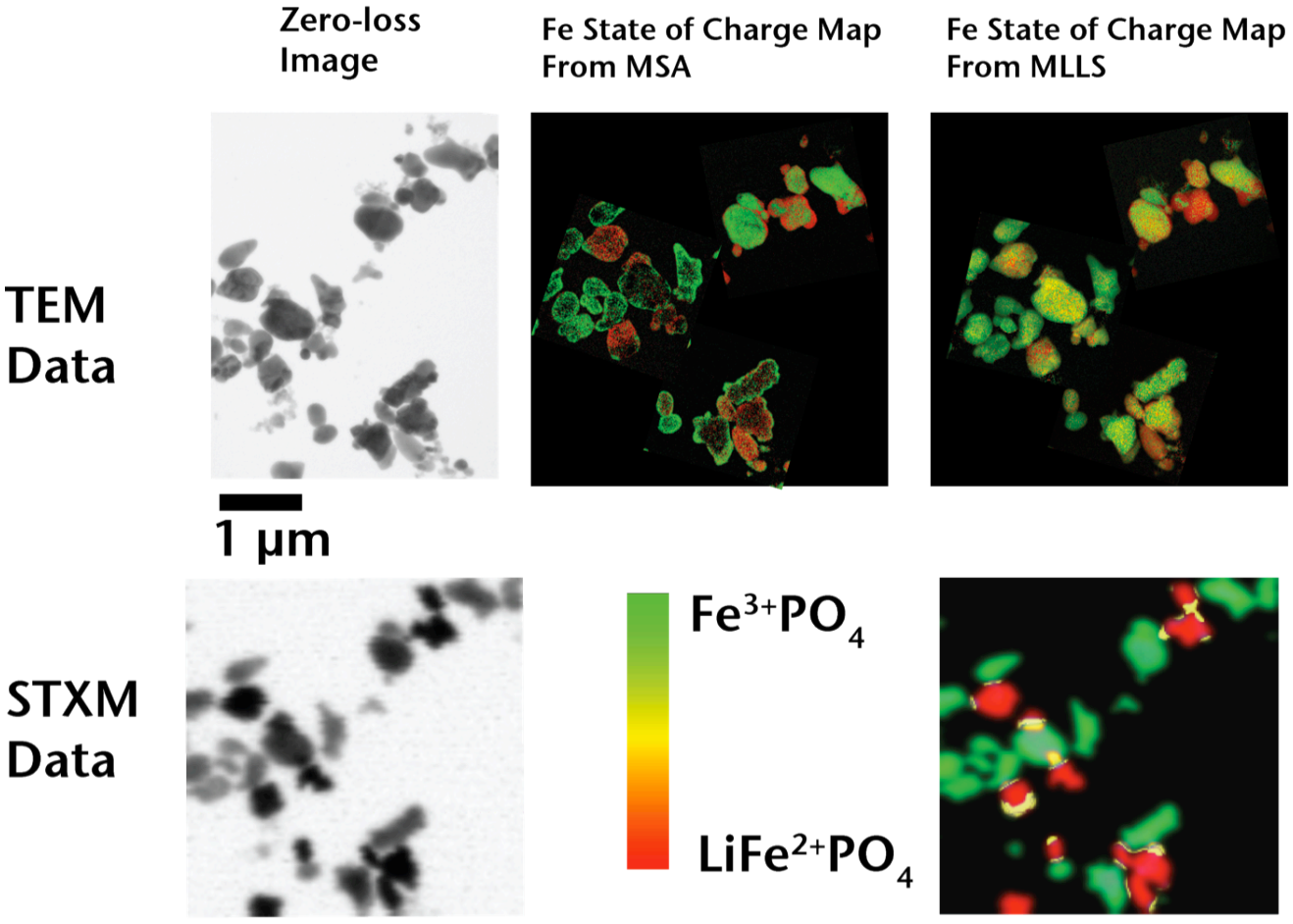

$$hue = \frac{I_{FePO_4}}{\left(I_{FePO_4} + I_{LiFePO_4}\right)}$$

Hue =0 red
Hue =1 green
Hue=0.5 yellow

Thinner samples are required for good spectroscopy

Making Thin Damage-Free Samples

- Sample Preparation Options
  - Particles on Grid – Too thick
  - Ion milling – Redeposition and too thick
  - FIB – Redeposition and damage
  - Ultramicrotome -Microstructure Preserved

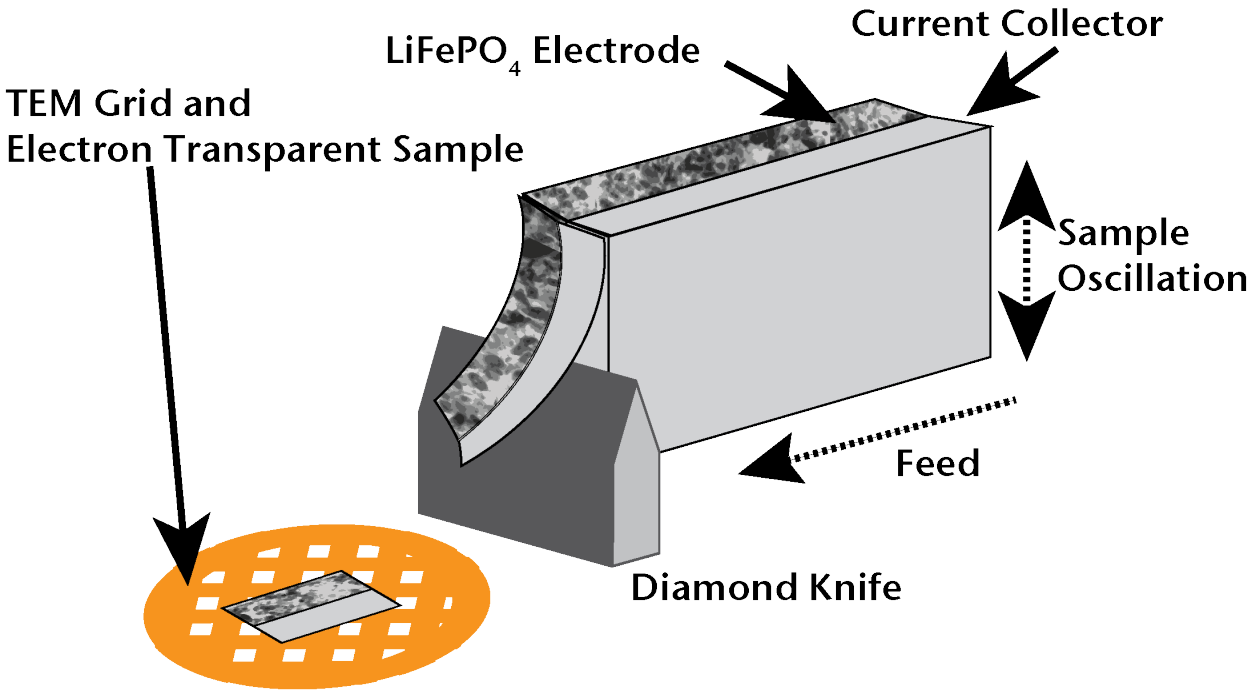

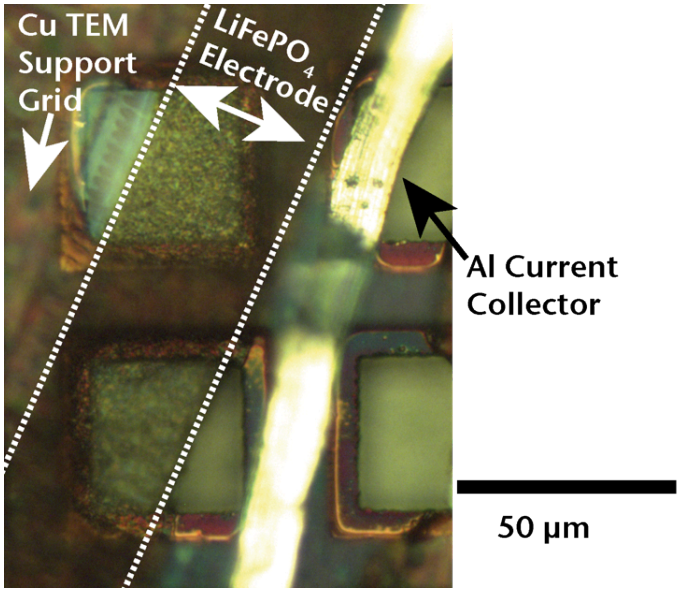

Validated Microtome Results

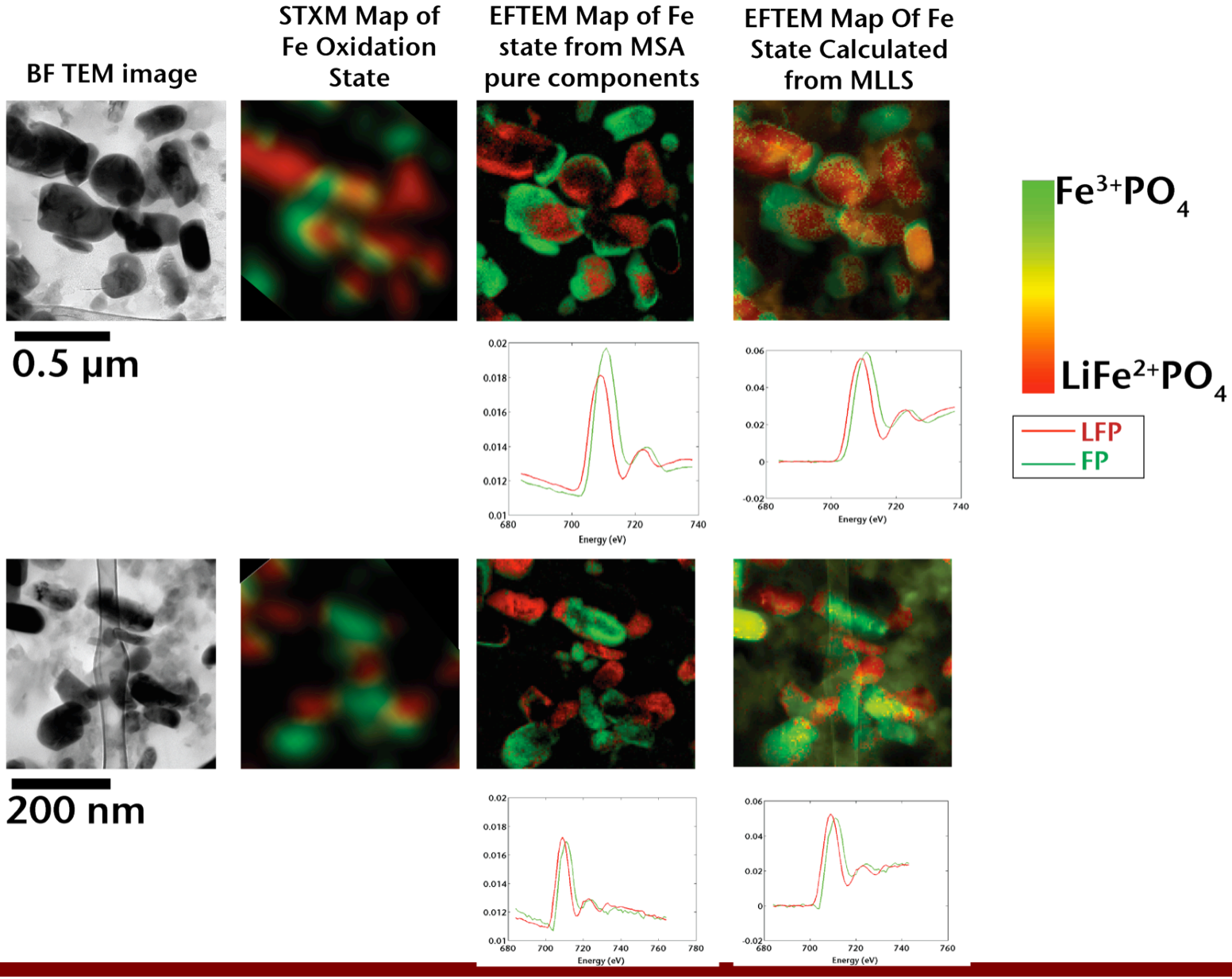

Large Areas Show Binary Phase Distribution

Sandia National Laboratories

BF TEM image

EFTEM Map of Fe state from MSA pure components

EFTEM Map Of Fe State Calculated from MLLS

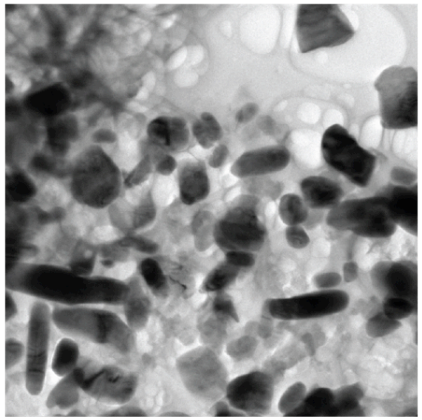

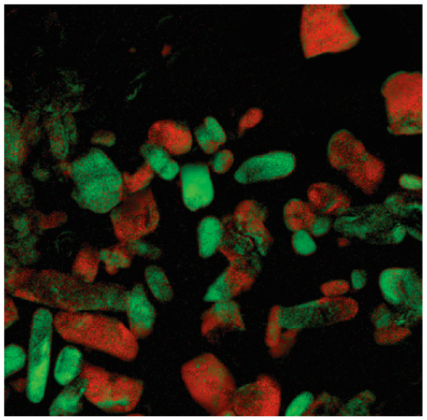

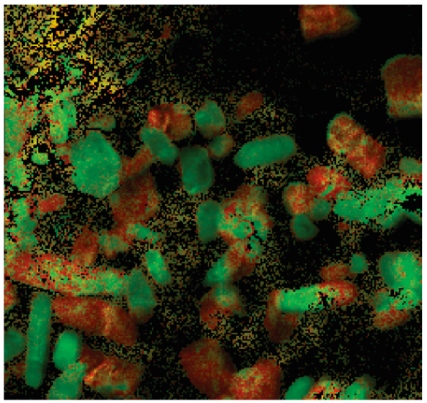

$Fe^{3+}PO_4$

$LiFe^{2+}PO_4$

1 µm

LFP

FP

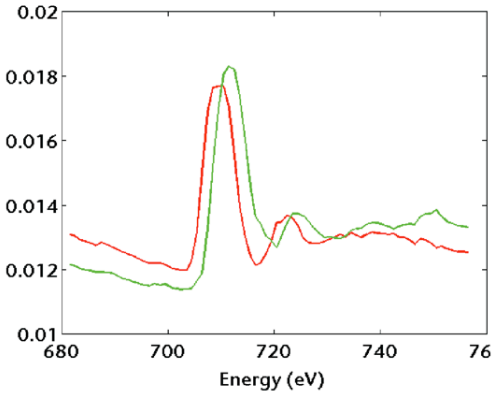

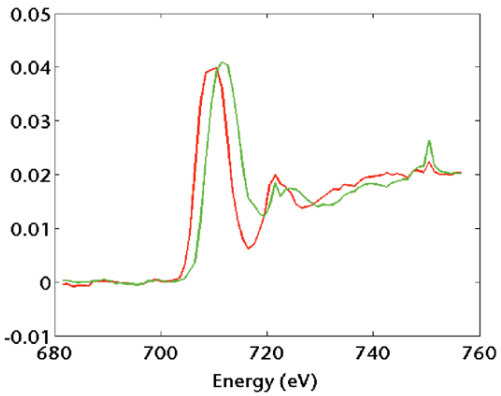

Large Statistical Information from combined STXM/TEM

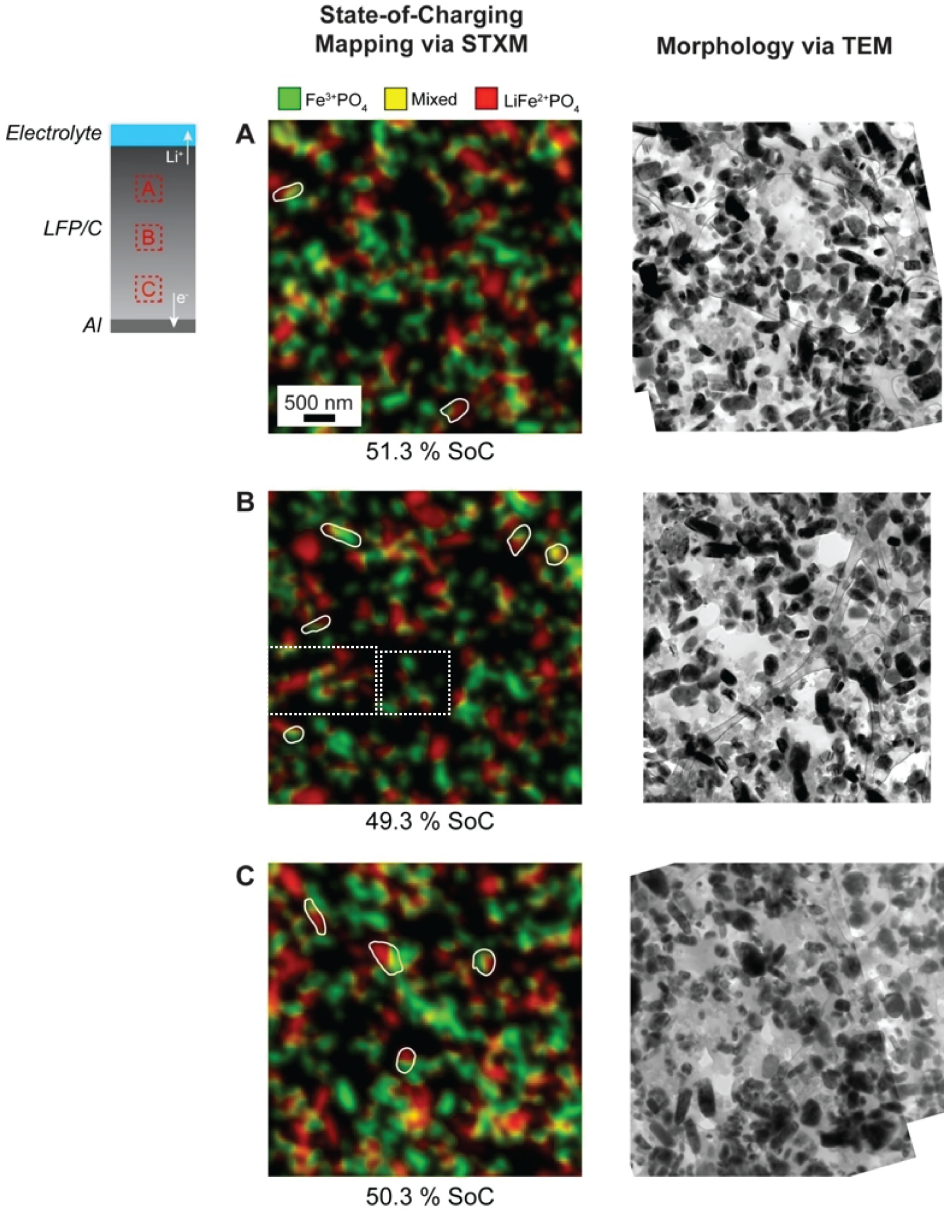

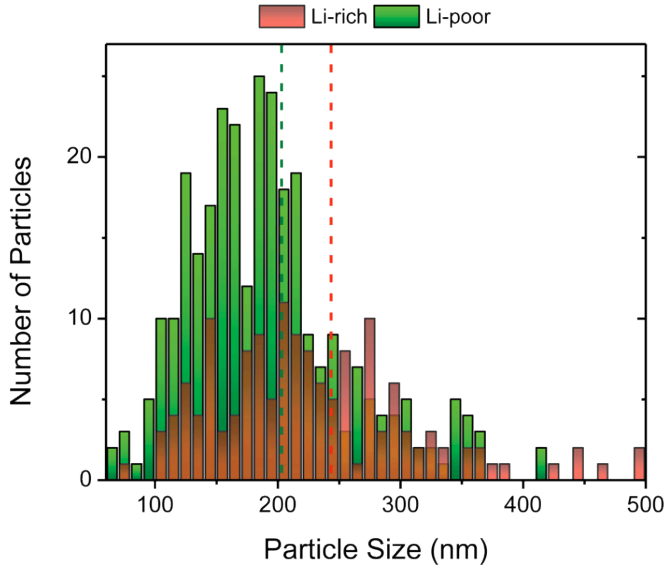

- Only 2% of particles are in a mixed state of charge (11/450)
- Particles that overlap can not be counted as one or the other
- There is a slight preference for smaller particles to transform first

Once the transformation has started, it goes fast

Chueh et al. *Nanoletters, 13, 2013, p.866*

A Simple Phenomenological Model: Nucleation-Limited Transformations

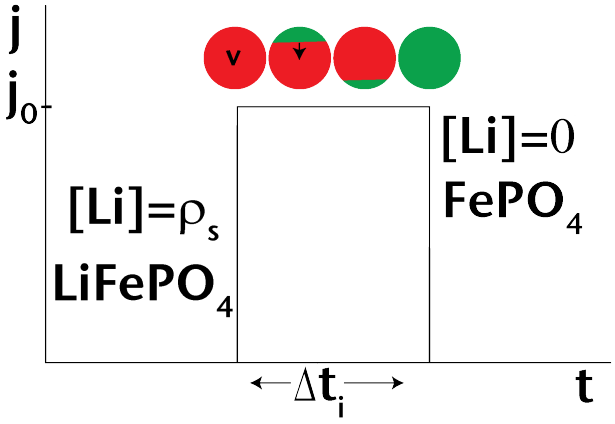

$$q = \rho_s v$$

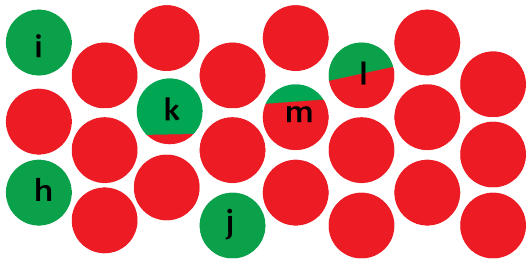

$$\Delta t_i \ll \Delta t_{\text{charging}}$$

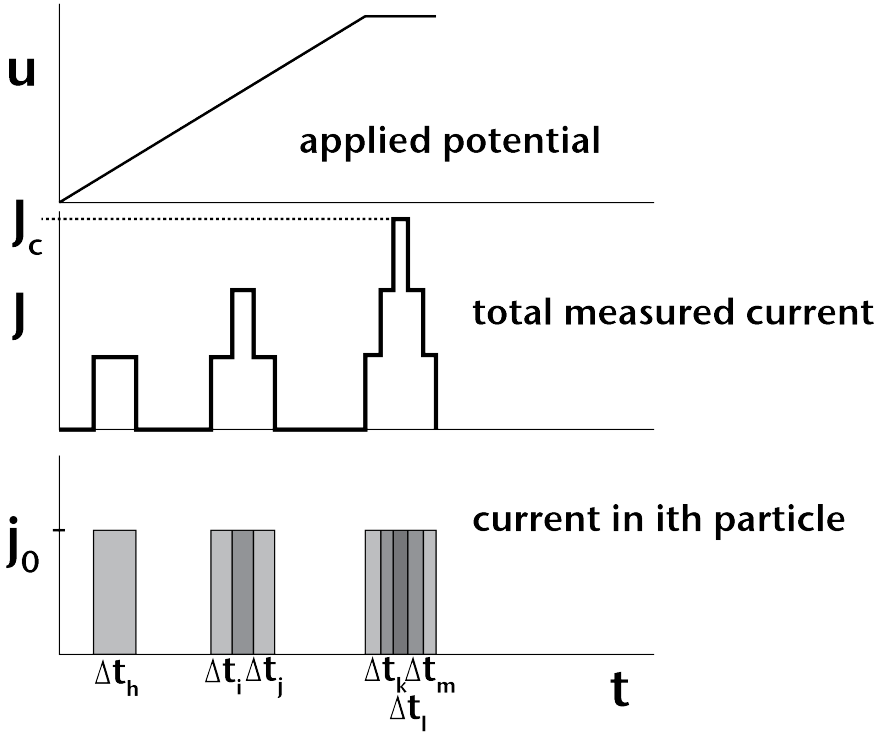

$$J = \frac{\Delta Q}{\Delta t} = q(v)\frac{\Delta N}{\Delta t} = q(v)\frac{dN}{dt} = q(v)\underbrace{g(v,t)}\underbrace{N(v,t)}$$

Probability of transformation i.e. nucleation rate (requires nucleation of new phase)

Untransformed Particles

$$g(v,t) = f(v)u(t) \quad \Rightarrow J_c \propto \int_0^\infty v\frac{\partial N}{\partial t}dv = u(t)\int_0^\infty vf(v)N(v,t)dv = \text{constant}$$

We know N(v,0), solve for N(v,t)

A Simple Phenomenological Model: Nucleation-Limited Transformations

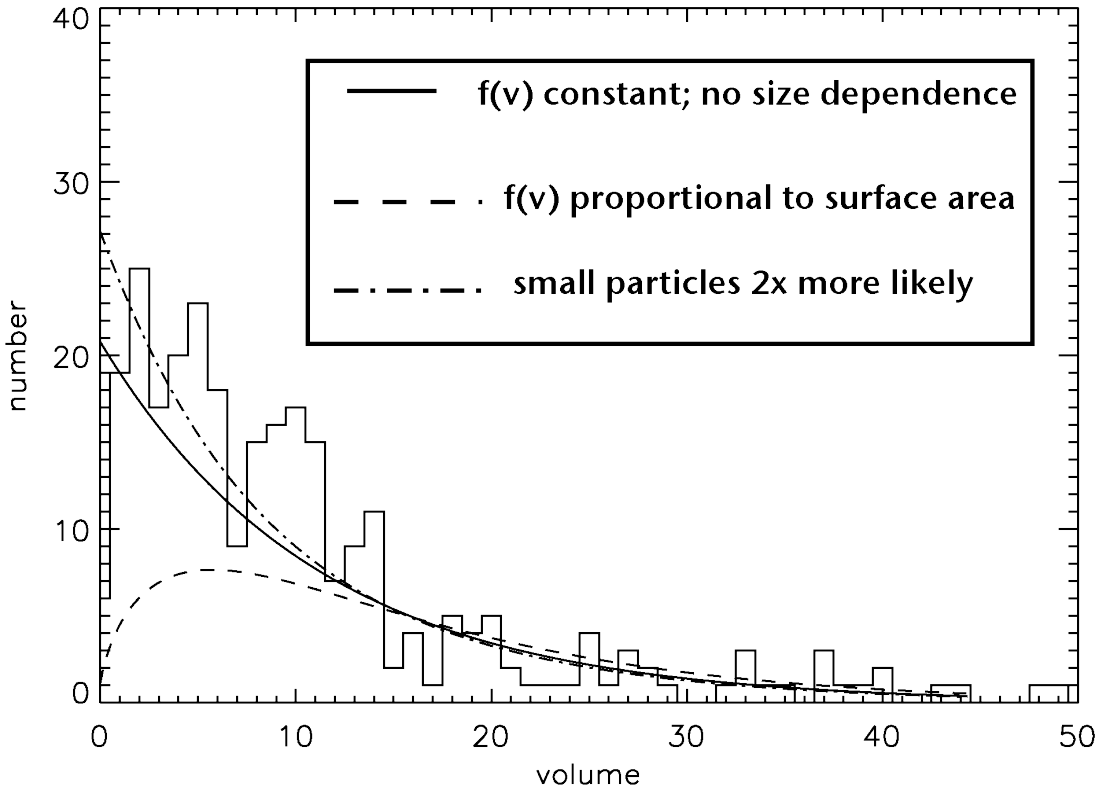

Particle Size distribution when 60% of particles have transformed

Given a theory for how nucleation rate depends on overpotential, u(t) would give overpotential as a function of time

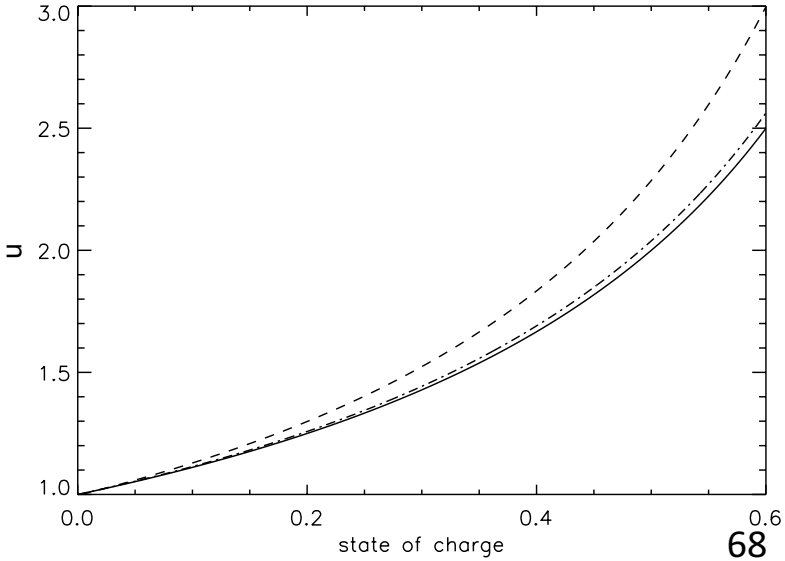

Reduce nucleation barrier to charge with less overpotential

At Large Overpotential More Nucleation of New Phase

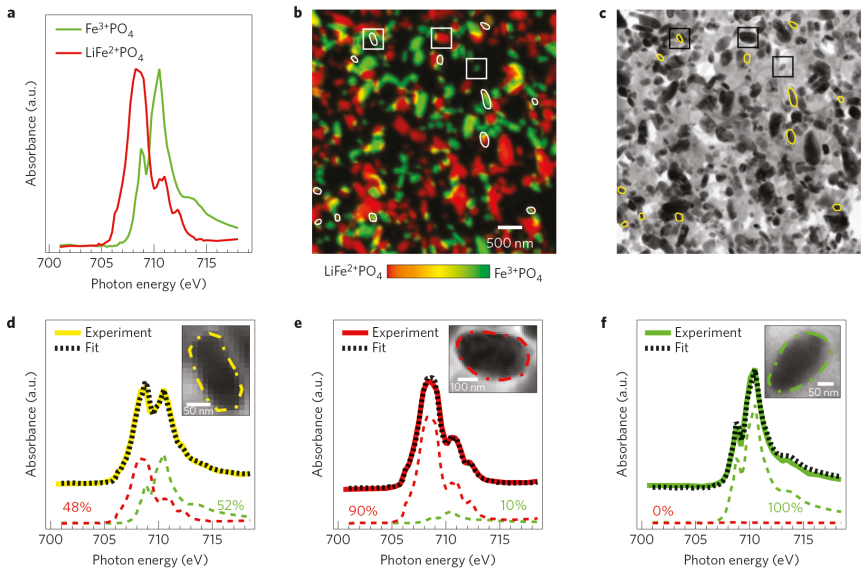

5 C Charge rate

Faster charge/discharge rate more actively intercalating particles carrying the current, but the current/particle remains the same

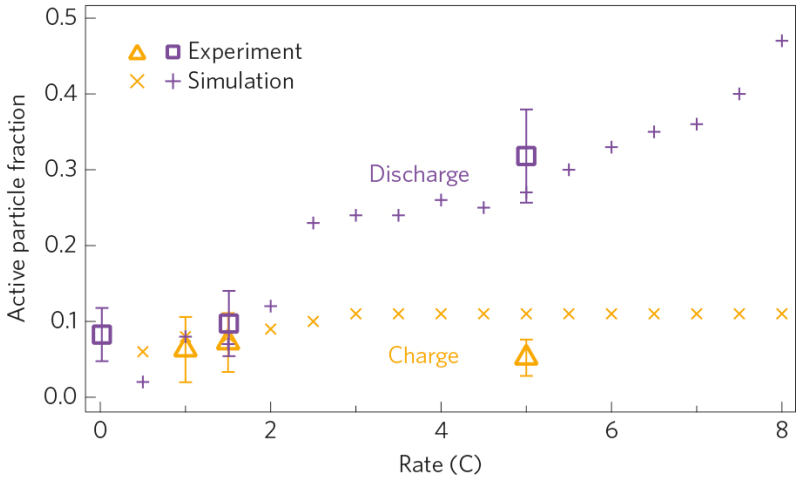

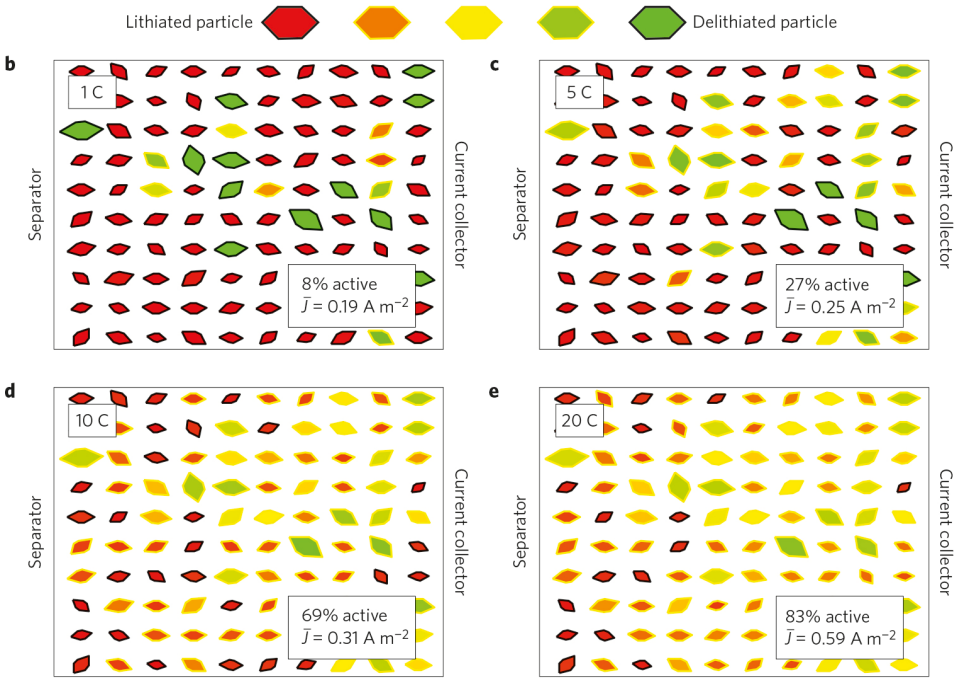

Linking Microstructural Measurements to Transport Phenomena

Sandia National Laboratories

- Helium bubbles formed by ^3H β decay, α decay, neutron (n, α) reactions
- Rh-ion transport during fabrication of nanoporous hydrogen storage materials
- Li-ion transport during charge/discharge of $LiFePO_4$ electrodes
- Reliability of aged electronic components with variability in manufacturing process

Poor Electrical Performance in JFET

Some parts exhibited higher contact resistance

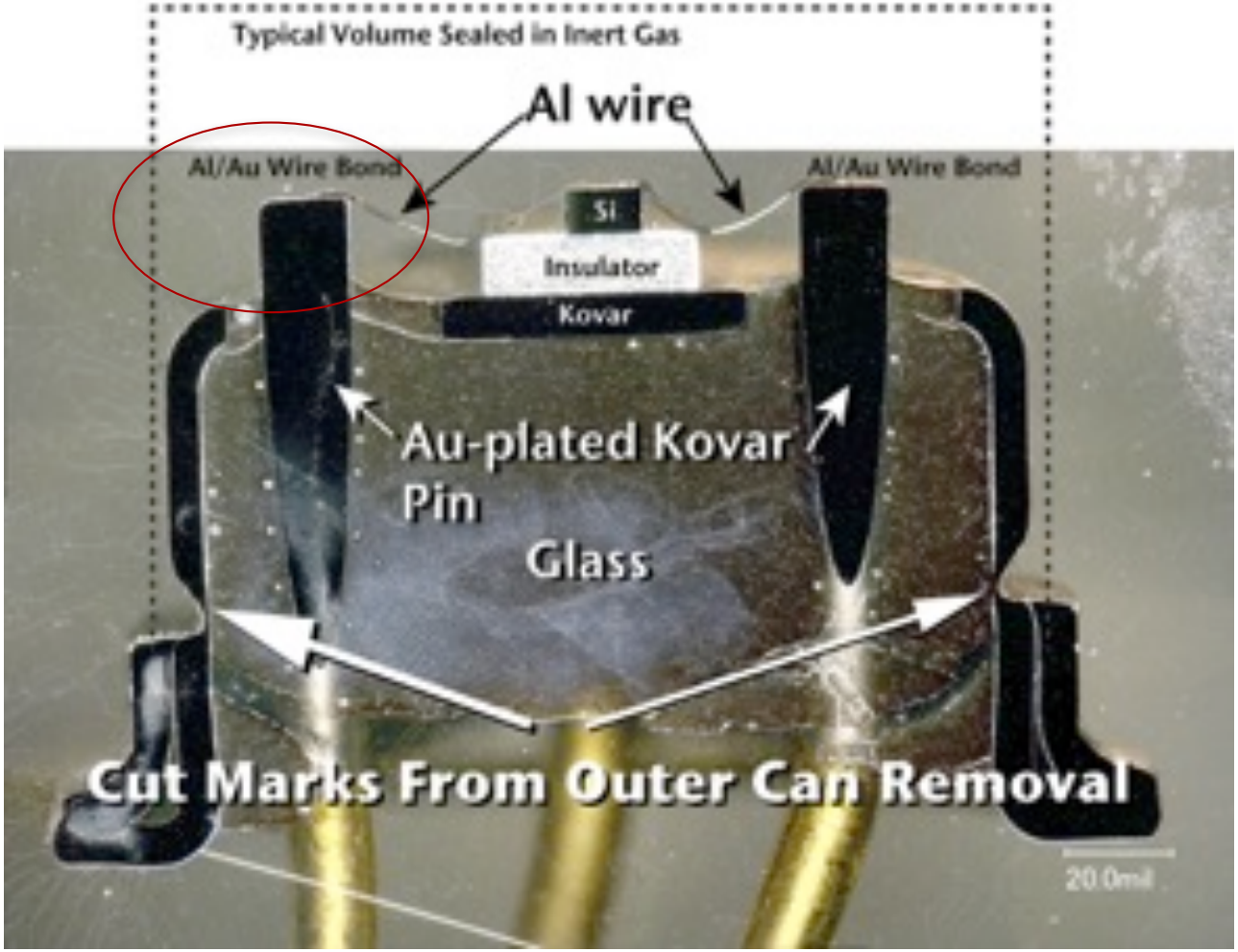

Poor Electrical Performance in JFET

Sandia National Laboratories

Contact Resistance was too high

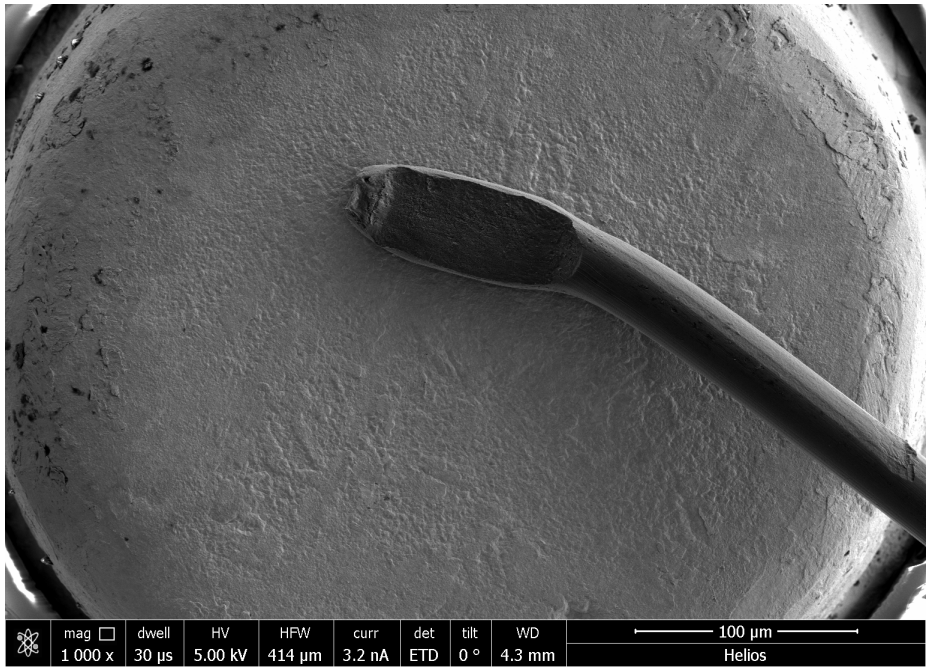

Smooth Au surface

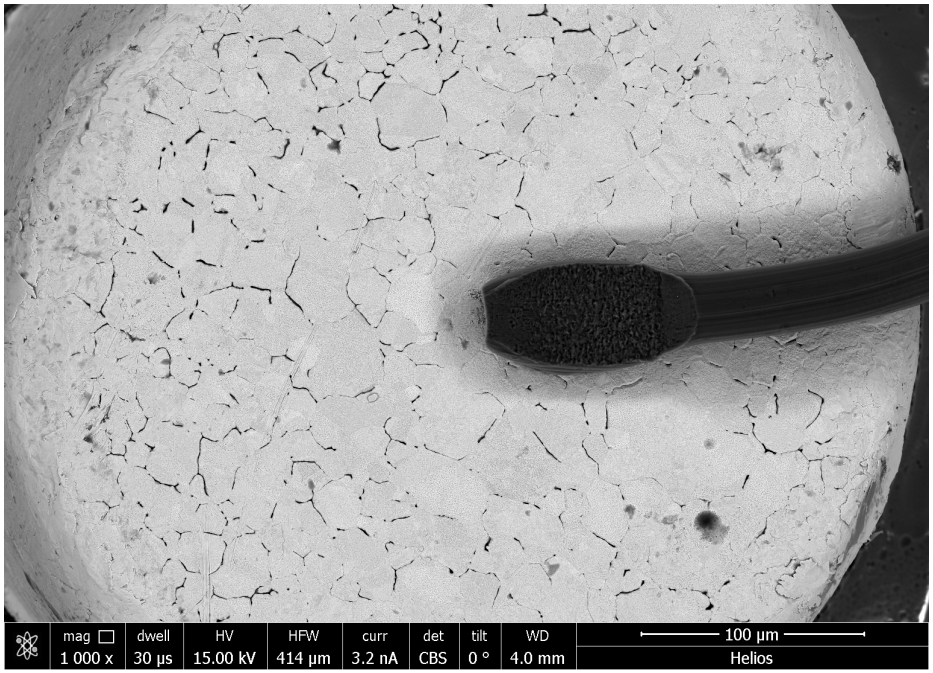

Mud-cracked appearance

Why do these exhibit different electrical performance, and does the mud-cracking have something to do with it?

-A microscopic forensic investigation

Explanation for Intergranular Corrosion

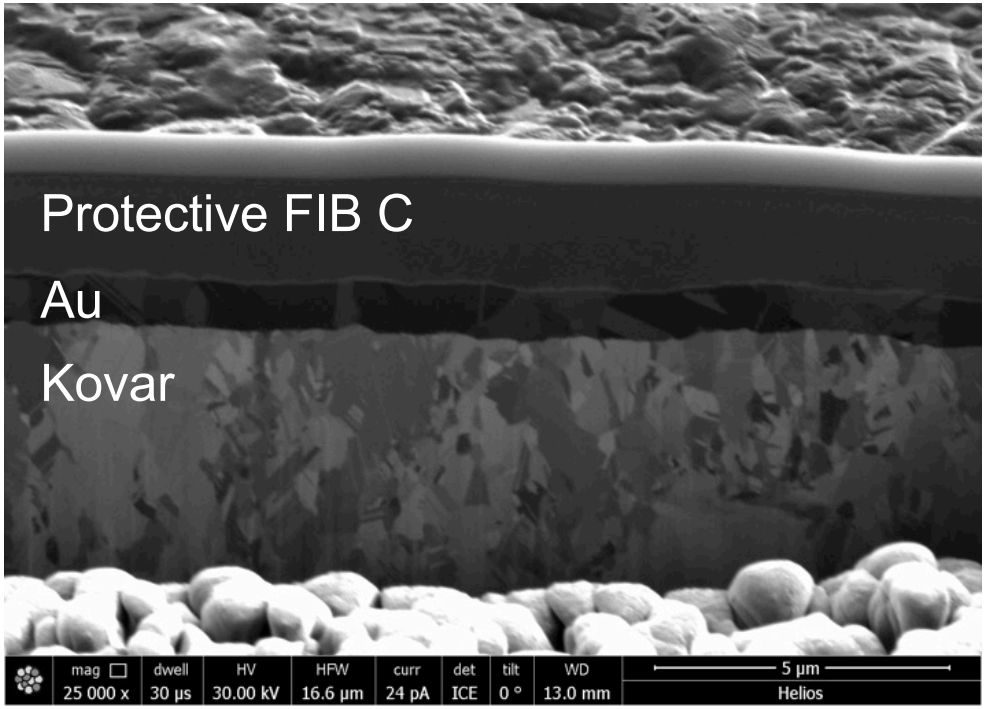

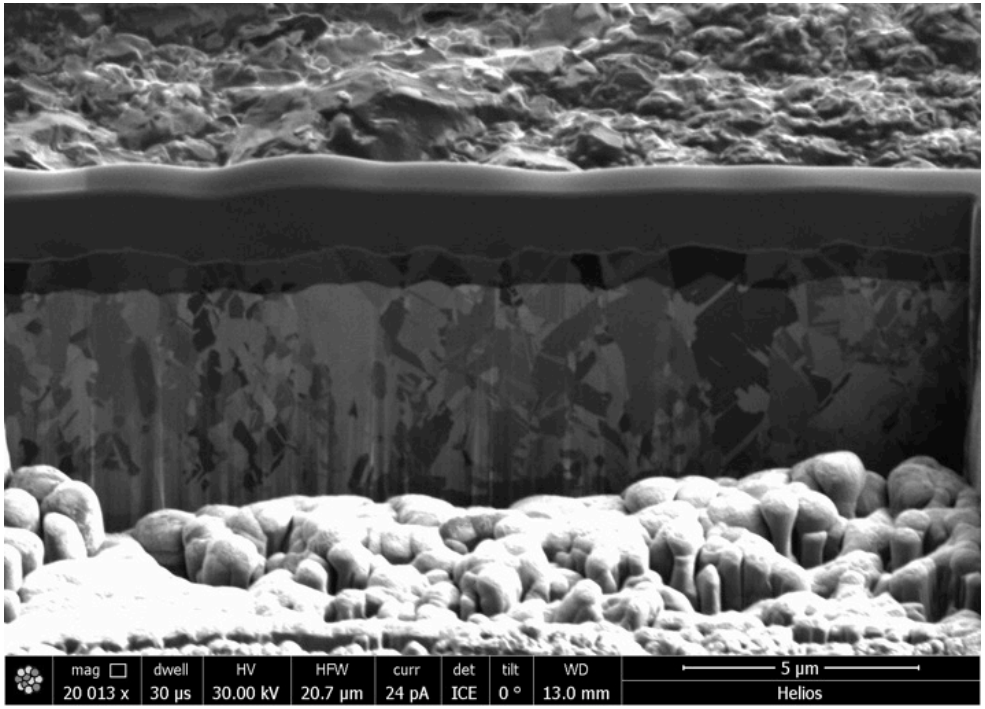

Typical Au plating/Kovar microstructure

Cross sectional images of posts from storage show a fine grain structure in the kovar. These channeling contrast images suggest a grain (subgrain) boundary structure with a length scale of approximately 1 µm.

Explanation for Intergranular Corrosion

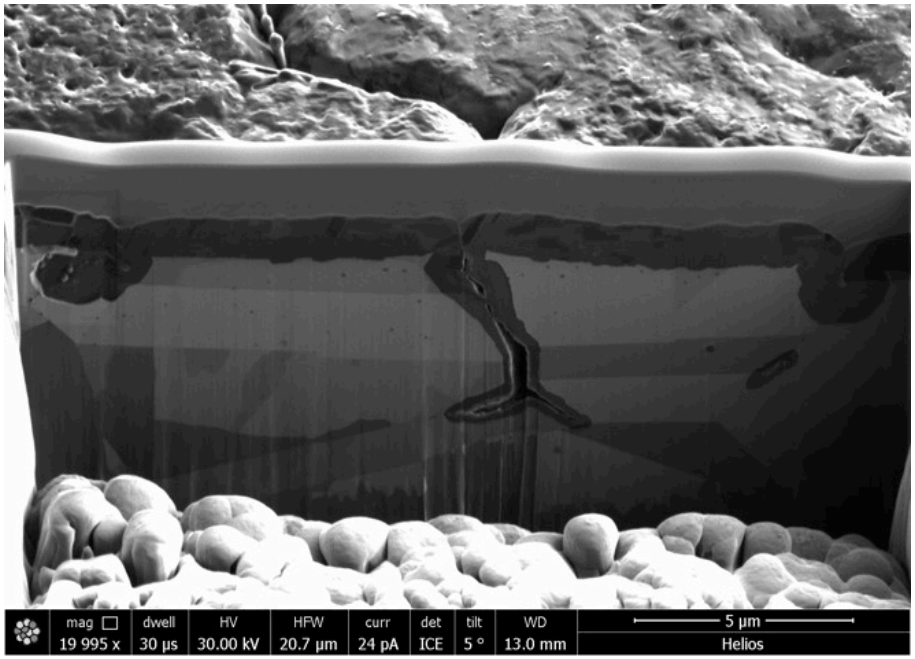

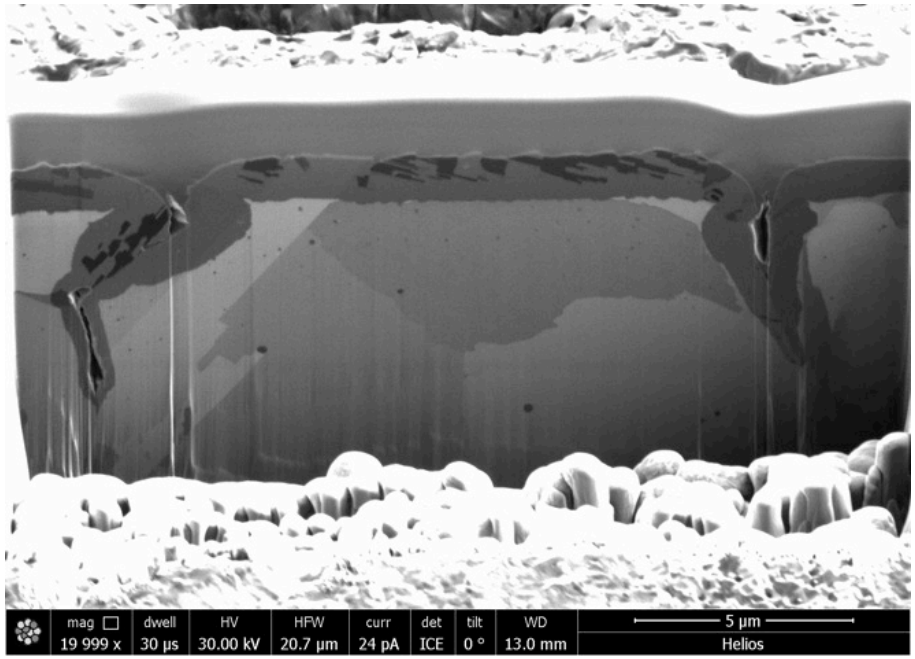

Atypical Au/Kovar Microstructure

In these images the relevant grain (subgrain) structure has a length scale of approximately 5 µm. The images show that the subgrain structure is much larger than in the previous images. This suggests that the kovar pins experienced a different thermal history.

Explanation for Intergranular Corrosion

- There is not a likely heat source with sufficient thermal energy in the operating environment to do this
- This thermal history can have two origins:
  - It is the result of the manufacturing processes. Either the as-received kovar had a different structure to begin with,
  - Or the glass-to-metal sealing process was different and the kovar pins got hotter in a subset of the parts.
- When the oxide cleaning process is applied to a kovar pin with a larger grain structure, the same process parameters could lead to over-etching the kovar and enhanced etch of the grain boundaries (intergranular corrosion).
- When the subsequent Au film was plated onto a rougher kovar surface, it plated into the etched grain boundary regions, this results in the mud-crack appearance on the surface of the Au plating.

Interfacial Defects Associated with Atypical Part

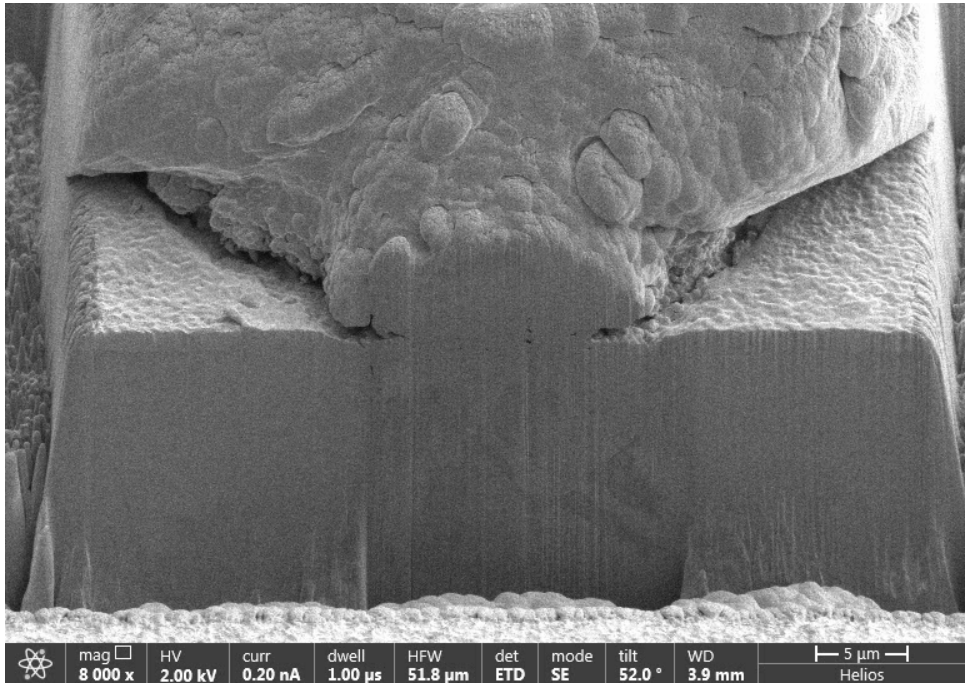

Typical Consistent Interface

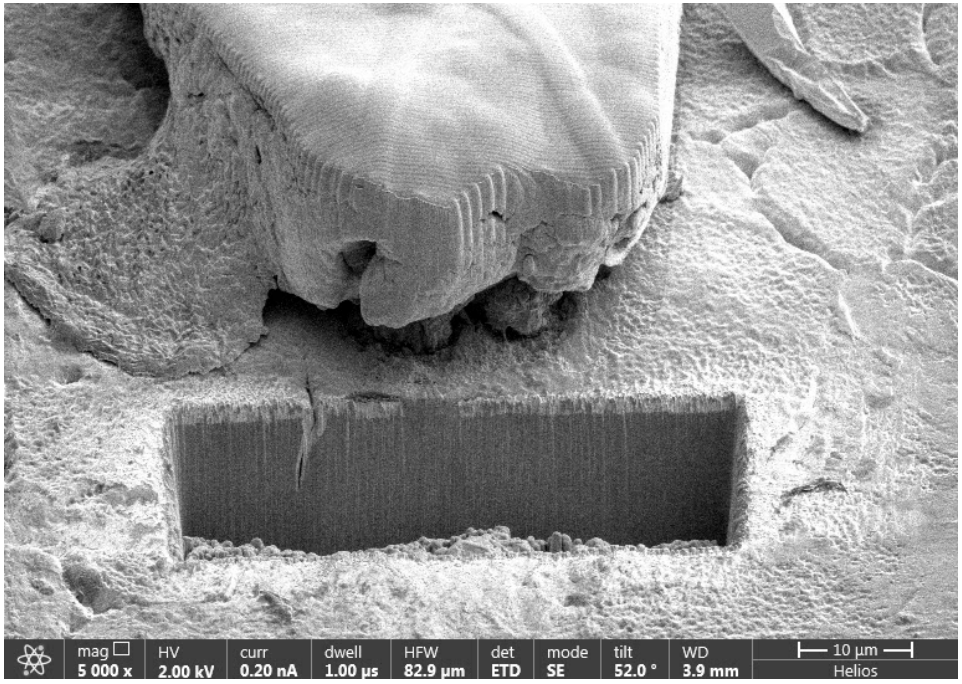

Highly Defective Atypical Interface

Interfacial Defects Associated with Atypical Part

- There are more interfacial features observed in atypical part that can cause an increase in contact resistance relative to normal

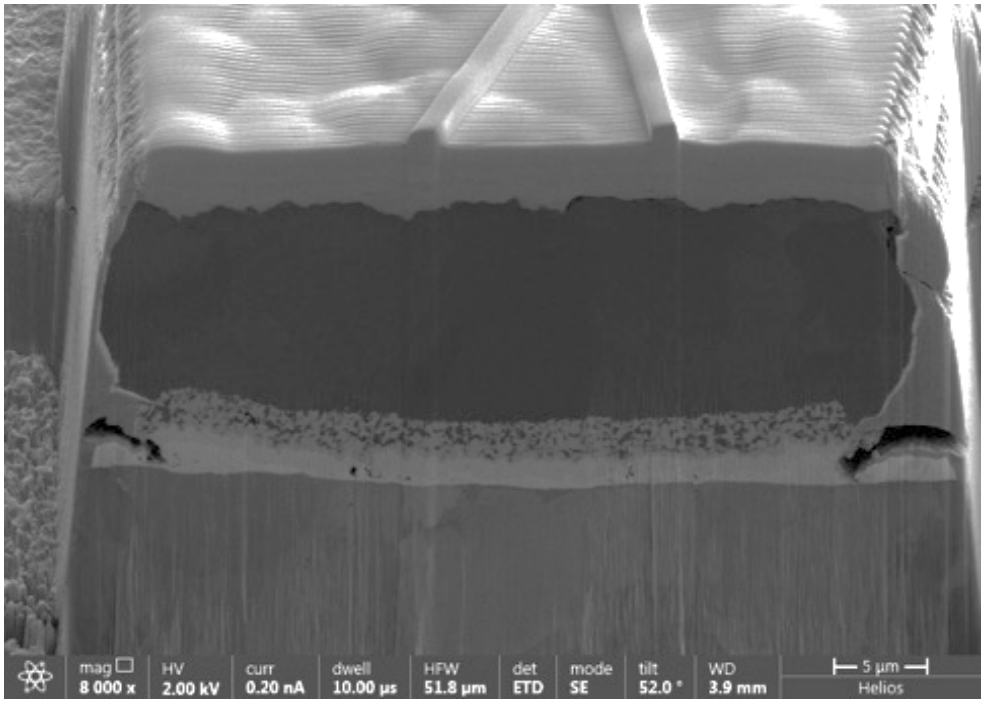

Typical Consistent Interface

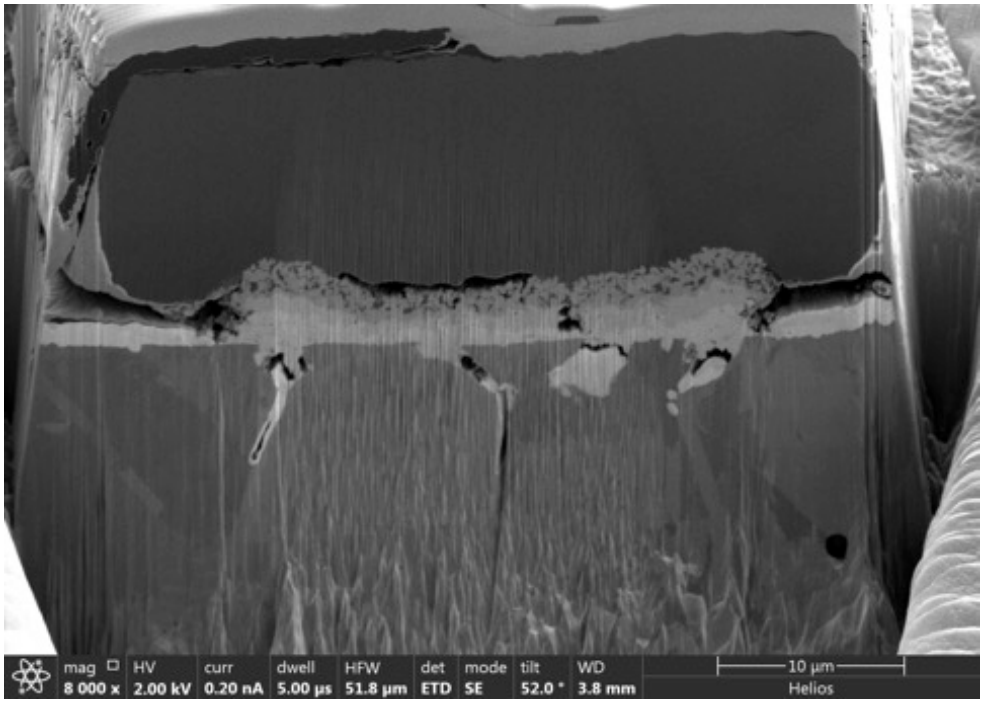

Atypical Defective Interface

Are these defects consistent with lower strength and a source of higher resistance?

Al Wire Bond Pull Tests: Bonnie Antoun and Kevin Connelly

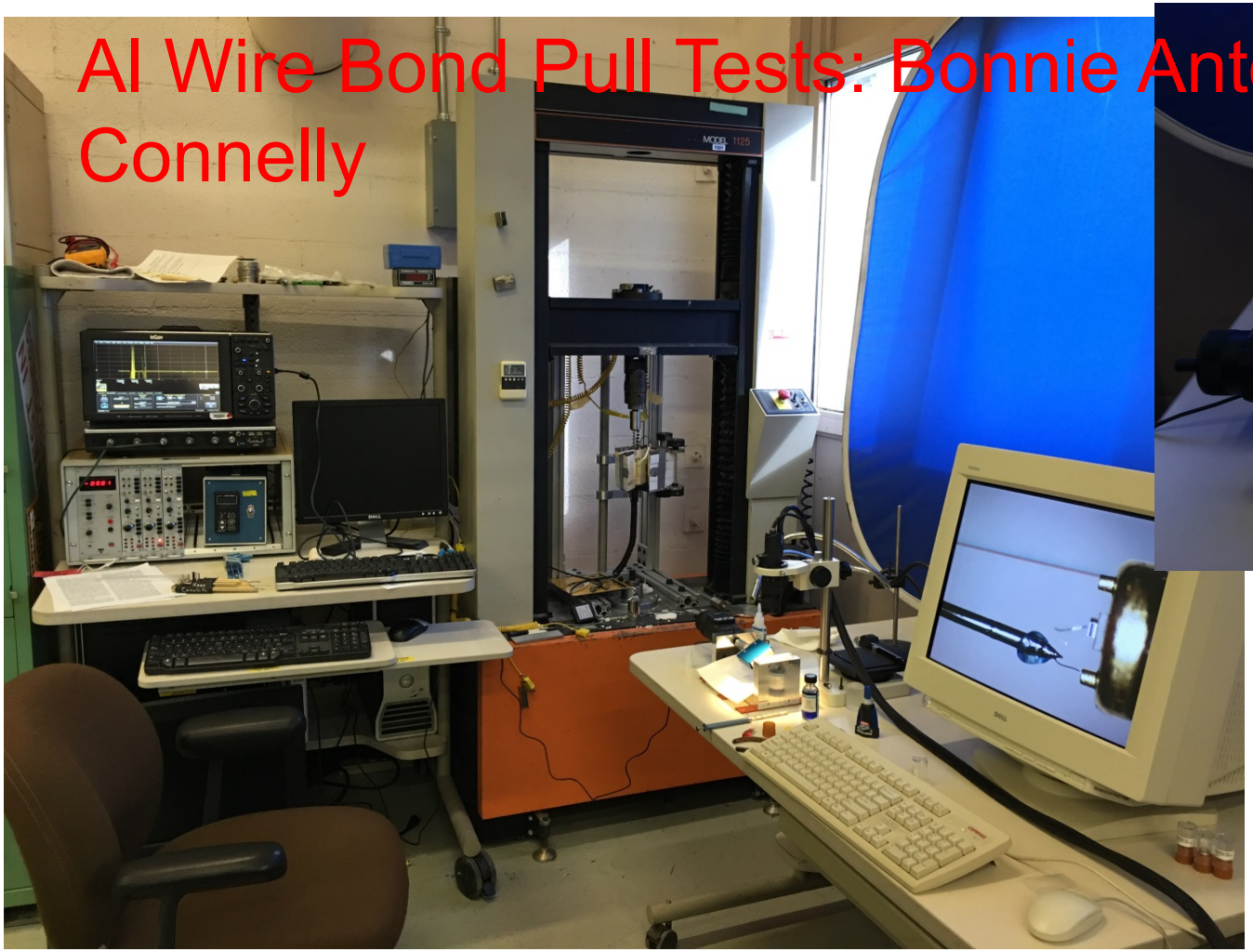

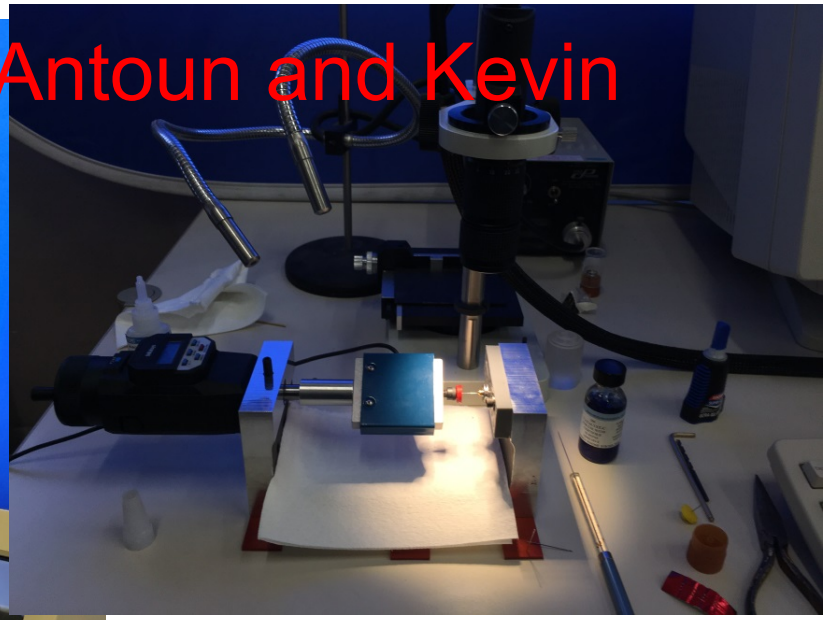

Custom tabletop test apparatus for measuring load to separate wire from gold post

- Using older Keyence microscope to allow viewing of small wire and parts in order to test properly (alignment, gluing wire to loading pin)
- Custom aluminum frame (modification to an existing part from our lab) holding: 1 lb load cell, Mitutoyo digital micrometer head, adjustable part/post holder, oscilloscope
- Final iteration used a steel pin pushed through a printed plastic holder to preserve each wire after failure

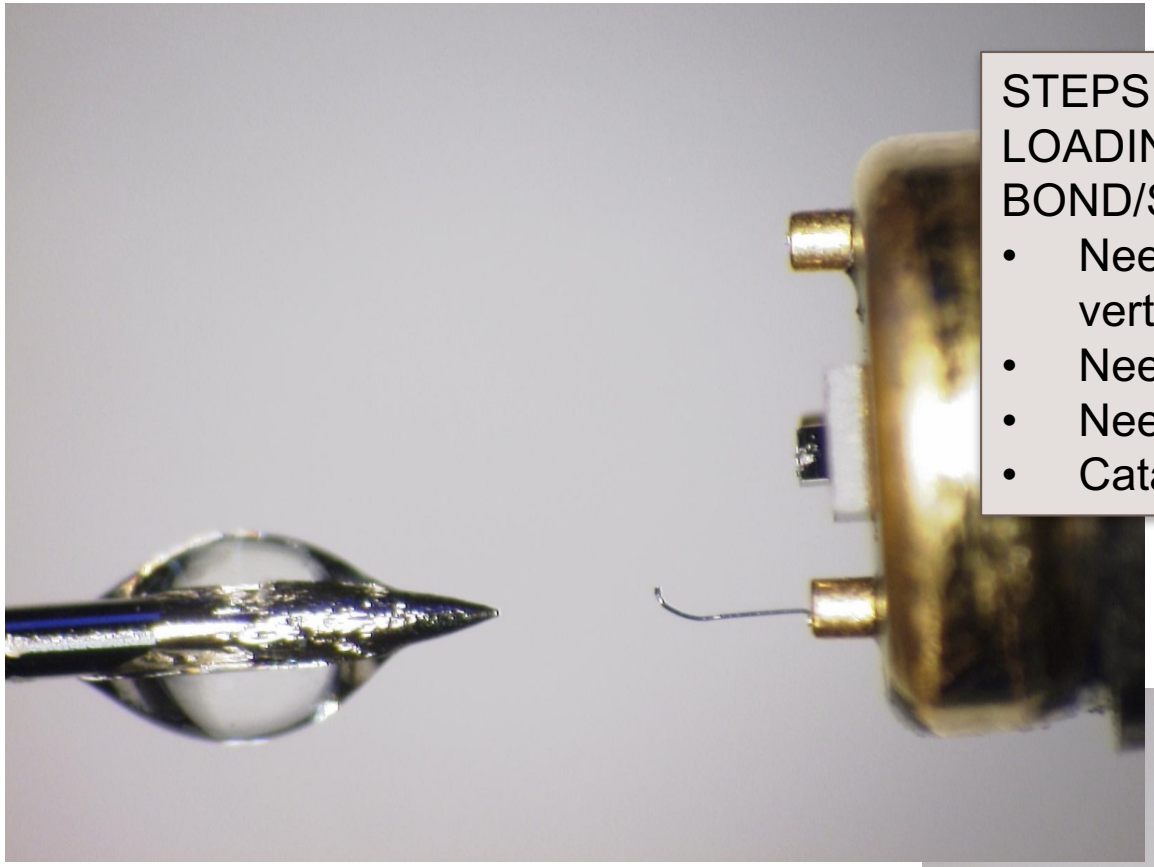

STEPS TO ATTACH WIRE FOR TENSILE LOADING UNTIL FAILURE AT GOLD POST BOND/SPOT WELD

- Needle aligned to wire (horizontally and vertically)
- Needle pulled back, MB200 applied to Needle
- Needle re-aligned with wire
- Catalyst C applied twice and allowed to dry

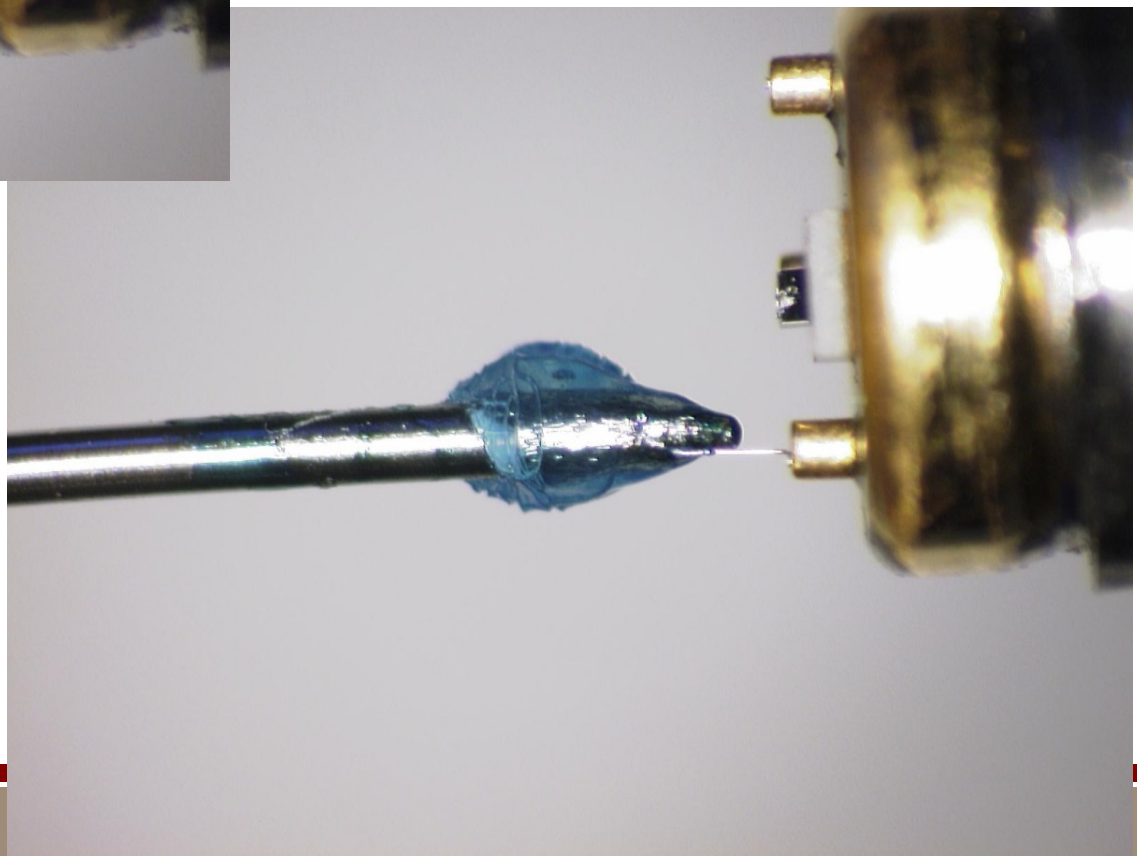

39 Tests: 6-10g Load to Failure Typical from Historical Records

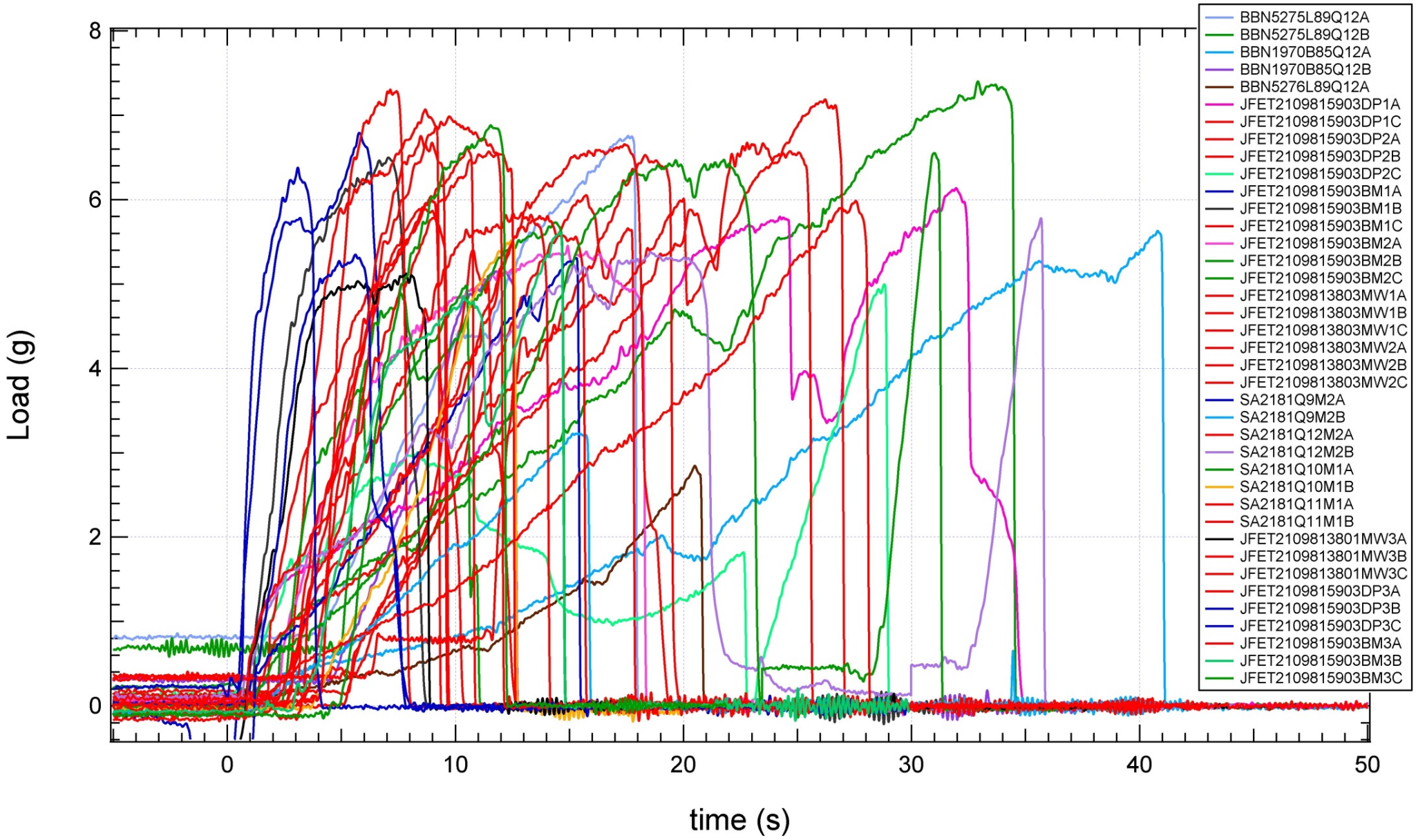

Pull Test Results

- Loads to Failure
- All tests
  - 5.98 ± 0.97 g
- Average results consistent with previous measurements
- Two lowest tests cause higher standard deviation

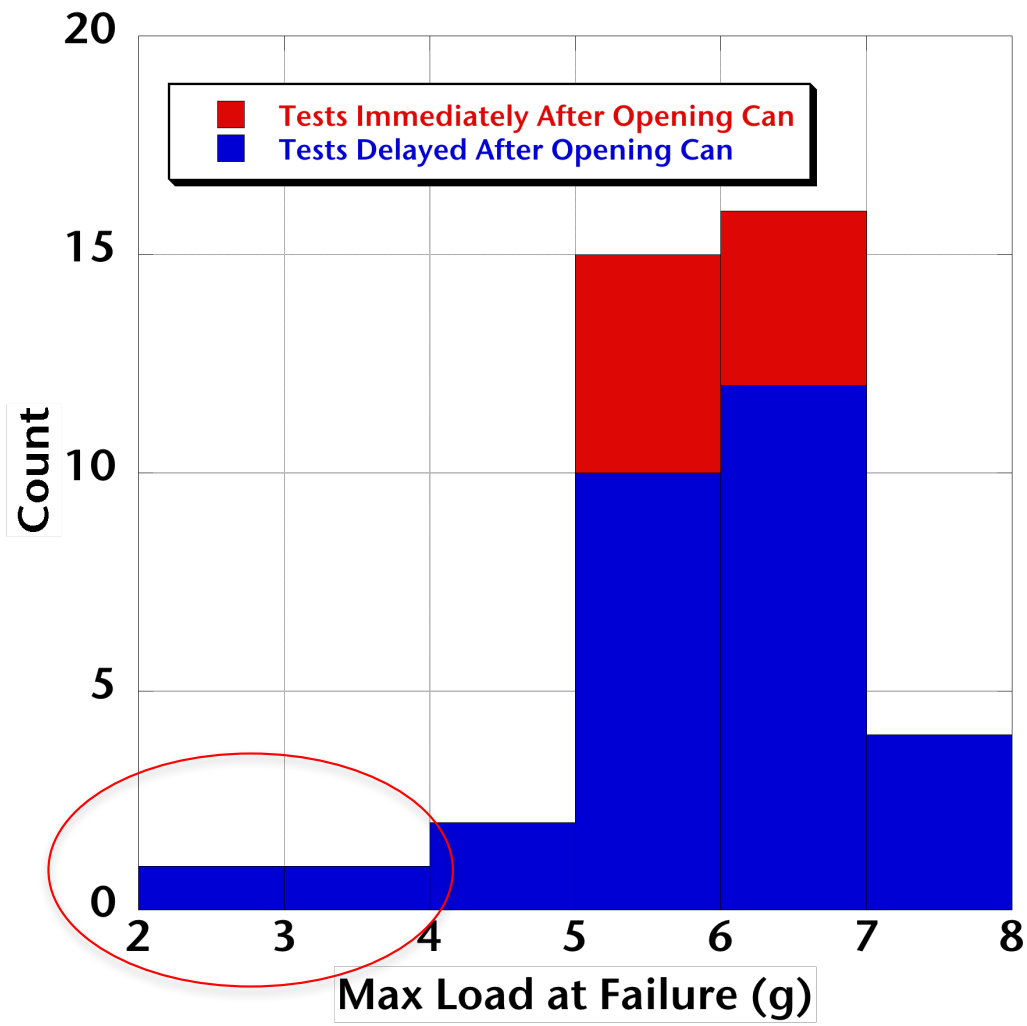

Carbon contamination and exposure to air does not affect pull test results.
Results are consistent with previous studies except for 2 low outliers.

Poor Electrical Performance Correlates with the Mechanical Performance of the Wire Bond

Sandia National Laboratories

Fracture always occurred in Al wire, not at Au/Al interface → the cause of high contact resistance does not affect interface strength

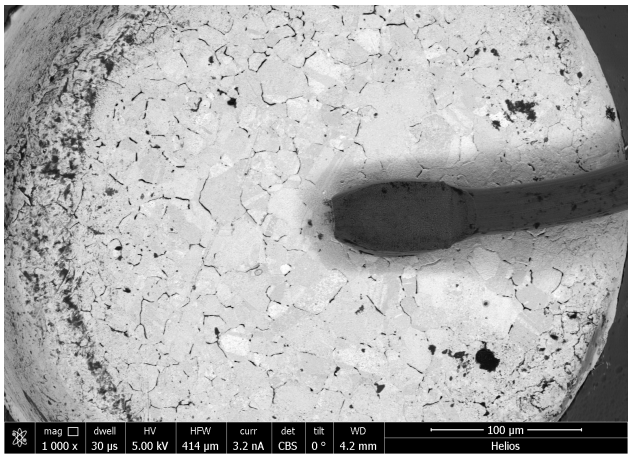

Our suspect part failed at 3.23 g

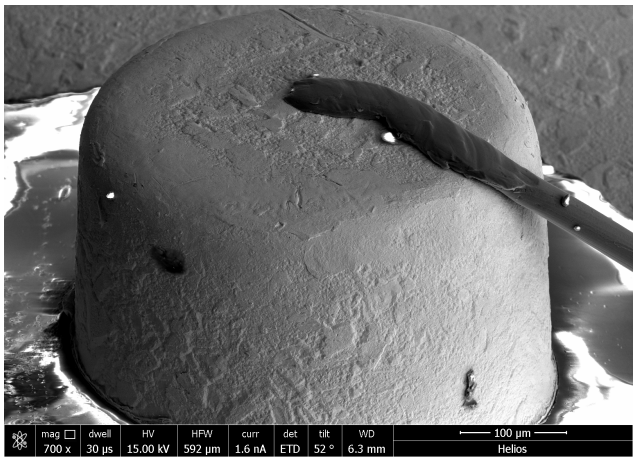

This failed at 2.84 g

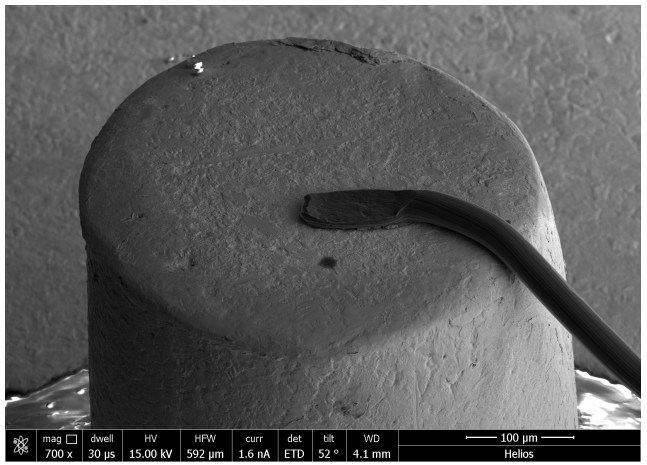

Typical part ~6 g failure

Mud cracking only appears on one part, but the deformation of the Al wire is suggestive that this could be related to low strengths

Evidence for Additional Deformation of Al in our "Suspect" Part

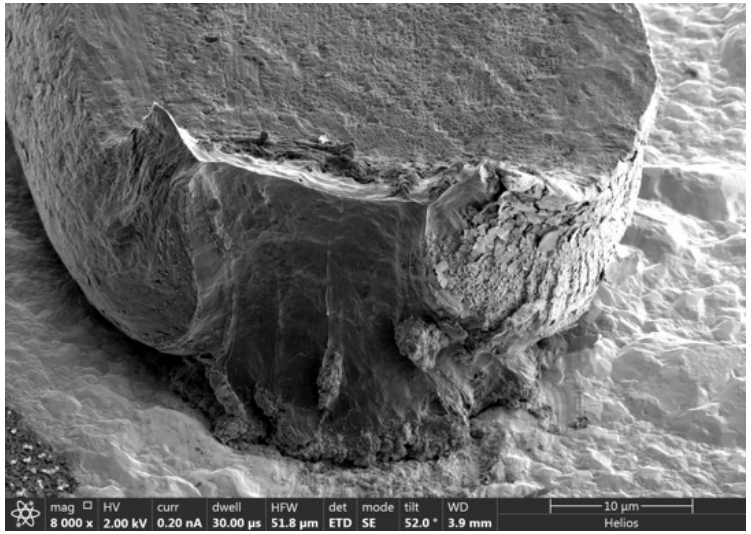

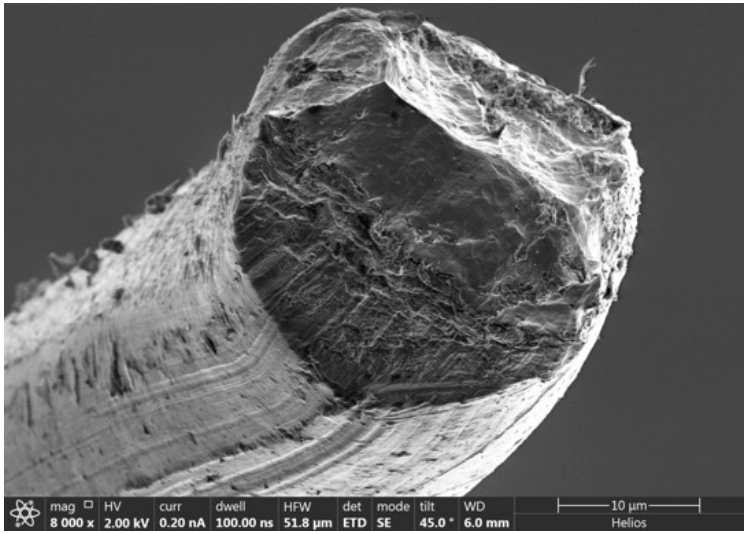

Typical wire shows smooth necking to knife edge

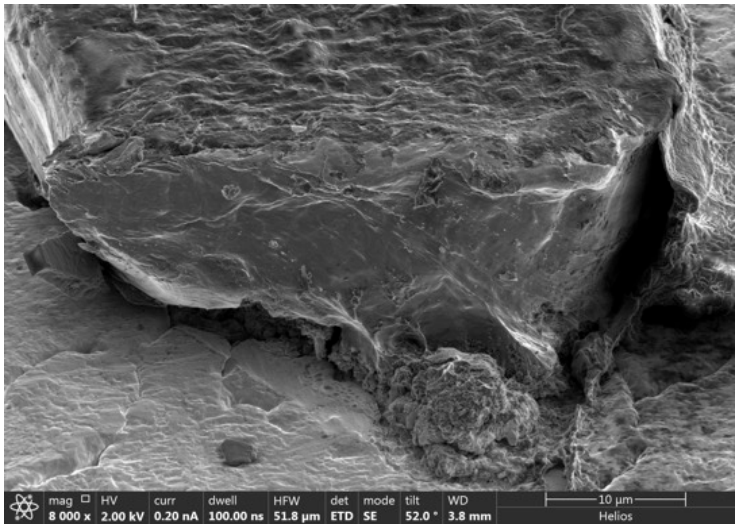

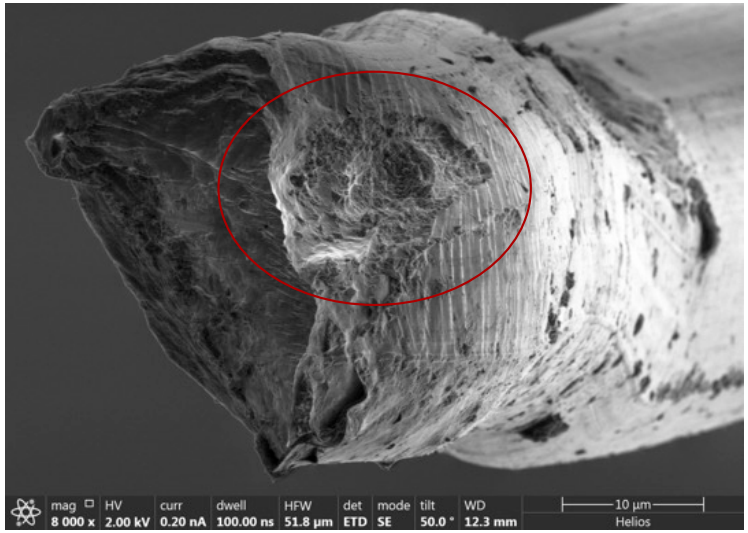

Atypical part shows a divot of additional unexpected deformation

Si precipitates Are Crack Initiation Sites

Sandia National Laboratories

- Al-Si alloy typically used for wire bonding
- Si not soluble at room temperature so driving force to precipitate
- The precipitates act as crack initiation sites during pull test and cause failures at low load

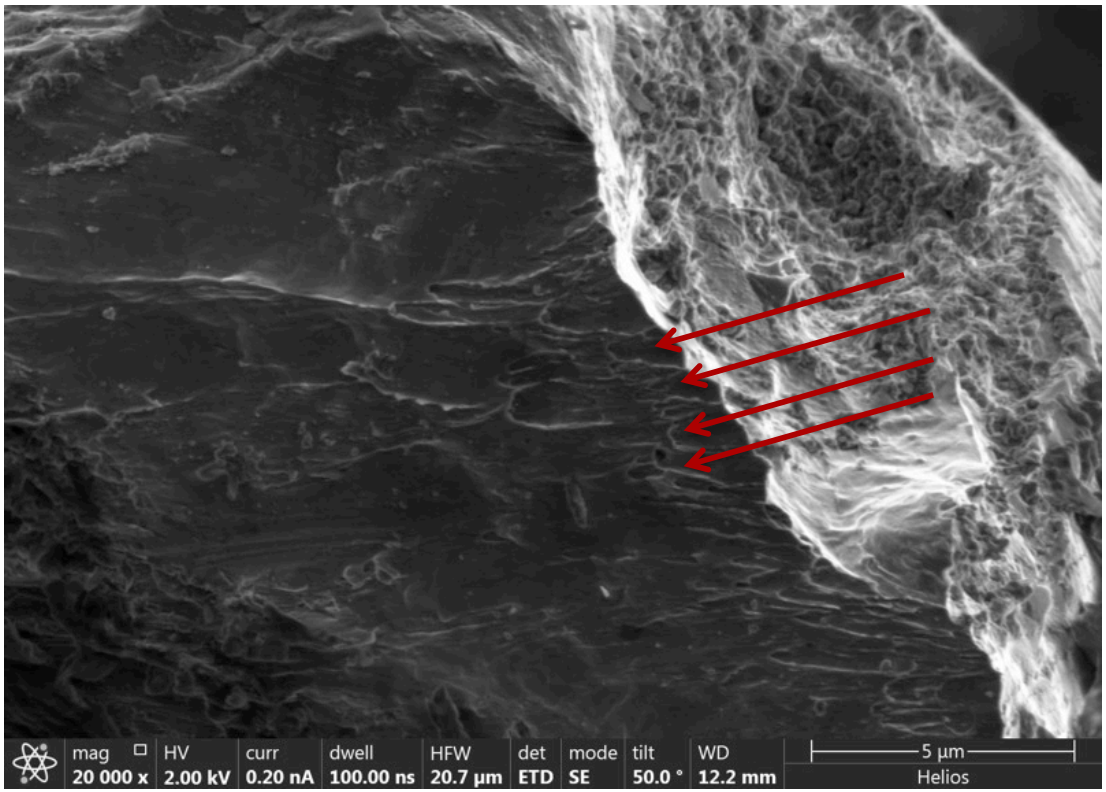

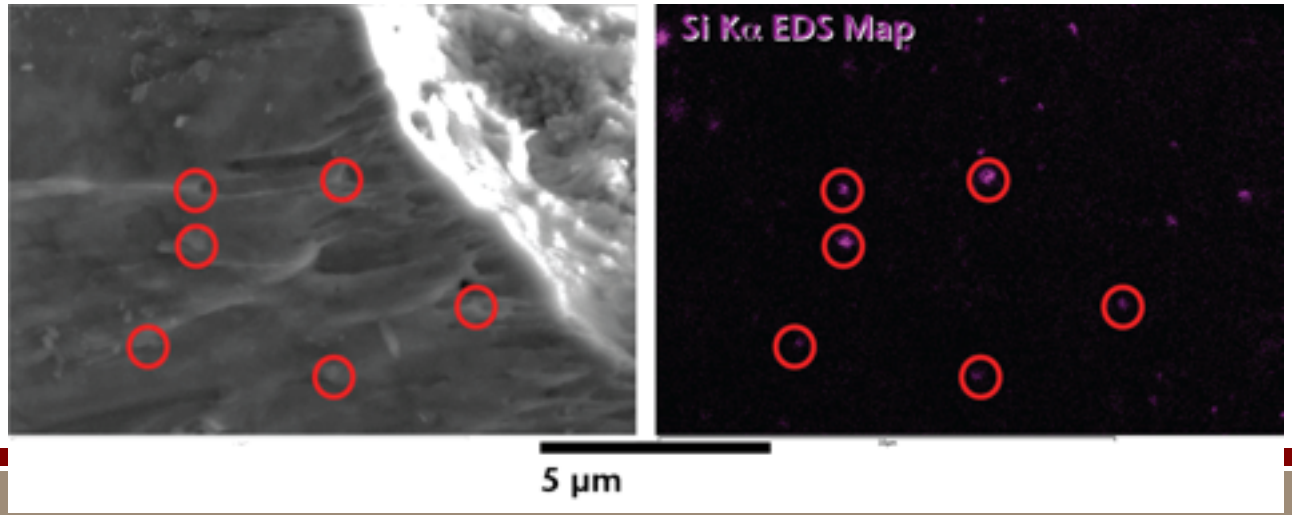

Connecting Electrical, Mechanical, and Microstructural Data

- All low load failures correlate with wires that experienced additional deformation beyond wire bond
- Consistent with Si precipitates acting as crack nucleation sites
- It is known that Si prefers to precipitate near dislocation loops
  - Kim et al. Electronic Materials Letters, **5** (3), 2009, pp. 99-103.
- Evidence of previous contact to Au surface in deformed region

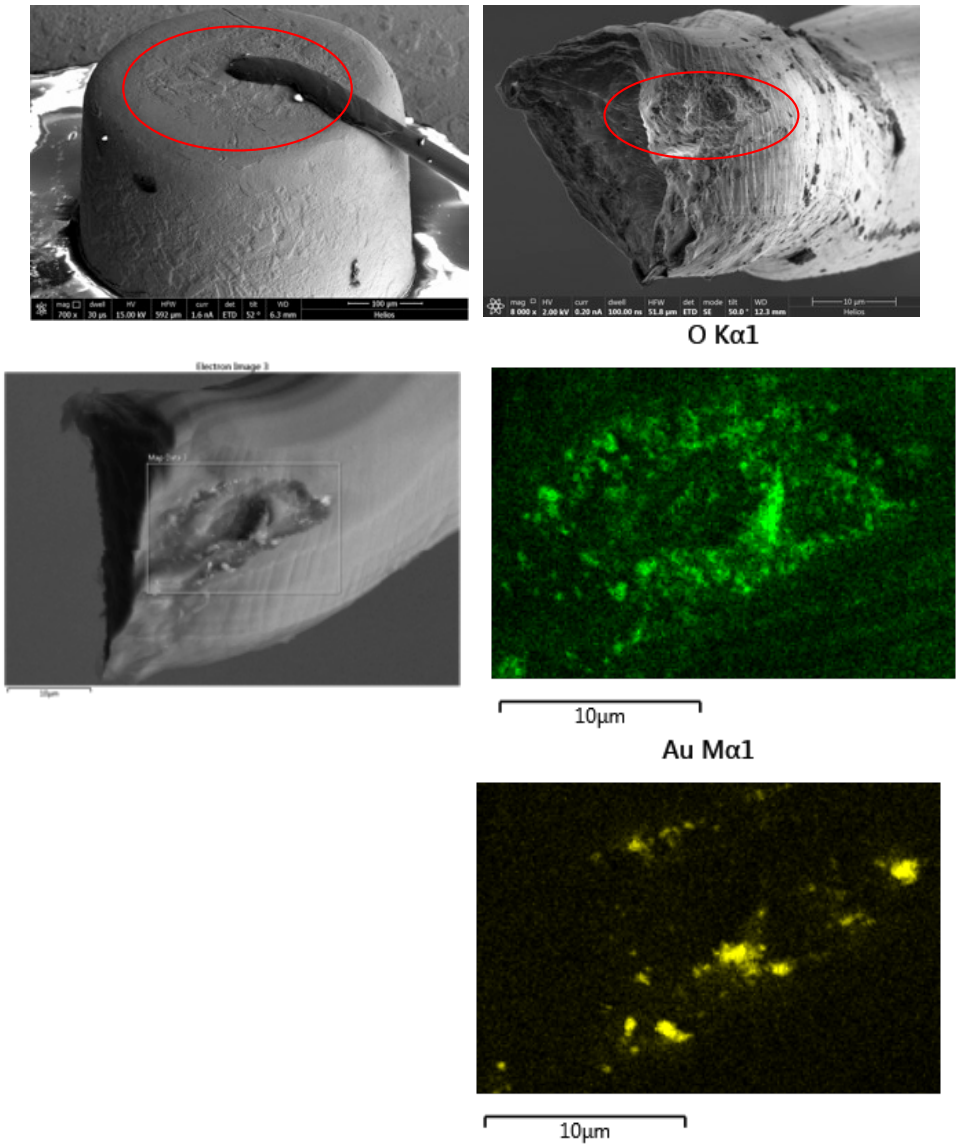

Additional deformation in wire can cause localized increase in Si precipitate density which causes failure at low strength. Additional deformation in wire could be explained by having to perform wire bonding twice

Reprocessing Caused a Series of Events that Reduced Reliability

Sandia National Laboratories

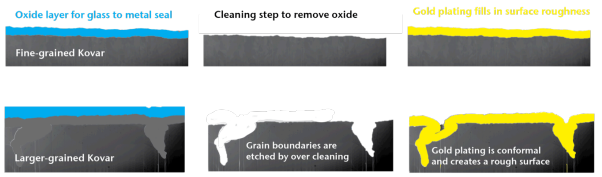

- Thermal history of kovar caused a larger grain size
  - Likely resulting from difficulty during glass-to-metal seal
- Cleaning step for fine-grained kovar resulted in intergranular corrosion
- Surface topography caused difficulty in forming Al wire bond
  - Additional deformation in wire suggests a reprocess
  - More interfacial defects present as a result
- Deformation caused dislocations in wire which serve as nucleation sites for Si precipitates
- The growth of Si precipitates as scattering centers over time, and trapping of contaminants at interface defects caused higher contact resistance

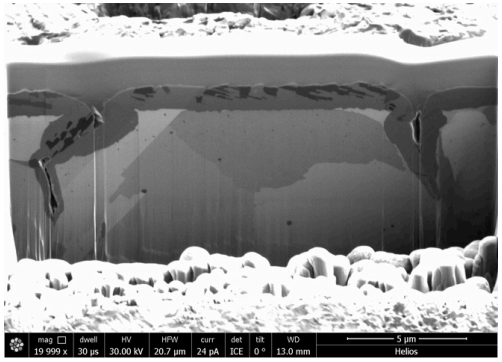

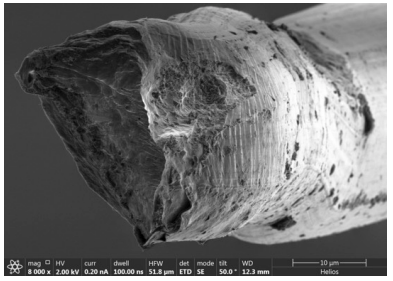

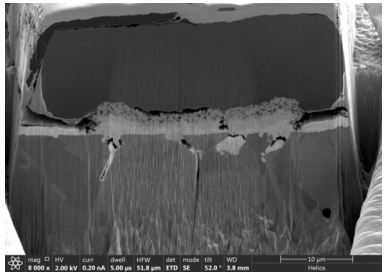

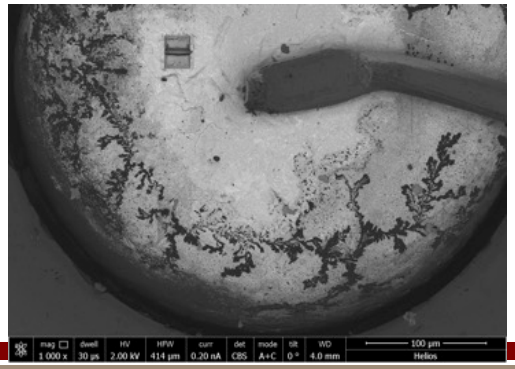

Variability in manufacturing can be hidden for decades if we don't have good control and understanding or processes.

Summary

- Model assuming early nucleation, diffusion limited growth, correlation of size/spacing of He bubbles does not explain all observations

- The distribution of Rh in nanoporous Pd/Rh particles effects the elevated temperatures stability of pores

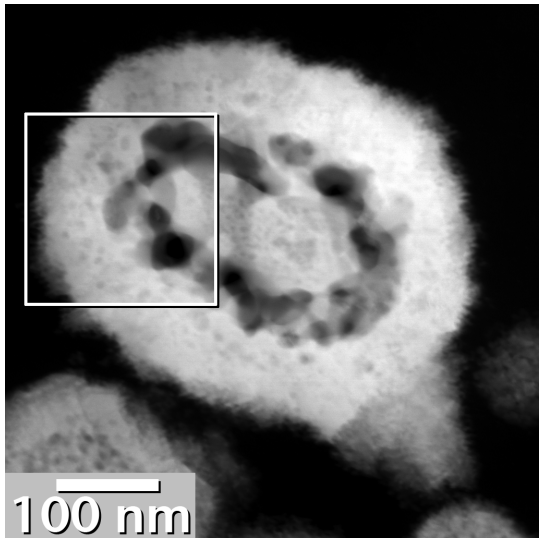

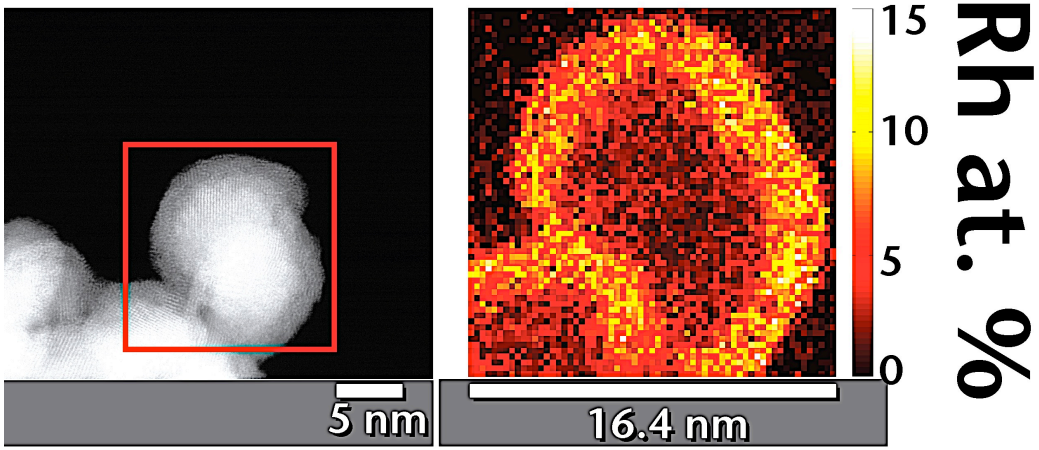

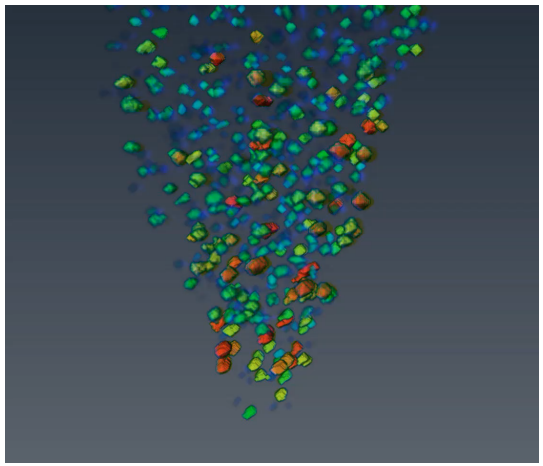

Summary

- Transformations is Li-ion battery electrodes are nucleation limited

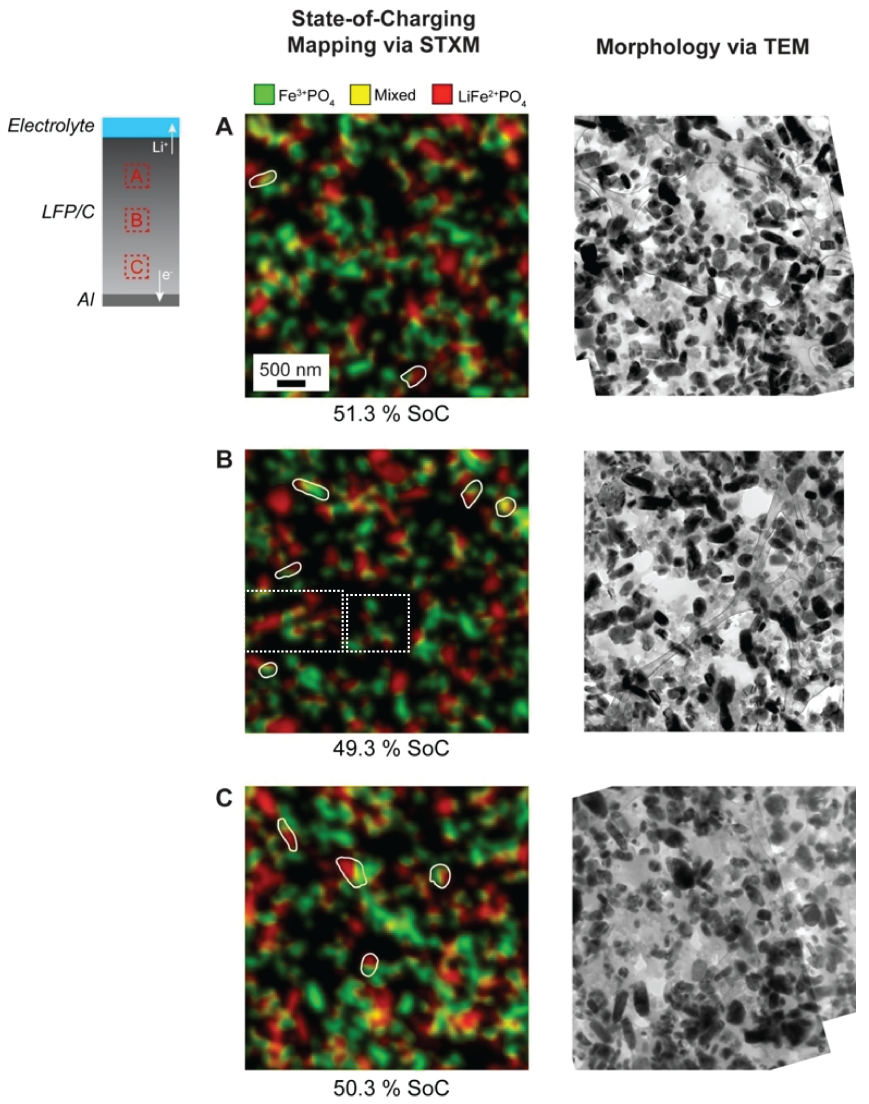

Summary

- Variability in manufacturing processes can cause performance issues decades after manufacturing
- The time scale of evolution of microstructures is much longer than typical modern products' life (2 years), but it is important for Sandia interests

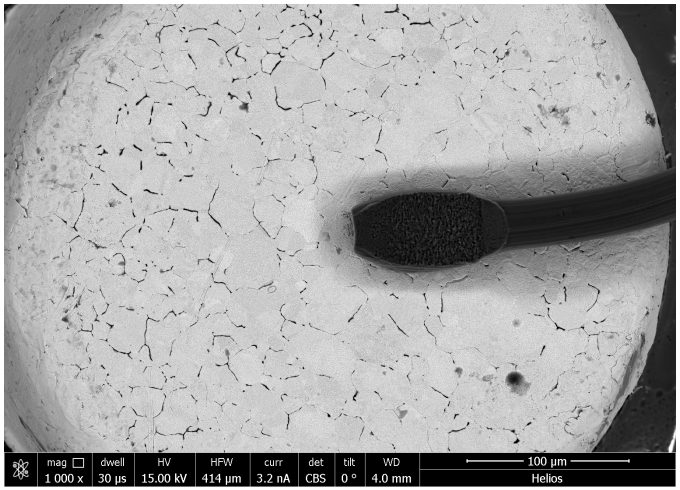

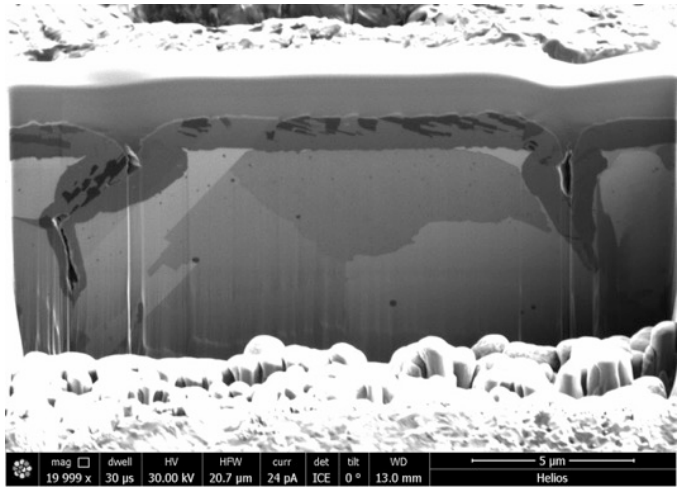

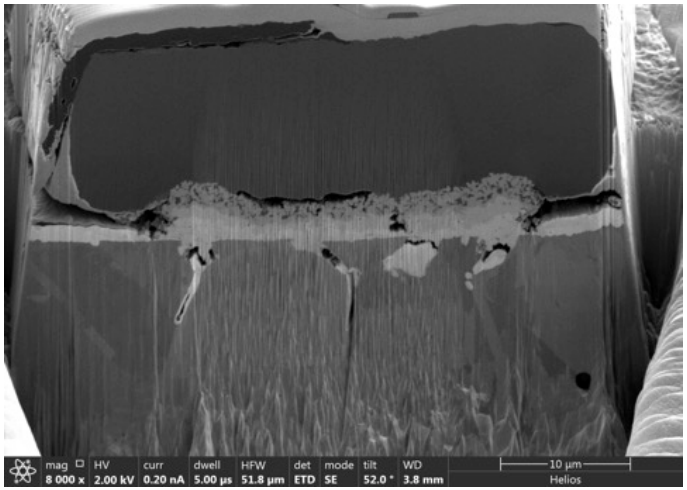

Conclusions

Sandia National Laboratories

- By going beyond just the pictures that are obtained from electron microscopy we can learn a lot about the evolution and behavior of materials and make informed engineering decisions
- Carnegie scientists and Sandia materials scientists look at the same microstructural phenomena but over millennial time scales rather than decades